

FOUNDED 1925
INCORPORATED BY
ROYAL CHARTER 1961

*"To promote the advancement
of radio, electronics and kindred
subjects by the exchange of
information in these branches
of engineering."*

THE RADIO AND ELECTRONIC ENGINEER

The Journal of the Institution of Electronic and Radio Engineers

VOLUME 38 No. 3

SEPTEMBER 1969

The Engineer's World

POLITICAL opinion determines the course of technology in much the same way as politics influence economic trends. Indeed, the whole business of politics, nationally and internationally, determines both by opinion and economic strictures the growth of technological development. Resistance to such development may be argued on the grounds of arresting expenditure on potential defence equipment, on the greater social needs of public services not needing a particular engineering service, or perhaps just bias against the social change created by applying science for the benefit of mankind.

Since the creation of the wheel, almost all technological achievement has found application to war-like ends: but often, for reasons of political economy, less encouragement has been given to the application of these inventions to release man from heavy labour or to create higher standards of living. Accordingly, the technological history of the twentieth century so far shows that our defence needs have largely provided the impetus to technological development, resulting in the varied communication systems, synthetic materials, etc., which now dominate the everyday life of society.

Given the necessary economic conditions, is the engineer able to make a major contribution toward improving the lot of man? Affirmative answers may be based on the apparent affluence of such comparatively small countries as Great Britain, Holland, Sweden, Switzerland (in terms of area and population) or the larger units as the U.S.A., Germany, and now Japan. The technological success of all these countries fades into insignificance, however, when measured against the international background which shows that the vast majority of the world population has scarcely benefited, if at all, from technological innovation. To argue that deficiency of economic well-being frustrates purchase of technical 'know how' and products merely invokes the merry-go-round of political opinion being the regulator of economic—but not necessarily technological—development. The solution lies in the ability of man to create wealth by providing the economic conditions essential for such advancement of technology as will enable all men to enjoy life far beyond the wheel and woad age.

The Radio and Electronic Engineer is not the medium in which to promote any hopeful panacea for men's ills. The Institution does, however, energetically resist any temptation to regard progress in its branch of technology as wholly dependent on war conditions, although admitting that like most other forms of human endeavour its progress was hastened in emergency and not retarded, as in peace time, by lack of economic foresight.

More pertinently, the Institution welcomes such international assemblies as the Commonwealth Engineering Conference which has this year adopted the theme 'Priorities in Public Works in Developing Countries'. Even if the Conference is restricted by economic or political considerations, it will nevertheless demonstrate that engineers, given both political and economic opportunity, are well able to fulfil the avowed object of every Chartered Engineer—"to advance science for the benefit of mankind".

G. D. C.

INSTITUTION NOTICES

Combined Programme of Meetings

Members of the Institution in the London area and in the Thames Valley and Kent Sections will receive with this issue of the *Journal* a copy of the 'Combined Programme of Meetings' issued by the I.E.R.E. and I.E.E. This programme, which covers meetings in October to January 1970, has been issued with the object of achieving closer collaboration in 'learned society' activities between the two Institutions.

All meetings in the programme are open to members of both Institutions (as well as to members of the Institute of Physics and the Physical Society and the Institute of Mathematics and its Applications). Copies of the booklet may be obtained by members in other parts of Great Britain by application to the Meetings Secretary, The Institution of Electronic and Radio Engineers, 8-9 Bedford Square, London, W.C.1.

The programmes for the East Anglian and Southern Sections of the I.E.R.E., which have for several sessions past been included with the London meetings, are now being published separately. However, for the convenience of members in the South East who are able to travel easily between these Sections and London, a complete programme of I.E.R.E. meetings for London and the East Anglian, Kent, Southern and Thames Valley Sections is contained as a 'tear-out' leaflet in the end-pages of this issue.

Technical Officer for the Indian Division

The Council has approved the appointment of Mr. M. T. Ranade, B.Sc., C.Eng. (Member), as Technical Officer for the Institution's Indian Division. He will take up his duties in November 1969 and will be based at the office in Bangalore. Mr. Ranade will edit *I.E.E.-I.E.R.E. Proceedings-India* and generally encourage 'learned society' activities in the five Zones of the Division, as well as membership development.

A graduate of Poona University, Mr. Ranade joined the Institution's headquarters staff in 1965 following experience in airborne radio and electronics and in sound recording and reproduction. He has been principally concerned with work on the editorial side of Institution publications, latterly as Assistant Technical Editor.

Study Tour of Japan and Expo '70

Members who are interested in the proposed study tour of the Japanese electronics industry combined with a visit to Expo '70 in Osaka in March/April of next year are reminded that they should advise the Institution without delay. No commitment on either side is involved at this stage but an idea of the numbers interested will enable further planning to proceed. Brief details of the tentative arrangements were given in the July issue of *The Radio and Electronic Engineer* (page 12).

Institution Dinner

Due to unavoidable circumstances the Institution Dinner announced for 27th November has had to be postponed until 1970.

The Council of the Institution expects to be able to announce the re-arranged date later this year and, at the same time, to announce the names of the principal guests.

Symposium on Satellite Communication

The Quebec Section of the Institution is planning to hold a symposium on 'The Canadian Aspects of Satellite Communication' in Montreal in May 1970. This is the first time that the Institution has organized such a meeting in Canada.

The Symposium will cover ground stations, communication links, and satellites themselves in both the experimental and operational environment. It will be particularly timely since a Canadian communication satellite is scheduled to be launched in 1970.

Contributions of papers of about twenty minutes' presentation time have been invited and synopses of proposed contributions should be sent to The Secretary, The Organizing Committee for the 'Canadian Aspects of Satellite Communication' Symposium, The Institution of Electronic and Radio Engineers, Room 300, Burnside Building, 151 Slater Street, Ottawa 4, Ontario, to arrive not later than November 30th, 1969. A synopsis should be long enough to enable the organizing committee to assess fully the proposed content of the paper and thus typically it should be of about 200 to 300 words in length.

1969-70 Programme of the Quebec Section

Meetings organized by the Quebec Section for the coming session include the following at which papers will be read:

- 5th November, 1969. 'Pseudo-Random Noise Generation, S. B. Mathews (*Canadian Marconi Company*)
- 4th February, 1970. 'Investing in Invention' P. Carey (*Central Dynamics*)
- 1st April, 1970. 'Fluidics' G. W. Standen (*Aviation Electric*)

All meetings will take place in the I.R.D. Conference Room of the Canadian Marconi Company, Aberdare Road (cross street Jean Talon), Montreal, and start at 7.30 p.m.

In addition there will be visits to the National Film Board and to the Canadian Overseas Telecommunications Corporation terminal. Full information on these visits, as well as further details of the meetings, may be obtained from the Meeting Secretary, Mr. K. E. Hancock, 78, 16th Avenue, Roxboro, P.Q. (Telephone 684-8584).

An Automatic Picture Transmission Cloud Cover Receiving Station

By

W. K. KENNEDY,
B.E. (Hons.)†

AND

J. K. BARGH,
M.E., Ph.D., M.N.Z.I.E., C.Eng.,
M.I.E.E.†

Presented at the Second New Zealand Electronics Conference (NELCON II) organized by the New Zealand Section of the I.E.R.E. and the New Zealand Electronics Institute and held in Auckland in August 1968.

Summary: The automatic picture transmission (APT) sub-system carried on weather satellites transmits, at facsimile rate, cloud cover photographs of the Earth below. Frequency modulation of a carrier in the 137 MHz band transmitted at a level of 5 watts is used to give pictures representing an area approximately 2400 km (1500 miles) square with an average resolution of 3 km (2 miles).

Major factors governing the design of a ground station which has been operational since early 1967 are presented. Signal/noise considerations show that a desirable combination is a tracking antenna having a gain of 10 dB followed by a receiving system having a noise figure not greater than 4 dB. Except for a doubling of line frequency a standard wire facsimile is used for final picture print-out.

Many additions to, and refinements of, the basic station are possible. A few of these are outlined and assessed in terms of operational convenience.

1. Introduction

In weather prediction, meteorologists have been, and still are, hampered by a lack of information on the current state of the atmosphere which they need to forecast the complex movements that determine the weather. Satellites are an obvious surveillance platform provided they can sense the atmospheric parameters from a distance. To date, the only useful link between our atmosphere and a satellite has been electromagnetic—either at the visible or infra-red wavelengths. Despite this limitation much valuable atmospheric information can be conveyed by cloud cover photographs.

Out-of-date information is of no use to the meteorologist except for research purposes. The Earth's atmosphere is a dynamic system with the situation changing hour by hour. Hence a means of automatic picture transmission (APT) direct from satellite to local ground stations was devised. An additional incentive for the development of such a system was the overloading of available data channels which would follow if the pictures were collected at a few central stations and distributed from there to the local forecaster.

This paper outlines the design of an APT station. Foremost objectives throughout the project were reliability and ease of operation by the meteorologist. Other major factors influencing the design decisions

were economics, ease of manufacture and maintenance and non-critical alignment—both electrical and mechanical.

2. Satellite Characteristics

To satisfy the meteorological requirement of complete Earth coverage at least once per day, weather satellites are injected into a near-polar orbit. Simultaneous consideration of camera characteristics, picture overlap, resolution and aspect-ratio limit the mean orbital height to between 900 and 1500 km, giving an orbital period between 104 and 116 minutes. Picture interpretation and latitude/longitude gridding problems are eased if the orbit is circular and the satellite is Earth-stabilized.

The satellite sub-system which is of concern for this paper is presented in Fig. 1. A picture sequence begins with 300 Hz modulation of the 2.4 kHz sub-carrier for 3 s as an alert signal, followed by 5 s of white level tone interrupted at line scan rate by a 12.5 ms black pulse for phasing purposes. In accordance with standard facsimile technique, no further synchronizing pulses are transmitted.

Concurrent with the above procedure the vidicon is exposed for 40 ms and the picture, typically representing an area 2400 km (1500 miles) square, is 'charge stored.' During the 200 seconds following the completion of the phasing sequence the picture is read from the vidicon at 4 lines per second and the video information is amplitude modulated on the 2.4 kHz

† Department of Electrical Engineering, University of Canterbury, Christchurch, New Zealand.

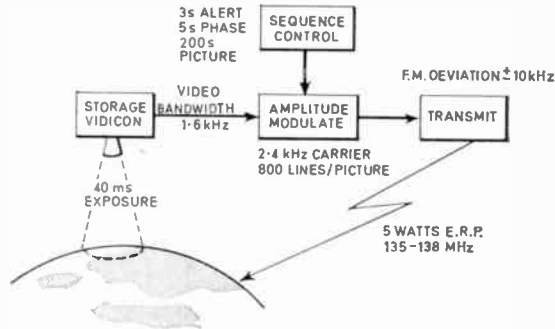


Fig. 1. Satellite sub-system.

sub-carrier; maximum carrier indicates white level and the video bandwidth is 1.5 kHz. The sub-carrier is frequency modulated on a 137 MHz r.f. carrier at a deviation of 10 kHz. Effective radiated power is 5 W.

Daytime cloud cover pictures may be supplemented by night-time infra-red transmissions for which the line scan rate is 48 lines per minute. Other differences occur in the picture format and an absence of phasing pulses in the infra-red system. However, since the main features determining ground station design are unaltered, this system will not be considered separately.

Further details on meteorological satellites are well presented in References 1-6.

3. Ground Station System: General Considerations

3.1 Antenna

A preliminary estimate of the station complexity may be obtained by calculation of the received signal/noise ratio. At an orbital height of 1500 km the path length of an horizon signal is 4000 km from which the signal received on a unity gain antenna is -140.2 dBW, increasing to -131.7 dBW when the satellite is overhead. (See Appendix).

At 137 MHz, antenna noise temperature due to natural sources⁷ is typically 1000° K to which an additional 1000° K is added to account for man-made noise. Assuming a system noise-figure of 4 dB, which may be readily obtained by careful application of standard techniques, the total equivalent noise temperature is 2450° K. Further, by use of the simplified formula,⁸

$$\text{r.f. bandwidth} = 2(f_m + \Delta f)$$

where f_m = maximum modulating frequency

Δf = frequency deviation,

the minimum pre-detection bandwidth may be calculated as 28 kHz. Allowing for receiver drifts and tuning inaccuracy the i.f. bandwidth, B , is taken to be 40 kHz. A noise temperature of 2450° K then corresponds to a received noise power of -148.7 dBW.

Siting to eliminate man-made noise reduces this figure to approximately -151 dBW.

An estimate of the base-band signal/noise ratio necessary for satisfactory picture quality must now be made. The dynamic range of the video signal handled by facsimile machines is typically 32 dB. If some 'spotting' in the black is tolerable a minimum base-band white signal/noise ratio of 38 dB would be permissible. By application of the formula⁹

$$(S/N)_b = 1.5 (S/N)_p (\Delta f/f_m)^2 (B/f_m)$$

where $(S/N)_b$ is the base-band signal/noise ratio and

$(S/N)_p$ is the pre-detection signal/noise ratio

it is found that a pre-detection S/N ratio of 18.3 dB is necessary. In the calculations above, the received signal and noise powers were -140.2 dBW and -148.7 dBW respectively, giving a $(S/N)_p$ ratio of 8.5 dB. Hence an antenna gain of 9.8 dB is required.

Since the antenna to be used in this service must be circularly-polarized (the incoming signal may have any polarization) either the helix or 'crossed' Yagi array is suitable. Table 1 summarizes the performance of these for a gain of 10 dB.

Table 1. Comparison of helix and Yagi antennas

Parameter	Helix	Yagi
General form	length 1.5λ 6 turn, 76 cm diameter	length 1.5λ 7 elements/plane
Polarization	naturally circular	λ/4 phasing section required
Axial ratio	closely unity	may vary widely
Beamwidth	45°	variable, but typically 40°
Side-lobes	less than -12 dB	variable; generally higher than helix
Bandwidth	50%	same order as received band; tuning critical
Feed	coaxial	balanced
Impedance	110Ω	variable, typically 40-100Ω (folded)
Size	lengths comparable, wind-load 30% higher on helix	
Construction	helix simpler, particularly in weather sealing	
Cost	comparable	

For both antennas the beamwidth is such that the ability to track during an orbit is required. If an 'elevation-on-azimuth' mount (el/az) is used a tracking speed of 6 degrees per second on both axes is sufficient for all orbits above 650 km and with maximum elevation angles less than 84 degrees.¹⁰ Orbits passing through greater elevations may be considered as either overhead or at 84° for tracking

purposes, since any reasonable pointing error is adequately offset by the lower signal path loss.

Other mounting arrangements may be used to advantage. For example, the X-Y mount avoids the infinite azimuth velocity required of the el/az mount for overhead passes. However, difficulties in mechanical arrangement, together with the ready availability of tables for the conversion of latitude, longitude and height data to azimuth and elevation co-ordinates, make the use of the el/az mount almost compulsory.

A few calculations comparing acceleration and wind-load forces¹¹ soon show the latter to be the more significant. Furthermore, it becomes obvious that to withstand winds over 100 km/h (60 miles/h) the pedestal and antenna structure must be large and robust with an all-up weight approaching 750 kg (1/2 ton). This, combined with a turning radius of 3.6 m (12 ft), introduces some minor siting problems when it is remembered that read-out at existing meteorological offices is required. At best it can be expected that a distance greater than 50 m and up to 240 m between the antenna and the operator's console must be allowed. Because of cable loss and consequential deterioration in signal/noise ratio, a pre-amplifier will be needed at the pedestal.

3.2 Tracking System

With the beamwidths listed in Table I it is apparent that an overall tracking accuracy within $\pm 10^\circ$ should be sufficient. However, to allow for other operational errors it would seem appropriate to design to closer limits. A $\pm 1\%$ accuracy (say $\pm 4^\circ$ in 360°) would seem a reasonable first specification which could be tightened or relaxed later when balanced against the cost of methods of system implementation.

Since accurate and up-to-date satellite orbital data are supplied regularly by N.A.S.A. there is no need for a completely automatic, self-locking tracking system. This leaves the possibility of various systems which basically fall into the categories of open- or closed-loop and which may be further subdivided into continuous or discrete types. The decision between open- or closed-loop system hinges mainly on operator convenience. Will more than one operator be required if the system is open-loop? Is there substantially less chance of error if a closed-loop system is used? Experience has shown that for general use an open-loop system is satisfactory, but for an experimental station, where the operator may be fully occupied with other equipment, the closed-loop system may have an advantage.

In general, with a moderate beamwidth antenna, it is likely that step-by-step or discontinuous tracking would be less expensive than continuous tracking provided that the stepping frequency required is not

too great. A continuous system must of course be a variable-speed type.

3.3 Signal Path

Typical losses in 9.5 mm (3/8 in) diameter coaxial cable at 137 MHz are 10 dB per 100 m. Any such loss arising prior to amplification must be added to the system noise figure which has been assumed to be 4 dB. Hence the need for a pre-amplifier.

To avoid the need for low-noise design in the receiver a pre-amplifier gain at least 10 dB in excess of cable losses should be provided. A noise figure of 4 dB without cable loss would then become 4.6 dB if the receiver noise figure were 6 dB.

The f.m. receiver design is governed by the standard considerations of spurious response, image response, and bandwidth, with the additional demand for facsimile signals of linear phase shift in the pass-band. Since the range of signal level to be handled is small, no a.g.c. is required, but the 2.4 kHz output level must be constant to within 0.2 dB. Discriminator linearity of $\pm 1\%$ is an advantage for infra-red transmissions. A pulse-averaging discriminator seems most suited to this and limits the maximum usable intermediate frequency.

Because of the 'one-shot' nature of the transmitted signal the display device must be readily operated with a minimum of skill. Furthermore, there is the meteorological requirement to have the picture available within a few minutes of reception. Both the above, without further consideration of the associated technical problems, eliminate an oscilloscope display.

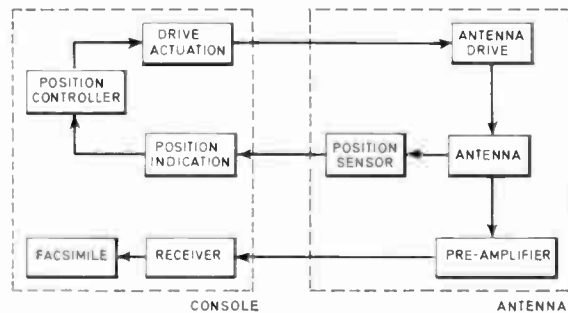


Fig. 2. System functional diagram.

A facsimile machine using either photographic or electro-sensitive paper seems to be the most reliable available picture display device. The photographic machine gives the better resolution and grey tone range but is more expensive and difficult to operate than the electro-sensitive type. The latter has the advantage that the picture may be viewed as it is formed.

The above considerations lead to a system for which the functional block diagram is as shown in Fig. 2.

4. Design Solutions

A more detailed indication of the design solutions incorporated in the station under discussion will now be given.

4.1 Antenna

Since the overall size of the antenna and pedestal structure is dependent solely on wind-loading, an early decision on allowable wind conditions had to be made. A maximum operating wind-speed of 130 km/h (80 miles/h) and a survival speed of 200 km/h (120 miles/h) were finally chosen as suitable for local conditions.

On the basis of the factors outlined in Table 1, with emphasis being placed on the absence of critical alignment and the comparative ease of manufacture, the helix was chosen. To obtain a little extra gain¹² it was designed for a centre frequency of 125 MHz which with 6 turns gives a calculated gain of 10.5 dB and an expected beamwidth of 43°. Although the design formula of Kraus¹² applies to an axially-terminated helix, it was found that performance was not noticeably impaired with circumferential termination.

Difficulty was experienced in obtaining a reliable measure of antenna gain but the beamwidth was within $\pm 1^\circ$ of that calculated. Since less than 20% of the system noise power is introduced by the amplifier any small deviation of antenna gain from optimum will have a second-order effect on system signal/noise ratio. Thus it was deemed unnecessary to make extensive gain measurements.

To reduce the necessary driving torque the antenna was counterbalanced against both weight and wind.

4.2 Pre-amplifier

Since the helix impedance is 110 Ω it was decided to mount the pre-amplifier directly behind the ground plane to use it for impedance matching to the 50 Ω cable.

A two-stage amplifier mounted on printed circuit board and enclosed in a cylindrical housing was designed following the mismatch techniques outlined by Ghausi.¹³ Active components used were Fairchild SE5020 transistors. Interstage coupling and input and output matching utilized single-tuned circuits. A stability factor of 11 was obtained for an alignability of 0.3, and a typical gain of 28 dB over a bandwidth of 3 MHz. The noise figure, measured by the noise doubling technique, was 3.3 dB.

Some difficulty due to condensation of water within the pre-amplifier has been experienced.

4.3 Receiver

In outline, the receiver is double superheterodyne using intermediate frequencies of 10.7 MHz and 1.5 MHz. It would be more usual in a receiver of this

type to choose a higher first i.f. but initially it was envisaged that a standard 10.7 MHz crystal or block filter might be used in the 1st i.f. Five switchable crystal frequencies are provided. The measured receiver noise figure is 4.5 dB.

The single 10.7 MHz stage is followed by three stages of amplification at 1.5 MHz using integrated circuit i.f. amplifiers chosen for their excellent limiting action. This completely eliminates the need for a.g.c. All the bandwidth determination of 40 kHz is done using double-tuned interstage coupling within the 1.5 MHz amplifier. Both Foster-Seeley and pulse-averaging type of discriminators are provided; the output from the latter is too low to drive the tuning indicator without introducing drift problems. Signal strength indication is derived from the first stage in the 1.5 MHz chain.

4.4 Facsimile

A commercial unit is used. It should be noted that the line-scan frequency is double the maximum usually provided in facsimile machines.

4.5 Pedestal Structure

Mechanical details of the pedestal will not be elaborated in this paper. Figure 3 shows the general structural form.

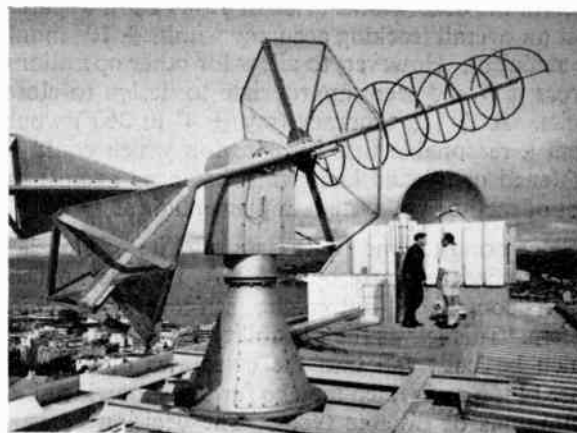


Fig. 3. Pedestal structure.

The antenna is mounted directly on the output shaft of the main elevation gearbox, which is driven from a subsidiary gearbox and $\frac{1}{2}$ hp 3-phase induction motor housed in the upper structure. This unit is rotated in azimuth by similar gearboxes and motor housed in the lower cone.

Signal, power and control cables limit the azimuth rotation to 370°, but the elevation may travel $\pm 92^\circ$ from vertical to allow continuous tracking for all possible orbits.

4.6 Position Control System

Velocity calculations¹⁰ show that if step-wise tracking is used with 10° increments the average stepping rate is a little greater than 1 per minute, with a maximum rate (for an orbit with a maximum elevation angle of 84°) of four in any one minute. This rate is well within the capability of small three-phase induction motors, which are more robust, reliable and less expensive than the more usual d.c. motors. Other methods of drive, notably hydraulic, were rejected as unsatisfactory at an early stage.

By fitting the motors with a brake, a very simple closed-loop control system was devised. This is pictured diagrammatically, together with the switching characteristic of each direction, in Fig. 4. The combined switching characteristic is shown in Fig. 5, where the guardband must encompass brake operating time and overrun during braking. Insufficient guardband will lead to hunting oscillations of the control system.

Most of the control system block diagram is self-explanatory except perhaps, the first-order interpolation unit. This enables satellite positions at one minute intervals to be programmed but the desired position fed to the error-detecting network to be a linear time interpolation between these positions.

Potentiometer feedback, as compared to synchro, was used because the signal indicating the desired position was more simply derived electrically. Furthermore, in view of the likely cable lengths of 240 m, a d.c. system was judged to be preferable. Errors were well within bounds at ± 0.4° for potentiometer linearity and ± 0.9° for worst case potentiometer loading. These figures are quoted for azimuth and must be halved for the elevation axis.

Not represented in Fig. 4 but incorporated in the final design are three possible modes of operation. The input from the interpolation unit may be replaced

by a single desired position with the backlash in the switching characteristic reduced accordingly. Further, there is facility for open-loop manual control both at the console and at the pedestal, with appropriate interlocks where necessary.

5. Refinements

The requirements of a basic APT station capable of successful operation by a non-technical operator with the minimum of training are presented above. However, there are a few refinements which would increase the versatility of the station.

5.1 Tape Recorder

All the detail within a picture may not be obvious in a single mean level exposure. It may be that expansion of the white or black contrast will highlight additional features. Tape recording of the transmitted pictures allows these additional exposures to be taken. Further, it supplies 'back-up' in the case of facsimile equipment malfunction or operator error.

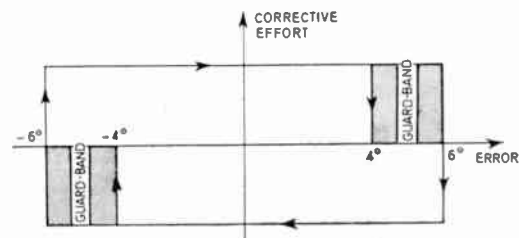


Fig. 5. Control system switching characteristic.

Most good-quality domestic tape recorders have satisfactory speed stability and bandwidth. However, since the signal to be recorded is amplitude modulated, 'drop-out' caused by head misalignment or low-quality tape contributes marked picture degradation. To overcome this the picture may be frequency-modulated on the tape, or alternatively, a high-quality tape must be chosen.

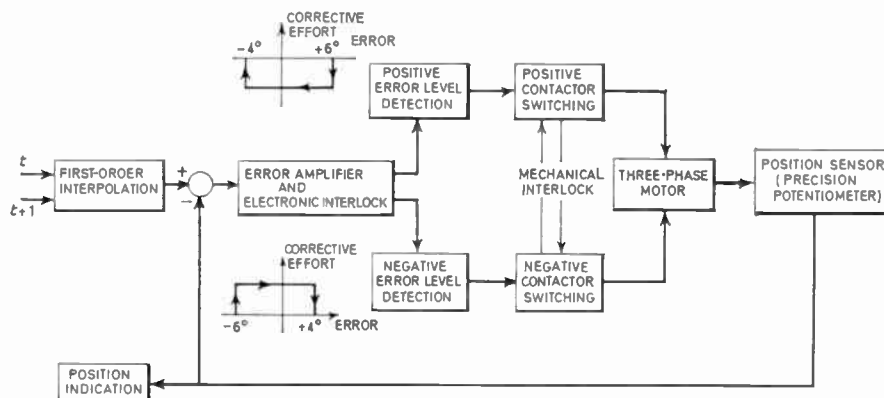


Fig. 4. Control system block diagram (Duplicate for second axis).

5.2 Video Remodulator

In Section 5.1 mention was made of contrast adjustment by photographic exposure level. However, electronic methods of implementing this are more convenient, repeatable and add considerably to the evrsatility of the station. Although adjustment may be made on the directly received picture it is more usual to use the remodulator in conjunction with the tape recorder.

As its name suggests this apparatus remodulates the incoming signal to alter overall contrast or to expand the contrast at either end of the grey scale, or to carry out both operations.

5.3 Control System

The control system outlined in Section 4.6 allows for a wide range of desired position input devices. If considered desirable it would be possible, without alteration of the present system, to control the antenna positioning from a punched paper tape. This would allow up to one month's orbits to be pre-computed and to be clocked to the control system at the appropriate time.

5.4 Interference

It is unfortunate that most meteorological offices are stationed at airports. This is one of the worst environments imaginable for the reception of low-level signals, particularly when these signals border on the aircraft communication band. Further, the level of man-made noise at airports is often high.

The most obvious solution to this problem is to site the antenna at a remote location but maintain control and read-out at the meteorological office. Such remote control would be readily incorporated in the station described above. The alternative is a rather stringent design of the receiving system; the most difficult requirement is the rejection of a 50 mV signal (satellite horizon signal is 2 μ V) at a frequency as close as 1 MHz to the 3 MHz wide satellite band.

A preliminary investigation has shown that blocking and intermodulation may be avoided by utilizing 3-pole Chebyshev filters as interstage and output coupling in the pre-amplifier. To maintain interstage losses within acceptable bounds helical resonator filters must be used.

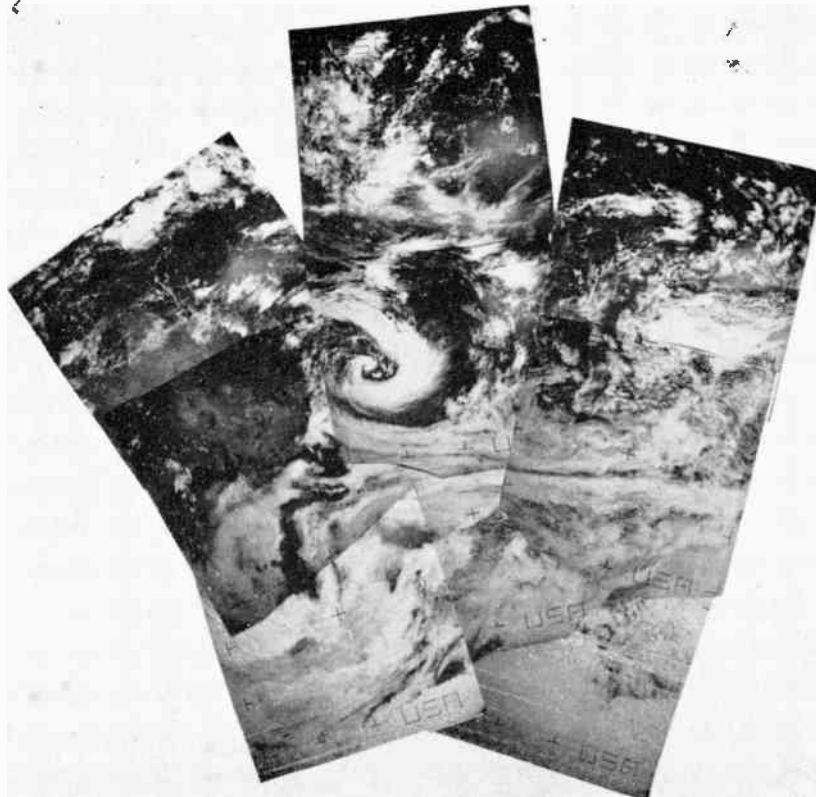


Fig. 6. Cloud montage of a single day's orbits.

6. Conclusions

An outline of the factors influencing the design of a meteorological satellite receiving station has been given. Throughout the design the overriding consideration has been the satisfaction of the meteorological objectives.

Over a period of operation of 16 months, during which at least 6000 orbits have been tracked, the total down-time has been 11½ hours involving the loss of five orbits. The loss of three of these orbits could be directly attributed to prototype faults, i.e. design features or manufacturing imperfections which were already noted as requiring correction in the production model.

The antenna structure has, without ill effect, withstood a measured 200 km/h (125 miles/h) gale. Azimuth backlash has settled down at a rather large $\pm 1.8^\circ$ but methods of eliminating this in future models have been devised.

Antenna beamwidth was measured as 43° with the maximum side-lobe level 14 dB down. With the pre-amplifier noise figure and gain measured at 3.3 dB and 30 dB respectively, combined with the receiver noise figure of 4.5 dB, a total cable loss of 21.3 dB could be tolerated before the system noise figure deteriorated to 4 dB. An average overall noise temperature was measured on site as 2600°K with fluctuations rising to 300°K above this in directions of industrial activity. Thus the detected signal/noise ratio, although not measured directly, should have been within 1 dB of the preliminary design estimates. Received pictures indicate that this was so. A typical set of pictures received from a satellite in one day has been assembled as shown in Fig. 6.

The meteorologist has found cloud cover photography an invaluable aid to weather prediction. However, before accurate forecasts are possible the meteorologist must have access to the measurement of atmospheric parameters at a large number of sample points. It would seem that satellites are destined to fill a major role in this instrumentation, both for operational and research purposes.

7. Acknowledgments

The building of this station was made possible by a grant from the New Zealand Meteorological Service. For this and subsequent advice and co-operation the authors are grateful.

Further financial assistance was received from the New Zealand University Grants Committee under Research Grant No. 66/41.

The generosity of various organizations in the U.S.A. in making the data from weather satellites freely available to all interested nations is acknowledged.

8. References

1. Stampfl, R. A. and Stroud, W. G., 'The Automatic Picture Transmission (APT) TV Camera System for Meteorological Satellites', NASA X-650-63-77, 1963.
2. Tepper, M. and Johnson, D. S., 'Toward operational weather satellite systems', *Astronautics and Aeronautics*, p. 16, June 1965.
3. Vaeth, J. G., 'Progress in satellite meteorology', *Spaceflight*, 7, p. 190, November 1965.
4. Hubert, L. F. and Lehr, P. E., 'Weather Satellites' (Blaisdell, Waltham, Mass., 1967).
5. Goldshlak, L., 'Nimbus III Real Time Transmission Systems (DRID and DRIR)', Technical Report No. 5, Contract No. NAS 5-10343, March, 1968.
6. Albert, E. G., 'The Improved *Tiros* Operational Satellite', ESSA Memorandum, NESCTM 7, August 1968.
7. Ko, H. C., 'The distribution of cosmic radio background radiation', *Proc. Inst. Radio Engrs*, 46, pp. 208-215, January 1958.
8. Krassner, G. N. and Michaels, J. V., 'Introduction to Space Communication Systems' (McGraw-Hill, New York, 1964).
9. Schwartz, M., 'Information Transmission, Modulation, and Noise' (McGraw-Hill, New York, 1959).
10. Rolinski, A. J., Carlson, D. J. and Coates, R. J., 'Satellite Tracking Characteristics of the X - Y Mount for Data Acquisition Antennas', NASA TN D-1697, 1964.
11. Brown, J. S. and McKee, K. E., 'Wind loads on antenna systems', *Microwave J.*, 7, p. 41, September 1964.
12. Kraus, J. D., 'Helical beam antenna design techniques', *Communications*, 29, pp. 6-9, 34-5, September 1949.
13. Ghausi, M. S., 'Principles and Design of Linear Active Circuits' (McGraw-Hill, New York, 1965).

9. Appendix

9.1 Received Signal Strength

Signal attenuation or path loss, L , between isotropic antennas separated a distance, D in free space may be expressed as⁸

$$L = \left(\frac{4\pi D}{\lambda} \right)^2$$

or more conveniently as

$$L \text{ (dB)} = 32.5 + 20 \log f + 20 \log D$$

if distance is expressed in km and frequency in MHz.

For $f = 137 \text{ MHz}$

$$D \text{ (horizon range)} = 4000 \text{ km.}$$

L may be calculated as 147.2 dB.

Transmitted signal power is 5 W or 7 dBW. Hence the received power (assuming unity gain antennas) is -140.2 dBW , which increases by $20 \log \left(\frac{4000}{1500} \right)$ or 8.5 dB when the satellite is overhead.

9.2 Noise Power

In general the received noise power may be expressed as

$P_n = KTB$ where the symbols have the following meaning:

- K Boltzmann's constant, 1.38×10^{-23} joule/deg K
- T equivalent input noise temperature, °K
- B pre-detection bandwidth, Hz.

Hence, if $T = 2450^\circ$ K and $B = 40$ kHz then $P_n = 1.35 \times 10^{-15}$ W or -148.7 dBW.

9.3 Signal/Noise Ratio

Above threshold the narrow-band noise model relates pre-detection and base-band signal/noise ratios by the following formula.⁹

$$(S/N)_b = 1.5 (S/N)_p (\Delta f/f_m)^2 (B/f_m)$$

where $(S/N)_b = 38$ dB = 6300

$$\Delta f = 10 \text{ kHz}$$

$$f_m = 4 \text{ kHz}$$

$$B = 40 \text{ kHz}$$

Hence $(S/N)_p$ may be calculated as 67.3 or 18.3 dB.

Manuscript first received by the Institution on 3rd March 1969 and in final form on 14th July 1969 (Paper No. 1276/AMMS23)

© The Institution of Electronic and Radio Engineers, 1969

Contributors to this Issue



Dr J. K. Bargh is currently a senior lecturer in electrical engineering at the University of Canterbury. After completing his M.E. degree at that University in 1956 he accepted a short service commission in the New Zealand Defence Scientific Corps. During this period he spent 3 years working in the Control Group of the Cambridge University Engineering Laboratories and

two years at the Naval Research Laboratory in Auckland, New Zealand. After leaving the Defence Scientific Corps, Dr Bargh spent some time as a systems engineer with Elliott Automation before returning to academic life. His main research interests are system identification and modelling.



L. Leng graduated from Manchester University with a B.Sc. Tech. degree in electrical engineering. He received his technical training at S.T.C.'s North Woolwich factory and also at B.T.H., Rugby.

His engineering experience was acquired on electrical drive and control gear while working with the consulting engineers, McLellan and Partners. He then joined the U.K.

Atomic Energy Authority where he was concerned with nuclear plant instrumentation and control.

At present, Mr. Leng is the head of Electrical Department of W. & T. Avery's weighing division and is responsible for the design and application of electrical and electronic equipment to weighing machines.



W. K. Kennedy joined the staff of the University of Canterbury after graduating with a B.E. degree in 1963. His teaching interests include circuit theory and service courses. At present his research is centred on machine recognition of photographic features, with particular reference to cloud cover photography.



Peter D. H. Cobham (M. 1968, G. 1963) was at the National Physical Laboratory for eight years, latterly as an assistant experimental officer in the Acoustics Section. In 1964 he became an assistant lecturer at Letchworth College of Technology and in 1968 was appointed lecturer in the Engineering Department at Twickenham College of Technology.

An Extension of Karnaugh Map Technique to Interface Design

By

P. COBHAM,
C.Eng., M.I.E.R.E.†

Summary: Karnaugh Map methods for designing counters and shift registers can be extended to parallel code conversion or interface design. A number of examples are shown, including the derivation of some well-known circuits. The possibility of steering J-K and D type flip-flops is considered. Finally, an example illustrating the use of a three-dimensional Karnaugh Map is given.

A recent paper by K. J. Dean‡ describes a method for the design of counters using Karnaugh maps. This method can easily be extended to obtain the logic required for parallel code conversion or interface design.

As an example consider the logic required to convert 8421 b.c.d. to the 7321 b.c.d. given in Truth Table 1, which has been chosen because the final logic is simple and unique. Let the inputs be A, B, C and D and the outputs be W, X, Y and Z, where D and Z are the most significant digits.

Truth Table 1

	8421 b.c.d.				7321 b.c.d.			
	A	B	C	D	W	X	Y	Z
0	0	0	0	0	0	0	0	0
1	1	0	0	0	1	0	0	0
2	0	1	0	0	0	1	0	0
3	1	1	0	0	0	0	1	0
4	0	0	1	0	1	0	1	0
5	1	0	1	0	0	1	1	0
6	0	1	1	0	1	1	1	0
7	1	1	1	0	0	0	0	1
8	0	0	0	1	1	0	0	1
9	1	0	0	1	0	1	0	1

AB	CD			
	00	01	11	10
00	0	8	X	4
01	2	X	X	6
11	3	X	X	7
10	1	9	X	5

Fig. 1. (a)
Key map for input 8421 b.c.d.

A key map (Fig. 1(a)) is now required to show the positions of the 8421 b.c.d. input states, and from it the four output maps for W, X, Y and Z are prepared. This may be shown as follows taking W as an example (see the maps comprising Fig. 1(b)): from the truth table it is known what W is required to be for 1, 2, 3, etc., so this is filled in on the map for W in the positions given by the key map, the immaterial states being completed with crosses. When all the maps have been completed the looping process is carried out, the same loop being duplicated on as many maps as possible, so as to produce the simplest logic for the system as a whole.

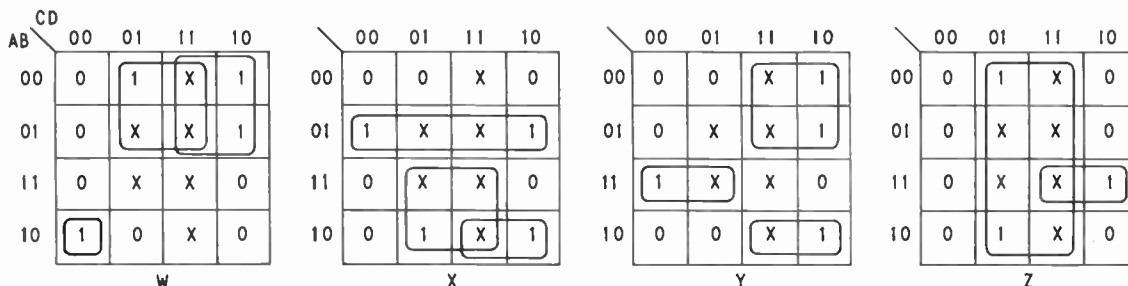


Fig. 1. (b) Derived maps to give 7321 b.c.d. in terms of 8421 b.c.d. input states A, B, C and D.

† Engineering Department, Twickenham College of Technology, Twickenham, Middlesex.

‡ Dean, K. J., 'Design of bidirectional coherent counters', *Proc. Instn Elect. Engrs*, 113, No. 11, pp. 1751-4, November 1966. (I.E.E. Paper No. 5098E.)

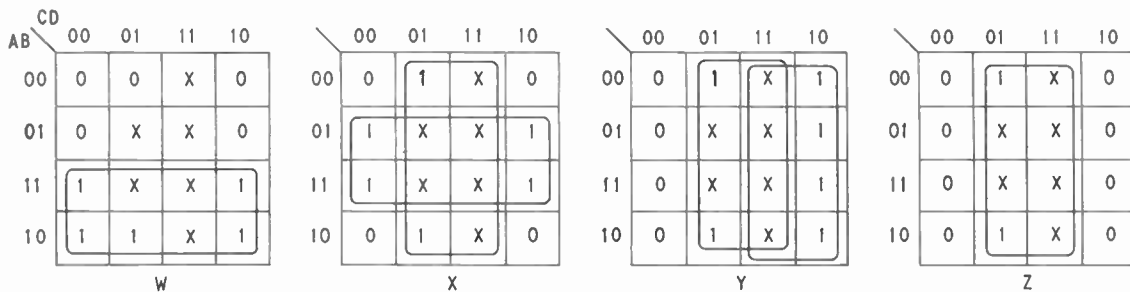


Fig. 2. Derived maps to give 2421 b.c.d. in terms of 8421 b.c.d. input states A, B, C and D.

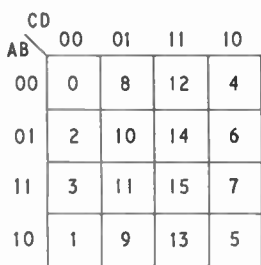


Fig. 3. (a) Key map for input binary.

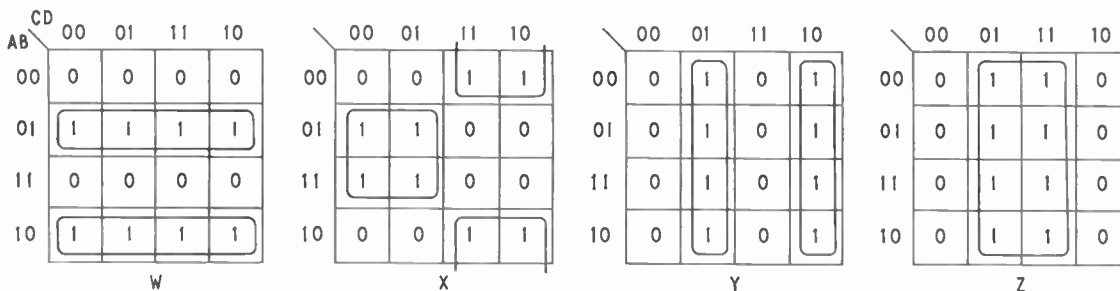


Fig. 3. (b) Derived maps to give Gray code in terms of the binary input states, A, B, C and D.

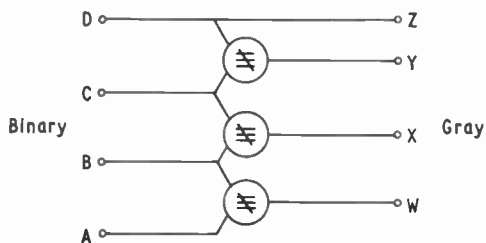


Fig. 4. Binary-Gray interface.

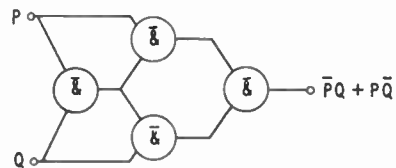


Fig. 5. Typical non-equivalence gate.

For example, Y bottom right-hand corner could otherwise form a loop of four with the top right-hand corner. However, in the case of Z, a loop of eight is preferred as this gives a single variable.

The final interface logic then becomes:

$$\begin{aligned} f_w &= \bar{A}D + \bar{A}C + ABC\bar{D} \\ f_x &= \bar{A}\bar{B}C + \bar{A}B + AD \\ f_y &= ABC + \bar{A}C + ABC \\ f_z &= ABC + D \end{aligned}$$

Although the above example serves very well to illustrate the method to obtain the interface logic, the code used is hardly a common one. However, the method can equally well be applied to any code and as examples it has been used to convert 8421 b.c.d. to 2421 b.c.d. and pure binary to Gray code. The truth tables of these codes are shown in Truth Table 2 and the appropriate maps are shown in Fig. 2 and 3.

From the maps the following results are obtained:

(i) To convert 8421 b.c.d. to 2421 b.c.d.

$$\begin{aligned} f_w &= A \\ f_x &= B + D \\ f_y &= C + D \\ f_z &= D \end{aligned}$$

(ii) To convert pure binary to Gray code

$$\begin{aligned} f_w &= \bar{A}B + AB \\ f_x &= \bar{B}C + BC \\ f_y &= \bar{C}D + CD \\ f_z &= D \end{aligned}$$

Truth Tables 2

	Gray				Excess 3				2421 b.c.d.			
	W	X	Y	Z	W	X	Y	Z	W	X	Y	Z
0	0	0	0	0	1	1	0	0	0	0	0	0
1	1	0	0	0	0	0	1	0	1	0	0	0
2	1	1	0	0	1	0	1	0	0	1	0	0
3	0	1	0	0	0	1	1	0	1	1	0	0
4	0	1	1	0	1	1	1	0	0	0	1	0
5	1	1	1	0	0	0	0	1	1	0	1	0
6	1	0	1	0	1	0	0	1	0	1	1	0
7	0	0	1	0	0	1	0	1	1	1	1	0
8	0	0	1	1	1	1	0	1	0	1	1	1
9	1	0	1	1	0	0	1	1	1	1	1	1
10	1	1	1	1								
11	0	1	1	1								
12	0	1	0	1								
13	1	1	0	1								
14	1	0	0	1								
15	0	0	0	1								

The binary to Gray logic leads to the well known interface which uses non-equivalence gates, and is shown in Fig. 4. A possible non-equivalence gate using NAND elements is also shown in Fig. 5.

The same process can be used to convert variously coded inputs to 8421 b.c.d. or pure binary, as examples excess 3, shown in Truth Table 2 and 7321 b.c.d. have been converted. The appropriate maps for these conversions are shown in Figs. 6 and 7 giving the following interface logic.

(i) To convert excess 3 to 8421 b.c.d.

$$\begin{aligned} f_a &= \bar{W} \\ f_b &= \bar{W}X + W\bar{X} \\ f_c &= \bar{X}\bar{Y} + \bar{W}\bar{Y} + WXY \\ f_d &= YZ + WXZ \end{aligned}$$

(ii) To convert 7321 b.c.d. to 8421 b.c.d.

$$\begin{aligned} f_a &= \bar{W}Z + \bar{W}Y + W\bar{Y}Z \\ f_b &= WX + X\bar{Y}Z + \bar{W}\bar{X}Z + \bar{W}\bar{X}Y \\ f_c &= WY + XY + \bar{W}\bar{X}Z \\ f_d &= XZ + WZ \end{aligned}$$

The logic in the latter example is a little complex but not too unwieldy, however the logic for conversion from Gray to binary as given by the maps comprising

WX	YZ			
	00	01	11	10
00	x	5	9	1
01	x	7	x	3
11	0	8	x	4
10	x	6	x	2

Fig. 6. (a) Key map for input excess-3 code.

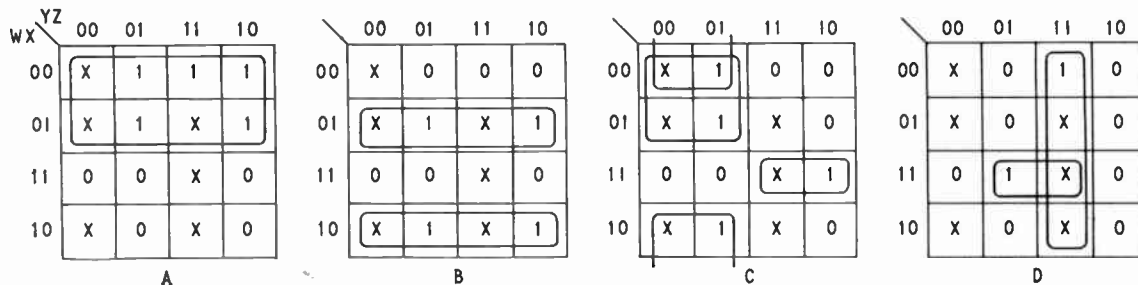


Fig. 6. (b) Derived maps for 8421 b.c.d. in terms of the excess-3 input states W, X, Y and Z.

Fig. 8 is clearly far too complicated to use. A relatively simple parallel circuit is known for this conversion and is shown in Fig. 9; if the map system works it should, and in fact is, able to produce the logic for this interface. Having considered the output in terms of the input logic, the possibility that a simple relation exists for the n th output state in terms

of the n th input and some other output state is now considered. This for example is certainly the case for a full adder where any digit sum depends on the carry from the next least significant digit. In the case of the Gray–binary interface shown in Fig. 9, the n th binary place depends on the n th Gray place and the $(n+1)$ th binary place.

	YZ	00	01	11	10
WX	00	0	7	X	3
	01	2	9	X	5
	11	X	X	X	6
	10	1	8	X	4

Fig. 7. (a) Key map for input 7321 b.c.d.

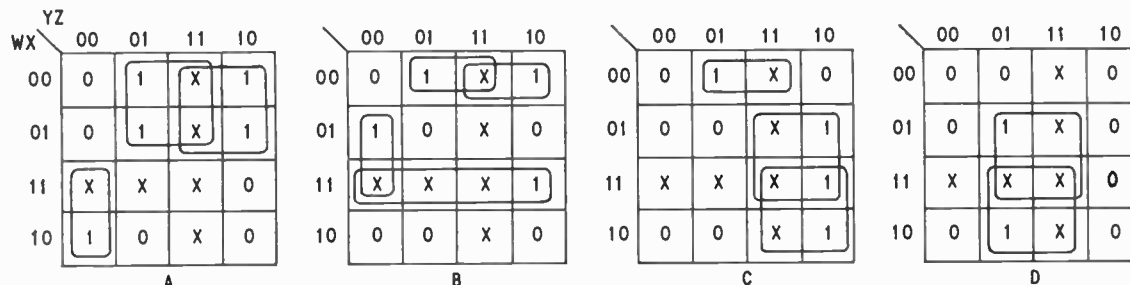


Fig. 7. (b) Derived maps for 8421 b.c.d. in terms of the 7321 b.c.d. input states W, X, Y and Z.

	YZ	00	01	11	10
WX	00	0	15	8	7
	01	3	12	11	4
	11	2	13	10	5
	10	1	14	9	6

Fig. 8. (a) Key map for input Gray code.

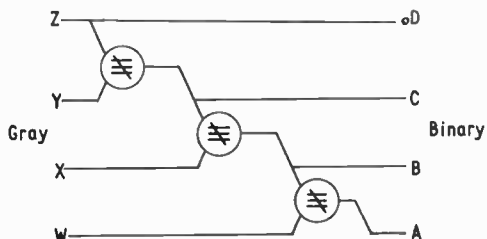


Fig. 9. Gray–binary interface.

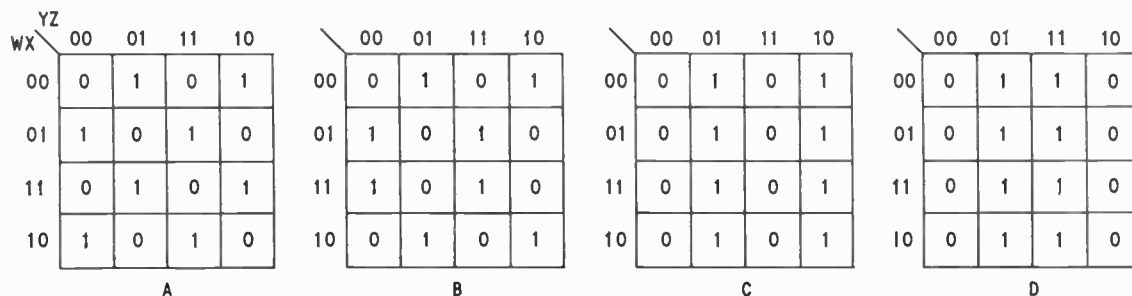


Fig. 8. (b) Derived maps for binary in terms of the Gray input states W, X, Y and Z.

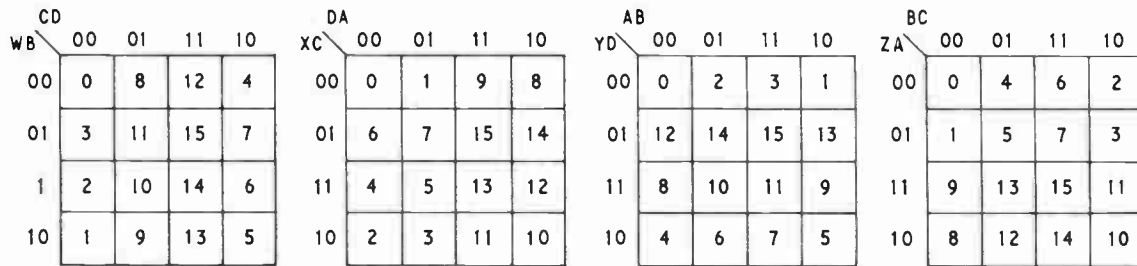


Fig. 10. (a) Key maps for A, B, C and D.

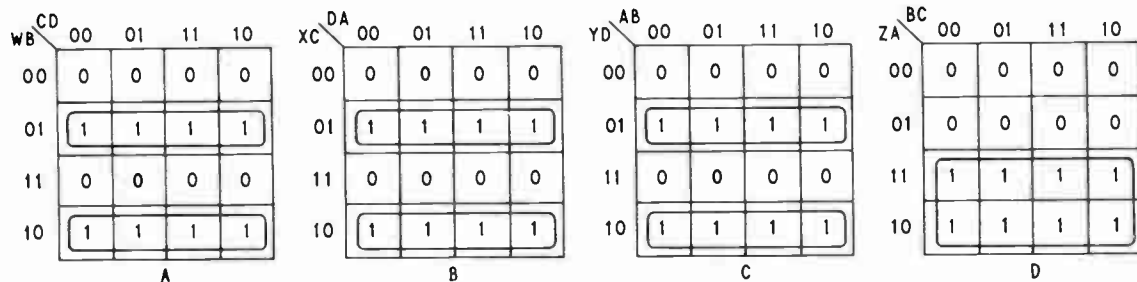


Fig. 10. (b) Derived maps for Gray-binary conversion interface.

$$\begin{aligned}
 f_a &= \bar{W}B + WB \\
 f_b &= \bar{X}C + XC \\
 f_c &= \bar{Y}D + YD \\
 f_d &= Z
 \end{aligned}$$

It is interesting to note that the method works whatever variables are chosen, provided that those upon which the logic depends are included on the map. For example, if A were included on the map for A, it merely comes out as a trivial solution that $A = A$. Figure 11 shows maps drawn for A in terms of WXBC, and B in terms of XYCD; here on the key maps two states occupy the same minterm but this does not matter as the required output for both states is the same and the output logic is the same

as that given above for f_a and f_b . Notice that if the output required for the two states within the minterms was not the same, the method terminates.

Following the modern trend towards integrated circuits and J-K flip flops, the possibility that the logic required to steer the J and K inputs of flip flops was considered. However, a look at the input truth table for a J-K flip flop shown in Table 3 reveals that this is no help. The steering logic requires that Q_{n+1} should go to 0 or 1 irrespective of the state of Q_n , which merely holds a previous solution for bit Q. In this case the steering equations become those given in Table 3 and $K = J$, so that the steering logic for J is identical to the interface logic determined for the same conversions and which is given above.

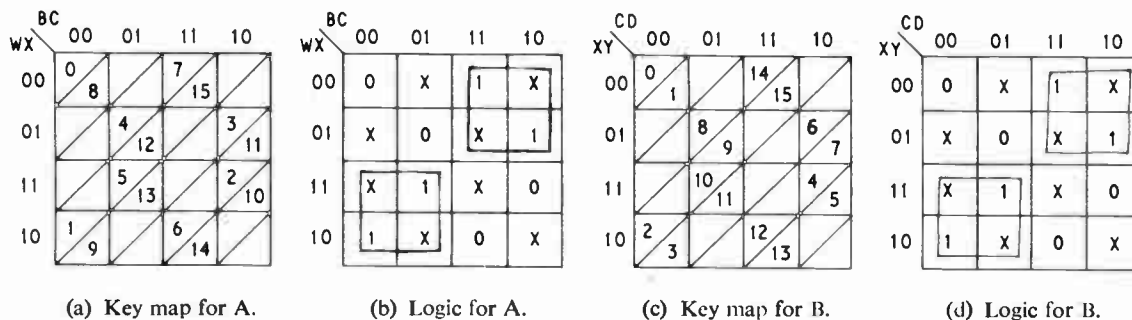


Fig. 11.

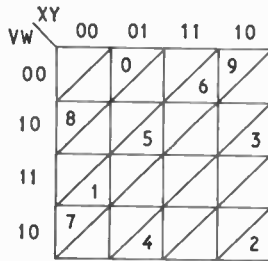


Fig. 12. (a) Key map for '2-out-of-5' code.

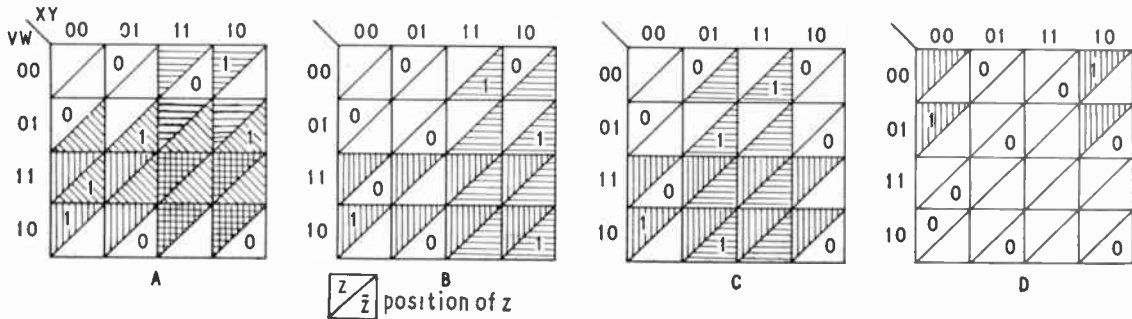


Fig. 12. (b) Derived maps for 8421 b.c.d. in terms of the '2-out-of-5' code states V, W, X, Y and Z.

Table 3

J-K truth table			J-K steering table			
J	K	Q_{n+1}	Q_n	Q_{n+1}	J	K
0	0	Q_n	0	to 0	0	X
0	1	0	0	to 1	1	X
1	0	1	1	to 0	X	1
1	1	\bar{Q}_n	1	to 1	X	0

$Q_{n+1} = 0$ if J = 0 and K = 1
 $Q_{n+1} = 1$ if J = 1 and K = 0

In order to avoid using a number of inverters to produce the logic for K, it may well be convenient to use D type flip-flops which only require one input. The D type flip-flop has only one input, the D input, and whatever (0 or 1) appears on that input is transferred to the output when a clock pulse arrives; this is illustrated by the truth table given in Table 4.

Table 4

D truth table		
Q_n	D	Q_{n+1}
0	0	0
0	1	1
1	0	0
1	1	1

$Q_{n+1} = 0$ if D = 0
 $Q_{n+1} = 1$ if D = 1

Using the Karnaugh map technique described by Dean† the above method can be expanded to cope with much larger problems, such as the parallel conversion of an eight-bit code to a six-bit code. This automatically implies that a number of states are not used and therefore it is feasible to use Dean's method. As a simpler example the method has been used to obtain the logic required to convert the 2-out-of-5 code shown in Truth Table 5 to 8421 b.c.d. The relevant maps which are shown in

Fig. 12 give the following logic:

$$\begin{aligned}
 f_a &= XZ + VZ + WZ \\
 f_b &= XZ + VZ \\
 f_c &= YZ + VZ \\
 f_d &= \bar{V}YZ
 \end{aligned}$$

Truth Tables 5

	V	W	X	Y	Z
0	0	0	0	1	1
1	1	1	0	0	0
2	1	0	1	0	0
3	0	1	1	0	0
4	1	0	0	1	0
5	0	1	0	1	0
6	0	0	1	1	0
7	1	0	0	0	1
8	0	1	0	0	1
9	0	0	1	0	1

Finally it must be pointed out that Boolean algebra takes no account of time. Thus when using this method to design interface and sampling circuits, care must be taken to allow for the propagation delays encountered when a change in the input logic takes place.

† Dean, K. J., 'An extension of the use of Karnaugh maps in minimization of logical functions', *The Radio and Electronic Engineer*, 35, pp. 294-6, May 1968.

Manuscript first received by the Institution on 26th November 1968 and in final form on 25th February 1969. (Short Contribution No. 121/Comp. 121).

A Wideband Amplitude Modulator as a Special Silicon Integrated Circuit

By

A. STEWART†

AND

C. H. JONES,
B.Sc.(Hons.)‡

Summary: A transistor circuit for silicon integrated circuit construction incorporating a new design of modulator is described. The circuit is associated with a microphone amplifier and r.f. input stage. The output consists of an amplitude modulated carrier in which the a.f. components have been suppressed. The circuit is suitable for modulation frequencies well into the video range and carrier frequencies up to about 20 MHz, the behaviour being predictable over a wide range of conditions. The specifications meet those laid down for integrated circuits generally.

1. Introduction

Full carrier amplitude modulation is still widely employed, not only in commercial broadcasting but in a variety of mobile communication systems. This type of modulation is currently performed by devices containing non-linear elements or on an analogue sample basis sometimes known as piecewise-linear-rectification type modulation. The latter type usually implies carrier suppression. However, the device described in this paper is a general-purpose circuit which produces a modulated carrier free of the audio component over a wide range of frequencies. The basic modulator is currently the subject of a patent application.¹

2. The Overall Circuit

The block diagram of the circuit is shown in Fig. 1.

The operation of the circuit may be described by considering it in three sections, the audio amplifier, the radio frequency amplifier and the modulator. The input from a microphone is amplified by a fully temperature-stabilized d.c.-coupled two-stage amplifier having a voltage gain of approximately 75. A phase splitter, the output levels of which depend upon the output of the amplifier, supplies the modulator with two antiphase audio signals at different stable d.c. potentials. A wideband single-stage r.f. amplifier is also directly coupled to the modulator and the audio

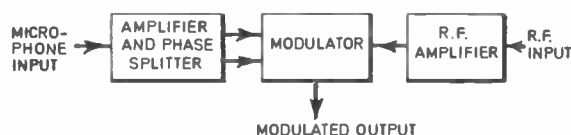


Fig. 1. Block diagram of modulator.

signals are sampled at the frequency of the carrier to produce a modulated output.

The component parts of the device will now be described, commencing with the modulator, the input requirements of which dictate the design of the rest of the circuit.

3. The Modulator

3.1. The Action of the Circuit

An idealized circuit with piecewise-linear characteristics is shown in Fig. 2(a), while the circuit of Fig. 2(b) illustrates the principle of the modulator described in this paper. The a.c. behaviour of the second circuit is self-evident, one diode being switched on by the positive-going voltage excursions of the carrier, the other by the negative-going excursions. The currents in the diodes combine to give the waveform shown in Fig. 3(a). The distortion in the resultant modulated carrier occurs during the non-linear portion of the

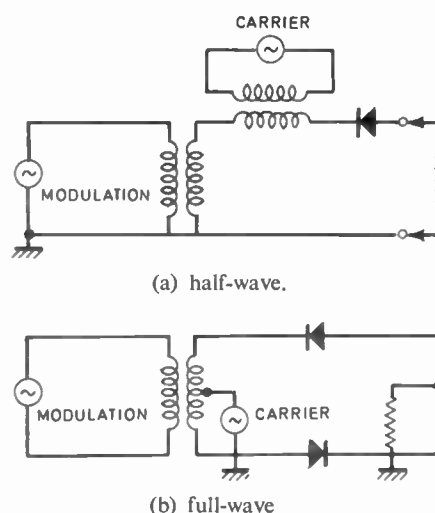
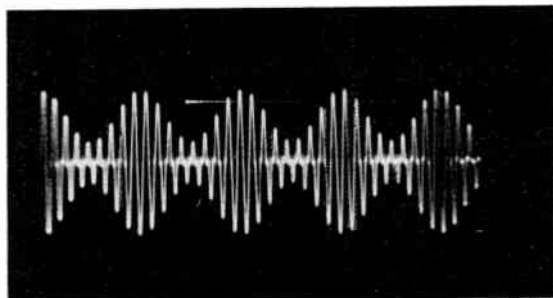


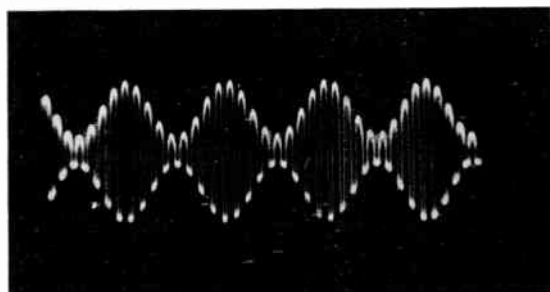
Fig. 2. Idealized piece-wise linear modulator circuits.

† Formerly at the Signals Research and Development Establishment.

‡ Signals Research and Development Establishment, Ministry of Technology, Christchurch, Hants.



(a) The output waveform of the circuit shown in Fig. 2(b).



(b) The output waveform of the circuit shown in Fig. 4.

Fig. 3.

diode characteristic, while in the case of the transistor circuit described below the distortion takes place at the waveform peaks. (Fig. 3(b).)

Figure 4 shows the modulator in its basic form and indicates its action. The emitters of TR1 and TR2 are maintained at a potential dependent on V_1 and V_2 respectively. As the collector and emitter of TR3 must also be maintained at these potentials its working range is limited to voltage swings not exceeding these limits. If TR3 is operated between cut-off and saturation by a high-frequency signal applied to its base it will act as a simple switch across TR2. Therefore if V_1 has superimposed upon it a modulating signal, and V_2 the same signal 180° out of phase, then the range over which TR3 can switch, and thus the excursions of the waveform at its emitter, is controlled by the modulating signal, leading to a completely symmetrical modulated carrier on R1. There is no component of the modulating signal present although the properties of the circuit are aperiodic.

If TR3 base is maintained at a quiescent potential of V_3 , approximately midway between V_1 and V_2 , TR3 will function as a symmetrical switch and the peak-to-peak swing of the carrier required to perform the action will be at a minimum. The modulated output is thus simply of the form (see Appendix 1):

$$y = (V_3 + v \sin \omega t) \sin pt,$$

plus harmonics of carrier.

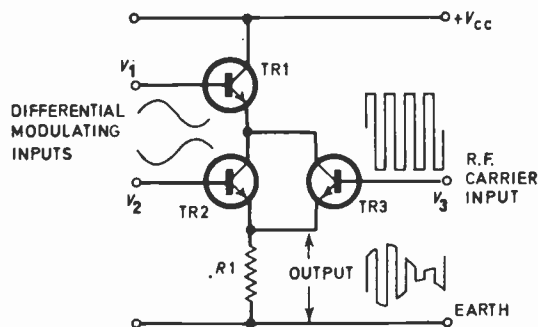


Fig. 4. The basic modulator.

3.2. Practical Details

To ensure a satisfactory switching behaviour for TR3, the carrier waveform excursions at its base will be in excess of the maximum signal displacement of V_1 and V_2 . In certain circumstances this large swing can lead to reverse voltage breakdowns of TR2 and TR3 emitter/base junctions during the positive and negative excursions respectively. In these cases the modulating waveform will no longer control the limits of the r.f. swing and peaks of carrier will occur beyond the envelope boundaries. To overcome this malfunction two emitter-base junctions are included in series with emitters of TR2 and TR3 to provide protection against such reverse breakdowns. (See final circuit in Fig. 11.) The net effect of the two diodes is merely to lower the level of the output by V_{be} .

The maximum depth of modulation at the peaks of the envelope is only limited by the applied signal amplitudes and the supply level, several hundred per cent being possible. At the envelope troughs the modulation depth is determined by the residual r.f. present. Complete 'punch out' is not achieved even when a phase splitter is employed which enables the modulating signals to overlap, due to the saturation voltage of TR3. Thus, because of tolerancing considerations, a residue of approximately 0.2 V dependent on temperature, is present. For a mean separation of 2.0 V between V_1 and V_2 this corresponds to a depth of modulation of 90%, which is not considered excessive in a repeatable practical circuit.

3.3. Modulator Input Level Requirements

The requirements are specified at a stabilized supply voltage of 10 V, this level being chosen to accommodate large variations in supply voltage. The typical signal inputs for 100% modulation at the output are as follows:

	d.c. (V)	a.c. (p.-p.) V
V_1 :	6.0 ± 0.25	1.5
V_2 :	4.5 ± 0.25	1.5
V_3 :	3.0 ± 0.50	3.0

4. The Microphone Amplifier

The amplifier consists of a four-transistor, three-stage, d.c.-coupled circuit having differential outputs. The source is low impedance and is fed to the base of the first transistor via a capacitor; the mean level is about 7 mV r.m.s. This defines an amplifier voltage gain for the levels quoted in Section 3.3 of approximately 75, this gain being maintained over the frequency range 300 to 3000 Hz. The requirements for an integrated circuit include temperature variations of from -40°C to $+70^{\circ}\text{C}$. The circuit is shown in Fig. 5.

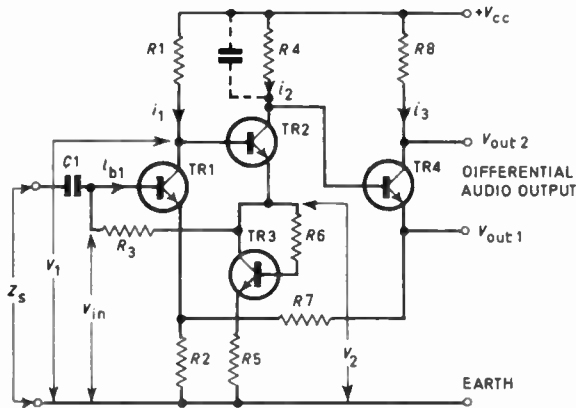
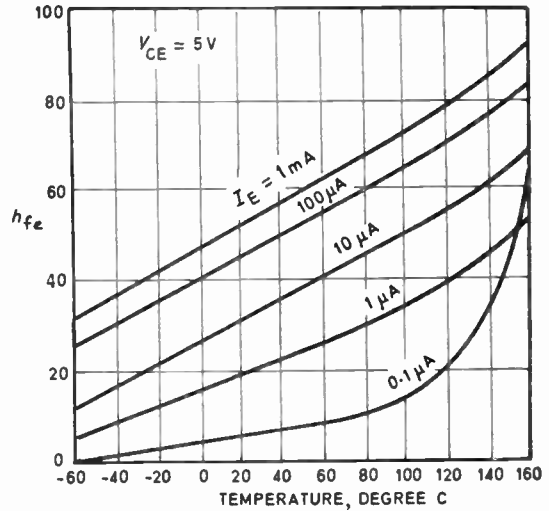


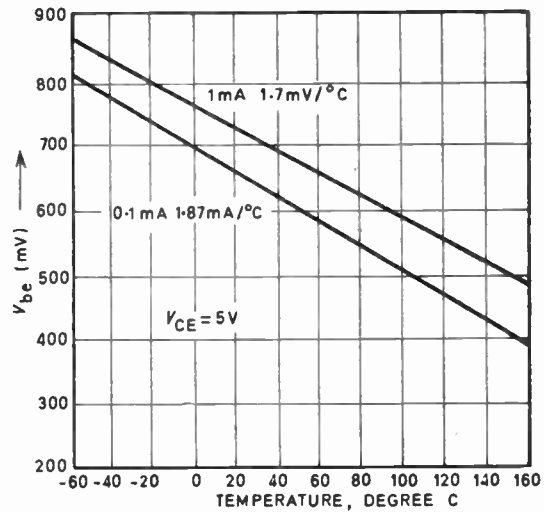
Fig. 5. The basic microphone amplifier.

4.1. The D.C. Condition

The d.c. behaviour of a directly-coupled transistor circuit is dependent upon the temperature characteristics of the components that constitute the circuit. In the case of the amplifier under consideration the transistors are of silicon integrated construction, their behaviour under changes in temperature being shown in Fig. 6. The variations in value of carbon resistors with temperature bear little relationship to those expected in an integrated circuit and the design objectives were to minimize the effect of resistor value variations whether due to temperature change or to tolerancing spreads. This was achieved by making use of the facility for accurate resistor ratioing available in s.i.c. technology by associating pairs of resistors of similar value but with opposing effects on the d.c. behaviour of the amplifier.



(a) D.c. gain against temperature.



(b) $V_{be(on)}$ against temperature.

Fig. 6. Temperature behaviour of the SL301 monolithic epitaxial transistor.

(These curves are reproduced from technical specifications by the Plessey Company, Swindon, Wiltshire.)

An analysis of the d.c. circuit conditions is included in the Appendix. Some approximations have been made in view of the fact that large spreads in the values of h_{fe} can be expected in s.i.c. form. The expression obtained for V_{out1} is:

$$V_{out1} = \frac{V_{cc} \left[\left(R_s - \frac{R_4 R_2}{R_1} \right) + \left(\frac{R_6}{h_{fe3}} - \frac{R_4 R_3}{R_1 h_{fe1}} \right) \right] - V_{be3} \left(R_s + \frac{R_6}{h_{fe3}} \right)^2}{R_s + \frac{R_6}{h_{fe3}} + \frac{R_2 R_4}{R_7}}$$

while that for V_{out2} (see Appendix 2) is:

$$V_{out2} = V_{cc} - V_{out1}, \text{ since } R_7 = R_8$$

The required differential outputs are at the levels detailed in Section 3.3 and by substituting the following values in the expression above the magnitude of the components R_5 and R_6 were calculated to give a variation of V_{out} within that specified:

$$\begin{aligned} V_{cc} &= 10 \text{ V}; h_{fe3} = h_{fe1} (15\%); \\ h_{fe3} &= 70 \text{ and } V_{be3} = 0.65 \text{ V}; \\ h_{fe3} &= 35 \text{ and } V_{be3} = 0.85 \text{ V}; \\ R_1 &= 10 \text{ k}\Omega; R_2 = 20 \text{ k}\Omega; \\ R_3 &= 2 \text{ k}\Omega; R_4 = 5 \text{ k}\Omega; \\ R_7 &= 2 \text{ k}\Omega; R_8 = 2 \text{ k}\Omega. \end{aligned}$$

Thus for $V_{out1} = 4 \pm 0.25 \text{ V}$, the value of R_5 and R_6 are 53.5 and 1130 Ω respectively.

Measurements on the lumped component circuit indicated that for a value of 1200 ohms for R_6 , the value of R_5 was very dependent on h_{fe1} and h_{fe3} in achieving the correct d.c. conditions. If the circuit associated with TR3 (Fig. 7) is considered:

$$R_{eq} = \frac{V_{be3}}{i_e} + \frac{R_6 + R_{b3}}{h_{fe3}} + R_5 + r_{e3}$$

assuming V_{be3} to be constant and letting

$$r_{e3} + R_5 + \frac{R_6 + r_{b3}}{h_{fe3}} = K$$

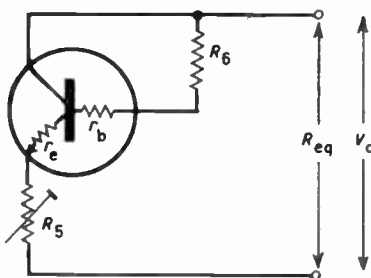


Fig. 7. Circuit associated with TR3.

The practical limits on this expression are:

$$K \ll \frac{R_6 + r_{b3}}{h_{fe3}} \text{ and } R_5 = K - r_{e3} \text{ when } h_{fe} \rightarrow \infty$$

Figure 8 shows the expression plotted as R_5 against h_{fe3} using a typical value for K of 1200 Ω . Over the acceptable range of h_{fe3} the curve is shown as a shallow slope indicating that only a small variation in the value of R_5 is required. Since this value is critical to the correct functioning of the modulator, this led to the conclusion that R_5 should be an external component to be adjusted under test conditions.

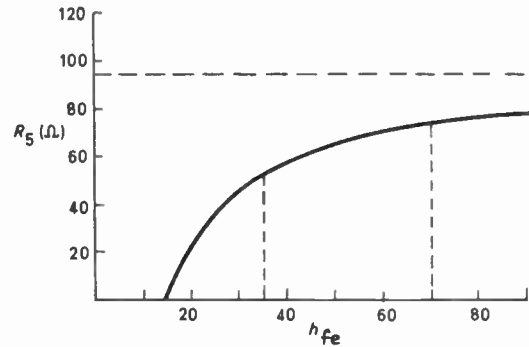


Fig. 8. Variation of preset resistor with d.c. gain.

In view of the analysis above, an attempt to maintain the relativity between outputs for up to a 50% variation in supply voltage would have involved complex modifications to the amplifier configuration. Thus it was considered that the simplest solution was to stabilize the supply voltage at 10 V using a series transistor regulator controlled by the sum of the Zener voltages of two further transistors. The variation of depth of modulation with no stabilizer is shown in Fig. 9.

4.2. Overall Gain

With the component values shown in Fig. 11, the closed loop gain of TR1 is approximately 7. The mean equivalent resistance of the stage TR3 is 125 Ω , leading to a stage gain of 40 for TR2. Thus the overall gain of the amplifier is 265. With the gain defining feedback loop R_7/R_2 incorporated, this drops to the required gain of 75 when the amplifier is employed with the microphone detailed below in Section 4.3. The full procedure used in computing the amplification is shown in Appendix 3.

4.3. Frequency Response

The frequency response of the electromagnetic microphone which had been specified for use with this modulator had been shown to have a rising characteristic of about 10 dB per octave for a constant sound

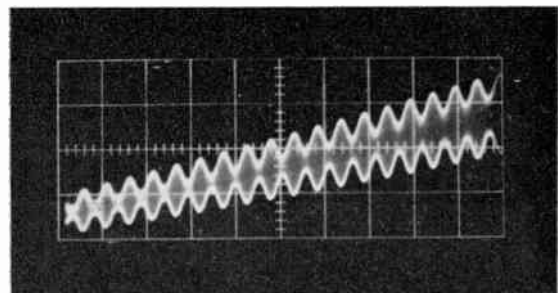


Fig. 9. Complete unstabilized modulator modulation level change with variation of supply voltage from 5–15 V. (2 V/cm).

pressure input. The output is rated at 10 mV and when used by the average talker, due to the 'falling characteristic' of speech, the output was reasonably flat within ± 3 dB over the frequency range 300 Hz to 4 kHz.³ To increase the 'roll-off' above 3 kHz and reduce the amplifier gain at high frequencies a capacitor is employed in shunt with R_4 . This capacitor is external to the integrated circuit.

For an insertion loss of less than 1.0 dB at 300 Hz the microphone coupling capacitor must exceed 0.5 μ F.

5. The R.F. Stage

The carrier input waveform is amplified to the required minimum swing of 3.0 V peak-to-peak for a modulation depth of 100% in the grounded base stage of Fig. 10. This circuit is d.c. stabilized against temperature variations by the emitter potential of TR1 being set by TR2 connected as a diode, the transistors being matched and sharing a common bias resistor, R_3 . Providing that the r.f. voltage excursions exceed those of the two modulating signals, the d.c. level is not critical. The grounded base configuration permits wideband operation in excess of 20 MHz despite the fairly large r.f. voltage swing required.

6. Performance of the Lumped Circuit Model

The performance of the modulator was measured in two ways, firstly by investigating the basic circuit suitably biased, the modulating and carrier signals being supplied externally, and secondly by testing the complete circuit shown in Fig. 11. The device is intended for a specific application in the mobile transmitter; as a general-purpose device the frequency

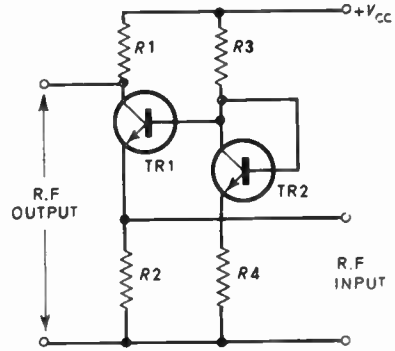


Fig. 10. The r.f. amplifier.

response of the audio amplifier would not be restricted as detailed.

6.1. The Modulator

The current consumption of the basic modulator shown in Fig. 4 at $V_{cc} = 10$ V is 1.7 mA excluding that of the biasing networks required. The circuit is independent of supply voltage variations and temperature changes and will operate satisfactorily at carrier frequencies of up to 20 MHz.

6.2. The Overall Circuit

The current consumption of the circuit of Fig. 11 is 13 mA at 10 V including about 1.0 mA in the stabilizer chain. The required minimum input levels are detailed in Section 4. Other parameters are detailed below:

- R.f. carrier upper frequency limit—20 MHz
- Audio amplifier input resistance—700 Ω

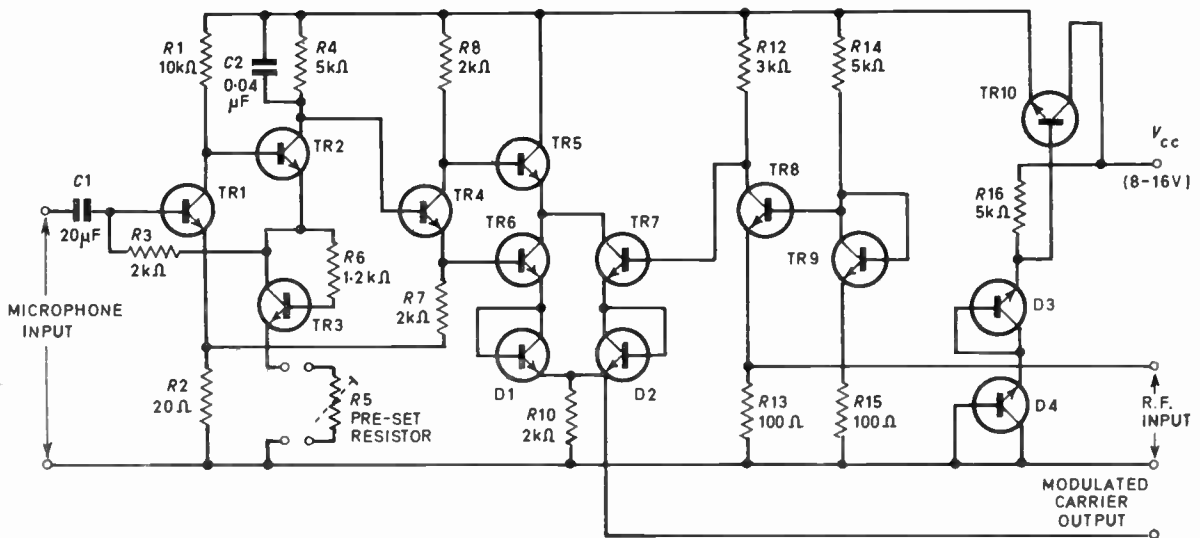
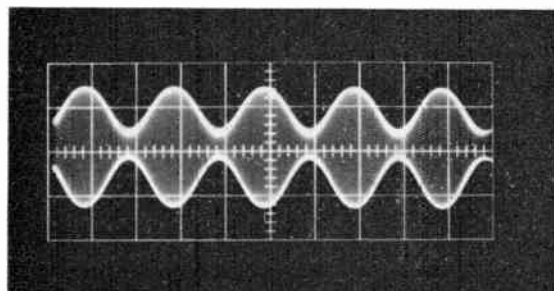


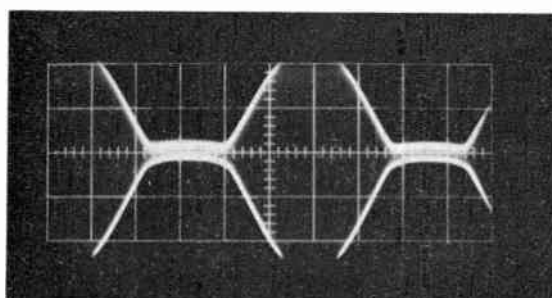
Fig. 11. Circuit diagram of complete modulator.

Carrier amplifier input impedance— 70Ω
 Modulator output impedance—approx. 50Ω

Output waveforms for different modulation levels and carrier frequencies are shown in Fig. 12.



(a) 10 MHz carrier, 75% modulation, 2 V/cm.



(b) 500 kHz carrier, over-modulated, 0.5 V/cm.

Fig. 12. Complete discrete circuit waveforms.

The temperature stability tests completed on the lumped circuit model indicated that there was no appreciable effect on the level or shape of the output waveform over the temperature cycle. The output was set for 50% depth of modulation at 23°C , the temperature being varied from $+80^\circ\text{C}$ to -27°C .

7. The Silicon Integrated Circuit

The stages in the preparation of a mask for the fabrication of an integrated circuit are generally well known and need not be described here. Figure 13 shows the composite mask prepared by the authors. There were no unusual features involved such as close tolerance transistors. The basic design aim involved is one of economy of space, every endeavour being made to reproduce the circuit layout in as conservative a manner as possible.

8. Conclusions

A new type of modulator has been described. Associated with suitable amplifiers, the design of which is

described, the device has been fabricated as a silicon integrated circuit.

The particular application of the device described in this paper is that of a modulator for a portable high-frequency transmitter; however it is also suitable for many general-purpose applications.

A voltage stabilizer is provided to accommodate large variations in supply voltage. The device has a thermal stability of the required standard for s.i.c.s. Although the carrier is present in the output, there is no audio component and this enhances the use of the circuit as a system element where it may often be convenient to locate the periodic portion of the circuit some distance from the modulator.

Finally, two such circuits supplied by anti-phase carrier signals may be used for suppressed carrier operation.

9. Acknowledgments

The authors wish to acknowledge the contribution made by the Plessey Company in the processing of the circuit using their Process I and their permission to reproduce Figs. 6 and 13.

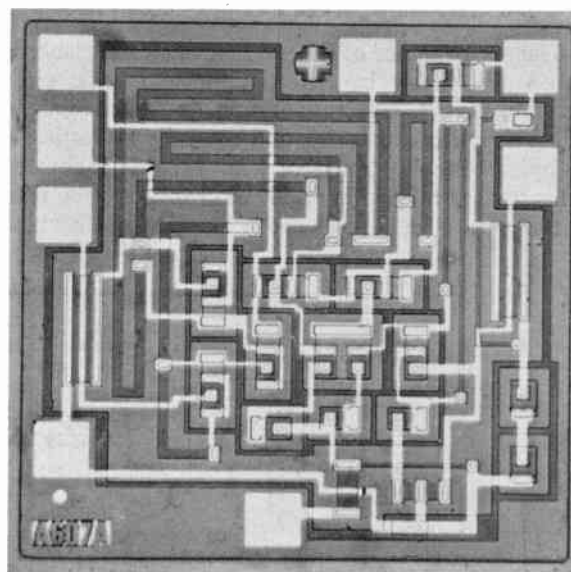


Fig. 13. The silicon integrated circuit—final mask ($\times 30$).

The authors are indebted to the Ministry of Technology for support and permission to publish this work.

The paper is reproduced with the permission of the Controller, Her Majesty's Stationery Office.

10. References

1. 'Improvements in or Relating to Transistor Modulator Circuits,' Provisional Patent Specification 1343/68, 9th January 1968.
2. Joyce, M. V. and Clarke, K. K., 'Transistor Circuit Analysis', (Addison-Wesley, Reading, Mass., 1961).
3. Butler, L. S., 'Real Voice Response of Electromagnetic and Carbon Microphones', Signals Research and Development Establishment, Ministry of Technology. Unpublished Report.
4. Jones, C. H. and Moore, D., 'The Development and Engineering of an Audio Amplifier and Modulator for Production in Silicon Integrated Circuit Form', Signals Research and Development Establishment, Ministry of Technology. Memorandum No. R7/67.

11. Appendix 1:

Fourier Analysis of Modulator Waveforms

An inspection of Fig. 14 indicates that the waveform involved in the action of the circuit may be resolved into a number of components. The inputs to the modulator consist of a limited carrier in the form of a

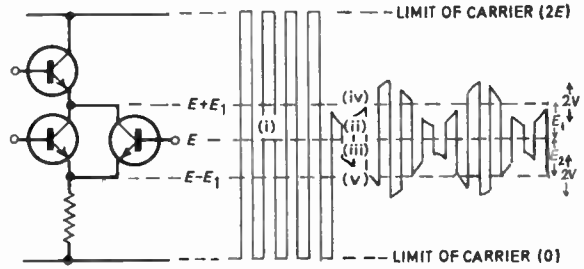


Fig. 14. Modulator waveforms.

square-wave and a mean d.c. level (i), an audio input and associated d.c. level (iv), and finally an anti-phase audio and d.c. (v). As one phase of the audio acts on one half-cycle of the carrier and the other phase on the other half-cycle, it is convenient in describing the action to treat the carrier as two separate waveforms (ii) and (iii). Hence the numbered waveforms shown in Fig. 14 may be described as follows:

- (i) $E + \frac{4E}{\pi} (\sin pt + \frac{1}{3} \sin 3pt + \dots)$ d.c. plus full carrier
- (ii) $(E + \frac{E_1}{2}) + \frac{2E_1}{\pi} (\sin pt + \frac{1}{3} \sin 3pt + \dots)$ upper half of carrier
- (iii) $(E - \frac{E_1}{2}) - \frac{2E_1}{\pi} (\sin (pt + \pi) + \frac{1}{3} \sin 3(pt + \pi) + \dots)$ lower half of carrier
- (iv) $(E + E_1) + v \sin \omega t$ audio
- (v) $(E - E_1) + v \sin (\omega t + \pi)$ audio phase shifted by π radians

The modulated output is defined by the expression:

$$\begin{aligned}
 & E + \left[\frac{2}{\pi} (\sin pt + \frac{1}{3} \sin 3pt + \dots) \{ (E + E_1) + v \sin \omega t \} + v \sin \omega t - \frac{2}{\pi} \left\{ \sin (pt + \pi) - \frac{1}{3} \sin 3(pt + \pi) + \dots \right\} \{ (E + E_1) + v \sin (\omega t + \pi) \} - v \sin (\omega t + \pi) \right] \\
 &= E + \left[(E + E_1) \frac{2}{\pi} \sin pt + \frac{1}{3} \sin 3pt + \dots + \frac{2}{\pi} v \sin \omega t \left(\sin pt + \frac{1}{3} \sin 3pt + \dots \right) + v \sin \omega t \right] - \left[(E - E_1) \frac{2}{\pi} \left\{ \sin (pt + \pi) + \frac{1}{3} \sin 3(pt + \pi) + \dots \right\} + \frac{2}{\pi} v \sin (\omega t + \pi) \left\{ \sin (pt + \pi) + \frac{1}{3} \sin 3(pt + \pi) + \dots \right\} - v \sin (\omega t + \pi) \right] \\
 &= E + \left[(E + E_1) \frac{2}{\pi} \left(\sin pt + \frac{1}{3} \sin 3pt + \dots \right) + \frac{2v}{\pi} \{ \cos (p - \omega)t - \cos (p + \omega)t + \text{harmonics} \} + v \sin \omega t \right] - \left[(E - E_1) \frac{2}{\pi} \left\{ \sin (pt + \pi) + \frac{1}{3} \sin 3(pt + \pi) + \dots \right\} - \frac{2v}{\pi} \{ \cos (p - \omega)t - \cos (p + \omega)t + \text{harmonics} \} - v \sin (\omega t + \pi) \right] \\
 &= E + \frac{4E_1}{\pi} (\sin pt + \frac{1}{3} \sin 3pt + \dots) + \frac{4v}{\pi} \{ \cos (p - \omega)t - \cos (p + \omega)t + \text{harmonics} \}
 \end{aligned}$$

The output components are thus d.c., carrier plus harmonics and sidebands plus harmonics; the audio component is absent.

12. Appendix 2:

D.C. Analysis of the Microphone Amplifier

The following analysis produces an approximate expression for the output levels in terms of the circuit resistors and relevant transistor parameters. These expressions indicate the sensitivity of the circuit to

the parameters of the transistor TR3. The method of reducing this is outlined in Section 4.1.

Consider the portion of the circuit shown in Fig. 5.

$$i_{b1} = \frac{V_2 - [V_{be1} + (i_1 + i_3)R_2]}{R_3}$$

$$i_1 = \left(\frac{V_2 - V_{be1} - i_1 R_2 - i_3 R_2}{R_3} \right) h_{fe1}$$

$$i_1 \left(1 + \frac{R_2}{R_3} h_{fe1} \right) = \frac{h_{fe1}}{R_3} (V_2 - V_{be1} - i_3 R_2)$$

Therefore,

$$i_1 = \frac{h_{fe1}(V_2 - V_{be1} - i_3 R_2)}{R_3 + R_2 h_{fe1}} \quad \text{but} \quad V_1 = V_{cc} - R_1 i_1$$

and

$$V_1 = V_{cc} - \left(\frac{R_1 h_{fe1}}{R_3 + R_2 h_{fe1}} \right) (V_2 - V_{be1} - i_3 R_2) \quad \text{also} \quad V_2 = V_1 - V_{be2}$$

$$V_2 = V_{cc} - \left(\frac{R_1 h_{fe1}}{R_3 + R_2 h_{fe1}} \right) \cdot (V_2 - V_{be1} - i_3 R_2) - V_{be2}$$

$$V_2 \left[1 + \frac{R_1 h_{fe1}}{R_3 + R_2 h_{fe1}} \right] = V_{cc} + \left(\frac{R_1 h_{fe1}}{R_3 + R_2 h_{fe1}} \right) (V_{be1} + i_3 R_2) - V_{be2}$$

But

$$V_2 = i_2 \left(R_5 + \frac{R_6}{h_{fe3}} \right) + V_{be3}$$

Therefore,

$$\left[i_2 \left(R_5 + \frac{R_6}{h_{fe3}} \right) + V_{be3} \right] \left(1 + \frac{R_1 h_{fe1}}{R_3 + R_2 h_{fe1}} \right) = V_{cc} + \left(\frac{R_1 h_{fe1}}{R_3 + R_2 h_{fe1}} \right) (V_{be1} + i_3 R_2) - V_{be2}$$

$$i_2 \left(R_5 + \frac{R_6}{h_{fe3}} \right) + V_{be3} + i_2 \left(R_5 + \frac{R_6}{h_{fe3}} \right) \left(\frac{R_1 h_{fe1}}{R_3 + R_2 h_{fe1}} \right) + \frac{R_1 h_{fe1} \cdot V_{be3}}{R_3 + R_2 h_{fe1}} = V_{cc} + \left(\frac{R_1 h_{fe1}}{R_3 + R_2 h_{fe1}} \right) (V_{be1} + i_3 R_2) - V_{be2}$$

But if

$$R_1 h_{fe1} \gg R_3 R_2 h_{fe1} \quad \text{and} \quad i_3 R_2 \gg (V_{be1} - V_{be3})$$

Then,

$$i_2 \left(R_5 + \frac{R_6}{h_{fe3}} \right) \left(\frac{R_1 h_{fe1}}{R_3 + R_2 h_{fe1}} \right) = V_{cc} - V_{be3} - V_{be2} + \frac{i_3 R_2 \cdot R_1 h_{fe1}}{R_3 + R_2 h_{fe1}}$$

Also,

$$V_{out1} = V_{cc} - i_2 R_4 - V_{be3}$$

Therefore,

$$V_{out1} = V_{cc} - R_4 \left[\frac{V_{cc} - V_{be3} - V_{be2} + \frac{i_3 R_1 R_2 h_{fe1}}{R_3 + R_2 h_{fe1}}}{R_1 h_{fe1} \left(R_5 + \frac{R_6}{h_{fe3}} \right) / (R_3 + R_2 h_{fe1})} \right] - V_{be3}$$

$$V_{out1} = V_{cc} - R_4 \left[\frac{(V_{cc} - V_{be3} - V_{be2})(R_3 + R_2 h_{fe1}) + i_3 R_2 R_1 h_{fe1}}{R_1 h_{fe1} \left(R_5 + \frac{R_6}{h_{fe3}} \right)} \right] - V_{be3}$$

But

$$i_3 \approx V_{out1} / R_7$$

Therefore,

$$V_{out1} \left[1 + R_4 R_2 / R_7 \left(R_5 + \frac{R_6}{h_{fe3}} \right) \right] = V_{cc} - R_4 \left[\frac{(V_{cc} - V_{be3} - V_{be2})(R_3 + R_2 h_{fe1})}{R_1 h_{fe1} \left(R_5 + \frac{R_6}{h_{fe3}} \right)} \right] - V_{be3}$$

$$V_{out1} \left[R_5 + \frac{R_6}{h_{fe3}} + \frac{R_4 R_2}{R_7} \right] = V_{cc} \left[R_5 + \frac{R_6}{h_{fe3}} \right] - R_4 \frac{(V_{cc} - V_{be3} - V_{be2})(R_3 + R_2 h_{fe1})}{R_1 h_{fe1}} - \left(R_5 + \frac{R_6}{h_{fe3}} \right) V_{be3}$$

$$V_{out1} \left[R_5 + \frac{R_6}{h_{fe3}} + \frac{R_4 R_2}{R_7} \right] = V_{cc} \left[R_5 + \frac{R_6}{h_{fe3}} - \frac{R_4 R_3}{R_1 h_{fe1}} - \frac{R_4 R_2}{R_1} \right] + \frac{(V_{be3} + V_{be2})(R_3 + R_2 h_{fe1})}{R_1 h_{fe1}} - \left(R_5 + \frac{R_6}{h_{fe3}} \right) V_{be3}$$

But it can be assumed that

$$R_5 + \frac{R_6}{h_{fe3}} \gg \frac{R_3 + R_2 h_{fe1}}{R_1 h_{fe1}}$$

Hence,

$$V_{out1} \left[R_5 + \frac{R_6}{h_{fe3}} + R_2 R_4 \right] \simeq V_{cc} \left[\left(R_5 - \frac{R_4 R_2}{R_1} \right) + \left(\frac{R_6}{h_{fe3}} - \frac{R_4 R_3}{R_1 h_{fe1}} \right) \right] - V_{be3} \left(R_5 + \frac{R_6}{h_{fe3}} \right)$$

Therefore,

$$V_{out1} \simeq \frac{V_{cc} \left[\left(R_5 - \frac{R_4 R_2}{R_1} \right) + \left(\frac{R_6}{h_{fe3}} - \frac{R_4 R_3}{R_1 h_{fe1}} \right) \right] - V_{be3} \left(R_5 + \frac{R_6}{h_{fe3}} \right)}{R_5 + \frac{R_6}{h_{fe3}} + \frac{R_2 R_4}{R_7}}$$

Also the d.c. level of the antiphase output from the collector of TR4 is:

$$V_{out2} \simeq V_{cc} - V_{out1} \quad \text{since} \quad R_7 = R_8$$

13. Appendix 3: Amplifier Overall Voltage Gain

For the signal conditions the circuit was driven from a low-impedance source $Z_s = (40 + j 300)$ ohms via the capacitor C_1 whose reactance was negligible within the pass-band. Within the circuit were several feedback loops which attempted to define the gain and interface impedances. The voltage gain of TR1 was controlled by the feedback path R_3 and Z_s , while the gain of TR2 was controlled by the resistor R_5 and the equivalent resistance of TR3. The overall gain was determined by the series feedback path R_7 and R_2 .

Consider the stage TR1. The open-loop gain is

$$\frac{R_1}{R_2 + r_e}$$

hence the closed-loop gain is given by

$$\frac{\frac{R_1}{R_2 + r_e}}{1 + \left(\frac{R_1}{R_2 + r_e} \right) \left(\frac{Z_s}{Z_s + R_3} \right)}$$

Consider the equivalent resistance of TR3 in Fig. 7

Manuscript first received by the Institution on 14th January 1969 and in final form on 27th May 1969. (Paper No. 1277/CC53).

© The Institution of Electronic and Radio Engineers, 1969.

$$V_c \simeq V_{be3} + \frac{i_c(R_6 + r_b)}{h_{fe3}} + i_c(r_e + R_5)$$

$$\frac{V_c}{i_c} \simeq \frac{V_{be}}{i_c} + \frac{R_6 + r_b}{h_{fe3}} + r_e + R_5$$

Hence the equivalent a.c. resistance,

$$R_{eq} = \frac{R_6 + r_b}{h_{fe}} + r_e + R_5$$

Consider the stage gain of TR2 in Fig. 5.

The shunting effect of R_3 and Z_s on R_5 and TR3 can be neglected, hence the stage gain becomes:

$$\frac{R_4}{R_{eq} + r_e}$$

Thus the overall amplifier gain with the series feedback path R_7 open is the product of the gains of TR1 and TR2 above:

$$1 + \frac{\frac{R_1}{R_2 + r_e}}{\left(\frac{R_1}{R_2 + r_e} \right) \left(\frac{Z_s}{Z_s + R_3} \right)} \times \frac{R_4}{R_{eq} + r_e}$$

and inserting values this equals a gain of 265. The feedback loop R_7 is selected for the final required gain.

Contributors to this Issue



Professor D. P. Howson (M. 1961, F. 1969) graduated with honours at Bristol University in 1952 with a degree in special mathematics. He received his industrial training when working as a design engineer with Standard Telephones and Cables from 1952 to 1957. In 1958 he received his M.Sc. degree in information engineering from Birmingham University and

was then appointed a lecturer in the Department of Electrical and Electronic Engineering. In 1967 he was appointed Professor of Electrical Engineering at the University of Bradford and is at present Dean of the Board of Studies in Engineering.

Professor Howson has been the author of several technical papers in the *Journal* and of the book, 'Mathematics for Electrical Circuit Design'. He has also served on the Council of the Institution as the Chairman of the West Midland Section.



M. J. Beale joined the Physics and Engineering Laboratory (then known as the Dominion Physical Laboratory) in December 1957 as a Technical Trainee. After obtaining a credit pass in the New Zealand Certificate of Science in 1965, he was employed as a Technical Officer in the Physics and Engineering Laboratory. In May 1969, he resigned to take up teaching at the Wanganui High School.



A. R. Morman (S. 1961, G. 1968) joined the Electronic Design Section of the Physics and Engineering Laboratory (D.S.I.R., New Zealand) in 1963. Prior to that he was employed with the New Zealand Post Office.

Co-author of a number of Laboratory publications, Mr. Morman's chief interest is in electronic analogue-type instruments.

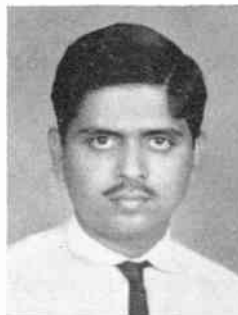
(A note on Mr. R. A. Morris, co-author with Messrs. Beale and Morman, appeared in the April 1969 issue.)



Dr. D. R. Wilson entered the Faculty of Technology, Manchester University (now UMIST) in 1957, after completing a six-year trade apprenticeship. He graduated in electrical engineering in 1960 specializing in control systems and obtained the M.Sc. degree by research in the following year. Subsequently, he was appointed to the staff of the electrical engineering department as a lecturer on control systems to graduate and post graduate courses. At this time he was concerned with the initiation of the first M.Sc. course in control systems that was offered by the college.

In 1965, Dr. Wilson joined A.E.I. Electronics Apparatus Division, now part of the G.E.C.-A.E.I. (Electronics), where he has been responsible for the servo design of a variety of antenna and military servo systems. He is shortly taking up a similar appointment with Plessey Radar.

Dr. Wilson has published fourteen technical papers and given numerous special lectures on servo control. He is also the editor of a manual entitled 'Modern Servo Design Practice', to be published early next year.



S. S. De, after obtaining his M.Sc. degree in physics in 1964, joined the Ionosphere Section of the Institute of Radio Physics and Electronics under the University of Calcutta as a research scholar. For the first two years, he was engaged in experimental work and since then has been working in the theoretical branches of the subject of scattering of radio waves in the ionosphere

in the presence of geomagnetic field and geomagnetic irregularities. He has also been concerned with different problems connecting wave propagation through the ionospheric plasma.



J. J. Sainsbury (G. 1966) was educated at Luton College of Technology. After serving three years in the R.A.F. as a ground radar technician Mr. Sainsbury first worked as a technician with G.E.C. and later with Texas Instruments.

In March 1961 he joined Fords (Finsbury) Ltd. where at present he is chief electronic engineer, responsible for design and development of new products. Mr. Sainsbury holds a number of patents in the instrumentation and control field.

Terminating Impedances in Diode Modulators and Mixers

By

Professor D. P. HOWSON,
D.Sc., C.Eng., F.I.E.E., F.I.E.R.E.†

Summary: Analysis of diode modulators and mixers is complicated by the need to examine the ratio of source to load impedance. In a number of circuits the optimum ratio is unity, and it is pointed out that a set of conditions can be developed, allowing this to be predicted in most cases before analysis.

Analysis of diode frequency changers, modulators and mixers by assuming the diode to be a periodically-varying resistance has been undertaken for at least thirty years.¹⁻⁴ It is always assumed in this work that the variation of diode resistance is completely controlled by a local oscillator current or voltage, any signal or modulation product currents or voltages affecting the diode being therefore very much smaller.

There are three fundamental types of circuits in common use, termed the series, shunt and ring modulators. These are shown in Fig. 1. The series and shunt modulators are equivalent for the diode variation assumed, and additionally most forms of ring modulator also have a series or shunt modulator equivalent circuit. Analysis of these circuits when terminated in resistances is straightforward, but not when terminated at either or both ports by filter structures. In the latter cases it is necessary to assume idealized forms for the filters in order to obtain a solution. For example, a modulator having a load impedance parallel resonant at the output frequency can have the impedance specified as Z (or R) at the latter frequency, zero at all other modulation product frequencies. In a similar way, a series resonant circuit can be approximated by an impedance (or resistance) at the resonant frequency, and an infinite impedance at all other circuit frequencies. There are a large number of possible arrangements of input and output filters, and details of the analysis, minimum conversion loss, and optimum terminating impedances can be found elsewhere.^{5,6} It will be noted on inspection of these tabulated results—or those found later in this paper—that in a substantial number of cases the optimum source and load impedances are equal. It is the purpose of this paper to draw attention to the fact that this can often be established before undertaking the analysis, which considerably reduces the labour involved.

In h.f. and microwave frequency changers—usually called mixers⁷—the local oscillator frequency, ω_p , is chosen to be almost equal to the signal frequency, ω_q , so that the output at the intermediate frequency,

$(\omega_p - \omega_q)$, is at a relatively low frequency. In consequence, it is found that in most circuits of this type the image frequency, $(2\omega_p - \omega_q)$, is sufficiently close to the signal frequency to dissipate power in the input

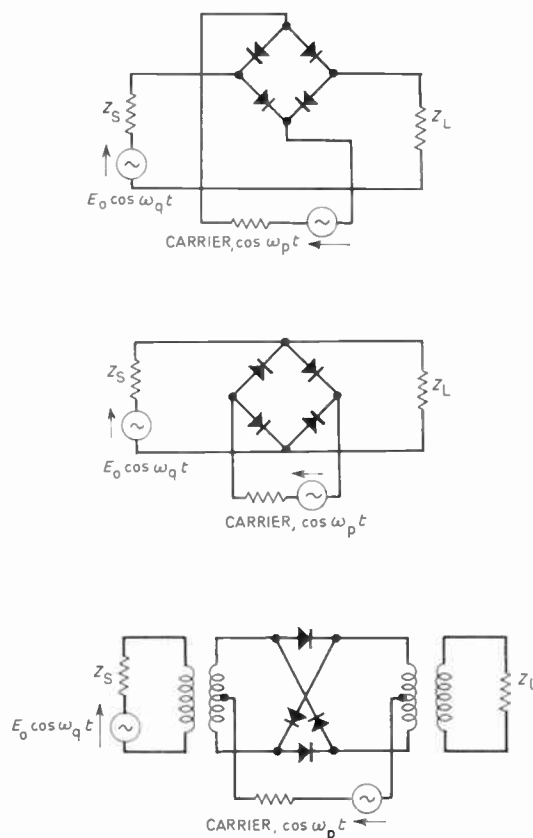


Fig. 1. Series, shunt, and ring modulators.

circuit. If equal currents at the two frequencies dissipate equal power in the input resistance the mixer is known as 'broad-band' mixer, otherwise it is termed a 'narrow-band' mixer.

The criterion to be suggested applies equally well to mixers or modulators. A general mixer or modulator circuit is given in Fig. 2, where the impedance Z

† Postgraduate School of Electrical and Electronic Engineering, University of Bradford.

represents the input and output impedances together with any other tuned circuits that may be added at other modulation product frequencies. $r(t)$ may be written quite generally as

$$r(t) = r_0 + 2 \sum_{n=1}^{\infty} r_n \cos(n\omega_p t + \theta_n) \quad \dots\dots(1)$$

since it varies periodically at the local oscillator frequency, ω_p . The current through the diode may be written

$$i(t) = \sum_{n=-\infty}^{\infty} i_n \cos(\omega_q + n\omega_p)t \quad \dots\dots(2)$$

where the i_n may be complex.

(The frequencies are written as $(\omega_q + n\omega_p)$, rather than $(n\omega_p + \omega_q)$ in order to facilitate analysis.^{3,8})

The mesh equation for the circuit is

$$E_0 \cos \omega_q t = [Z + r(t)]i \quad \dots\dots(3)$$

which may be separated out into components at all the modulation product frequencies,⁸ giving

$$\begin{bmatrix} \vdots \\ 0 \\ 0 \\ E_0 \\ 0 \\ 0 \\ \vdots \end{bmatrix} = \begin{bmatrix} \vdots & \vdots & \vdots & \vdots & \vdots & \vdots \\ \dots (Z_{-2} + r_0) & r_1(-) & r_2(-) & r_3(-) & r_4(-) & \dots \\ \dots r_1(+) & (Z_{-1} + r_0) & r_1(-) & r_2(-) & r_3(-) & \dots \\ \dots r_2(+) & r_1(+) & (Z_0 + r_0) & r_1(-) & r_2(-) & \dots \\ \dots r_3(+) & r_2(+) & r_1(+) & (Z_{+1} + r_0) & r_1(-) & \dots \\ \dots r_4(+) & r_3(+) & r_2(+) & r_1(+) & (Z_{+2} + r_0) & \dots \\ \vdots & \vdots & \vdots & \vdots & \vdots & \vdots \end{bmatrix} \begin{bmatrix} \vdots \\ i_{-2} \\ i_{-1} \\ i_0 \\ i_{+1} \\ i_{+2} \\ \vdots \end{bmatrix} \quad \dots\dots(4)$$

where $r_n \exp(\pm j\theta_n) = r_n(\pm)$

The rows and columns will be named from the centre of the matrix outwards, with reference to their associated modulation products.

The current at any modulation product frequency can be calculated as follows.

The current at a frequency $(\omega_p - \omega_q)$ is

$$\frac{i_{-1}}{E_0} = \frac{\Delta_{-1,0}}{\Delta} \quad \dots\dots(5)$$

where Δ is the circuit determinant in (4), and $\Delta_{-1,0}$ is the determinant formed by removing the (-1)th column and 0th row from Δ .

From this the conversion loss of the circuit can be calculated, for the appropriate input and output frequencies. Adopting the definition

conversion loss

$$= 10 \log_{10} \left[\frac{\text{available input power}}{\text{output power at output frequency}} \right] \quad \dots\dots(6)$$

in the case just examined,

$$\text{conversion loss} = 10 \log_{10} \left[4R_0 R_{-1} \left| \frac{\Delta_{-1,0}}{\Delta} \right|^2 \right]^{-1} \quad \dots\dots(7)$$

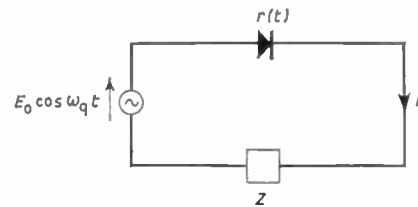


Fig. 2. General mixer circuit.

which can be generalized for an output frequency of $(\omega_q \pm m\omega_p)$ by substituting $\pm m$ for -1 in (7). The conversion loss is a minimum when the circuit is conjugately matched at the input and output ports, which leads to the results⁷ that

$$Z_0^* = Z_{11} - \frac{Z_{12}Z_{21}}{Z_{22} + Z_{\pm m}} \quad \dots\dots(8)$$

$$Z_{\pm m}^* = Z_{22} - \frac{Z_{12}Z_{21}}{Z_{11} + Z_0} \quad \dots\dots(9)$$

if the circuit equations (4) are written as

$$\begin{bmatrix} E_0 \\ 0 \end{bmatrix} = \begin{bmatrix} (Z_0 + Z_{11}) & Z_{12} \\ Z_{21} & (Z_{\pm m} + Z_{22}) \end{bmatrix} \begin{bmatrix} i_0 \\ i_{\pm m} \end{bmatrix} \quad \dots\dots(10)$$

by successively eliminating all other currents.

Now examine Fig. 3(a), which gives an equivalent circuit for the modulator, representing the time-varying resistance by a 'black box', with all the terminations shown outside the box.

The object of this work, it will be recalled, is to establish under what conditions minimum loss occurs when the load and source resistances are equal. Accordingly, take $R_s = R_L$. If this does not imply that $R_0 = R_{\pm m}$ (the sign being decided by the actual

output frequency),† it will be seen later that minimum loss will occur with R_s not equal to R_L .

If $R_0 = R_{\pm m}$, the circuit must be examined further. Adjust the values of the terminating resistances, preserving the equalities mentioned above, until the source impedance is conjugately matched to the input impedance, i.e. $Z_s^* = Z_{in}$. Then if $Z_L^* = Z_{out}$ in addition, the minimum loss condition has been achieved whilst $R_s = R_L$. This will be so if the circuit configuration appears the same in every respect when looking into the input and output ports, ignoring the difference in frequency of the signals present at the two ports. This is because the equation for Z_{out} will then be of exactly the same form as that for Z_{in} . Note that it is not possible to adjust Z_L separately to ensure that $Z_L^* = Z_{out}$, since this will upset the previous equality, $Z_s^* = Z_{in}$, as Z_{in} is a function of Z_L .

In order to examine the circuit configuration relative to the input and output ports it is convenient to consider each in turn as the input. The notation for the input and output frequencies may be formally interchanged, and the circuit equations and equivalent circuit rearranged in accordance with the new notation. If the result is an identical circuit matrix and equivalent circuit, the required condition will have been demonstrated. The currents present in the circuit are transposed from the original to the new notation as shown below

$$\begin{matrix} i_{\mp n} & \dots & i_0 & \dots & i_{\pm m} & \dots & i_{\pm(m+n)} & \dots \\ \downarrow & & \downarrow & & \downarrow & & \downarrow & \\ i_{\pm(m+n)} & \dots & i_{\pm m} & \dots & i_0 & \dots & i_{\mp n} & \dots \end{matrix} \dots(11)$$

and the notations for the terminating impedances are transformed in the same manner. The equivalent circuit transforms to the form shown in Fig. 3(b).

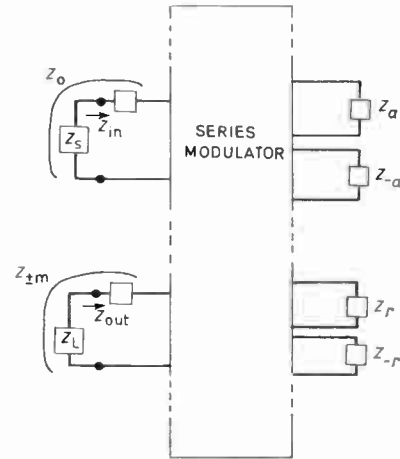
Inspection of the old and the new circuit matrices will immediately show if these are identical or not, and if identity is established this is equivalent to symmetry in the original matrix. An examination of the basic circuit matrix shows that symmetry will not, in general, be achieved unless

$$r_n(+) = r_n(-), \quad n > 0 \quad \dots(12)$$

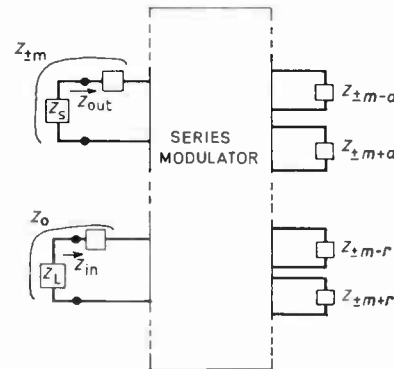
However, for the special case when only two currents

† R_s, R_L are the actual source and load resistances. Currents at many frequencies may flow through one or both of these. R_0 and $R_{\pm m}$, on the other hand, are the total resistances external to the diode through which currents at ω_q and $\omega_q \pm m\omega_p$ pass. As an example of a circuit in which $R_s = R_L$ does not imply $R_0 = R_{\pm m}$, consider the penultimate circuit described in Table 1, where the source impedance is R_s at all frequencies, and the load impedance is R_L except at ω_q where it is zero. Then if $R_s = R_L$, $R_0 = R_s$ and $R_{\pm m} = R_s + R_L \neq R_0$. Other resistances in the circuit matrix besides R_0 and $R_{\pm m}$ may be functions of R_s and/or R_L .

are present in the circuit, it can be seen from (8) and (9), in conjunction with (4), that no higher-order resistance coefficients than $r_1(+)$ and $r_1(-)$ occur. Moreover, Z_{12} and Z_{21} only occur in the form $Z_{12}Z_{21}$, and the product $r_1(+)r_1(-)$ is real and independent of the value of the phase angle θ . The restriction noted in (12) therefore will not apply in this case.



(a) viewed from input port



(b) viewed from output port.

Fig. 3. Equivalent circuit of series modulator ($a, r > 0$)

Having satisfied (12) where it may be applied, and assuming that a symmetrical set of modulation-product currents is present in the circuit, all that is left to compare in order to establish symmetry are the values of terminating impedances at the various frequencies present. From (11) the terminating impedances must, for symmetry, be equated as shown below

$$Z_{\mp n} = Z_{\pm(m+n)}, \quad m > 0, \quad \text{all } n > 0 \quad \dots(13)$$

where either the negative or positive sign is taken in a particular case, depending on whether the output frequency is respectively $(\omega_q + m\omega_p)$ or $(\omega_q - m\omega_p)$.

To summarize the results, therefore, minimum conversion loss will be achieved for equal source and load resistances if

- (a) for circuits in which currents at more than two frequencies flow, the time-varying resistance is (or can be made by a change of time origin), an even function of time,

and

- (b) equal source and load resistances imply equal terminating resistances at signal and output frequencies—see previous footnote.

and

- (c) the terminating impedance at a frequency of $(\omega_q \mp n\omega_p)$ is equal to the terminating impedance at a frequency of $\{\omega_q \pm (m+n)\omega_p\}$, for all non-negative values of n . The sign is negative when the output frequency is $(\omega_q + m\omega_p)$ and positive for $(\omega_q - m\omega_p)$, where m can be any positive number.

Take, as an example, the series modulator terminated in constant source and load resistances, R_S and R_L . The terminating resistances at signal and output frequencies, R_0 and $R_{\pm m}$, are given by $R_0 = R_m = R_S + R_L$, so that (b) is true. Similarly, $Z_{\pm n} = R_{\pm n} = R_S + R_L$, and the same is true for $Z_{\pm(m+n)}$, so that (c) is satisfied. Therefore we conclude that if (a) is satisfied this modulator will have minimum loss for $R_S = R_L$.

The results will also apply to all shunt modulator and mixer circuits, if voltage, conductance and admittance are substituted for current, resistance and impedance respectively. Table 1 shows the agreement between the second and third criteria established

above and the calculated results for a number of series modulators for which condition (a) holds. There are few data available in the literature on circuits for which (a) does not hold.

There are series and shunt equivalent circuits for the ring modulator⁵ from which corresponding deductions can be drawn. The equivalent circuits are only valid if the carrier waveform driving the diodes in the ring modulator contains only odd harmonics.⁸ With this restriction the input loop of the ring modulator contains only even-order modulation products, and the other external loop only odd-order

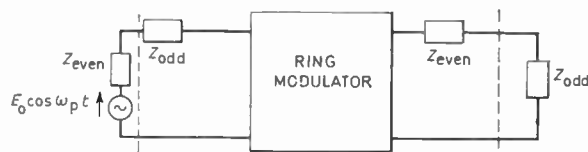


Fig. 4. Ring equivalent of series modulator.

products. Normally, the output will be taken at an odd-order product, usually either at a frequency of $(\omega_p - \omega_q)$ or $(\omega_p + \omega_q)$. However, the second-order ring modulator^{9,10} has some advantages, and in this the output is taken at a frequency of $(2\omega_p - \omega_q)$ from the same loop as the input. Figure 4 shows the ring modulator equivalent of a series modulator where the Z_{even} are the terminating impedances of the ring modulator at the input terminals, and the Z_{odd} terminating impedances at the other—usually the output terminals. The 'black box' represents the switched diodes of the ring modulator, here assumed time-varying resistances. From this equivalence the results

Table 1. Series modulators and mixers

Source termination	Load termination	Conditions satisfied (b)	Conditions satisfied (c)	Calculated terminations for minimum loss	Comments
R_s	R_L	yes	yes	$R_s = R_L$	
R_s at ω_q , 0 at $(\omega_q \pm m\omega_p)$	R_L at $(\omega_q \pm m\omega_p)$, 0 at ω_q	yes	yes	$R_s = R_L$	
R_s , except 0 at $(\omega_q \pm m\omega_p)$	R_L at $(\omega_q \pm m\omega_p)$, 0 elsewhere	yes	yes	$R_s = R_L$	
R_s at ω_q , 0 elsewhere	R_L , except 0 at ω_q	yes	yes	$R_s = R_L$	
R_s at ω_q , $(2\omega_p - \omega_q)$, 0 elsewhere	R_L at $(\omega_p - \omega_q)$, $(\omega_p + \omega_q)$, 0 elsewhere	yes	yes	$R_s = R_L$	
R_s at ω_q , $(2\omega_p - \omega_q)$, 0 elsewhere	R_L at $(\omega_p - \omega_q)$, 0 elsewhere	yes	no	$R_s = R_L$	For $r_2 = 0$ only, see note
R_s at ω_q , 0 elsewhere	R_L at $(\omega_p - \omega_q)$, $(\omega_p + \omega_q)$, 0 elsewhere		no	$R_s \neq R_L$	
R_s	R_L at $(\omega_q \pm m\omega_p)$, 0 elsewhere	no	no	$R_s \neq R_L$	
R_s	0 at ω_q , R_L elsewhere	no	no	$R_s \neq R_L$	
R_s at ω_q , ∞ at even products, 0 at odd products	R_L at $(\omega_q \pm m\omega_p)$, 0 elsewhere	yes	no	$R_s \neq R_L$	m odd

of Table 2 and Table 3 may be deduced, noting that the restriction on the carrier waveform and the

circuit symmetry ensures that condition (b) is automatically satisfied.

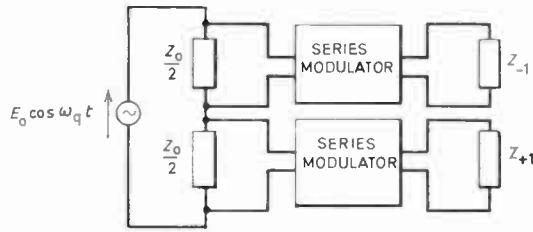


Fig. 5. Series modulator tuned to upper and lower sidebands, $r_2 = 0$.

Note. In Tables 1 and 2 it will be seen that there exist cases which do not satisfy the criteria but yet for which $R_s = R_L$ for minimum loss. These are all essentially the same circuits and so attention will be concentrated on the series modulator form of Table 1. Examination of the circuit matrix for this case when $r_2 = 0$ shows that it can be regarded as two simpler modulators paralleled at the input¹¹ as shown in Fig. 5. Each of these modulators satisfies the criteria, so that it is understandable that the same should be

Table 2. Ring modulators and mixers

Source termination	Load termination	Condition satisfied (c)	Calculated terminations for minimum loss	Comments
R_s at ω_q , any value elsewhere	R_L	yes	$R_s = R_L$	The same results apply to circuits with input tuned to ω_q , output to both upper and lower sidebands, $(\omega_p + \omega_q)$ and $(\omega_p - \omega_q)$
R_s at ω_q , ∞ elsewhere	R_L at $(\omega_q \pm m\omega_p)$ †, ∞ elsewhere	yes	$R_s = R_L$	
R_s at ω_q , 0 elsewhere	R_L at $(\omega_q \pm m\omega_p)$ †, 0 elsewhere	yes	$R_s = R_L$	
R_s at ω_q , ∞ elsewhere	R_L at $(\omega_q \pm m\omega_p)$ †, 0 elsewhere	no	$R_s \neq R_L$	
R_s at ω_q , 0 elsewhere	R_L at $(\omega_q \pm m\omega_p)$ †, ∞ elsewhere	no	$R_s \neq R_L$	
R_s at ω_q , $(2\omega_p - \omega_q)$, 0 elsewhere	R_L at $(\omega_p - \omega_q)$, 0 elsewhere	no	$R_s = R_L$ ‡	
R_s at ω_q , $(2\omega_p - \omega_q)$, 0 elsewhere	R_L at $(\omega_p - \omega_q)$, ∞ elsewhere	no	$R_s \neq R_L$	
R_s at ω_q , $(2\omega_p - \omega_q)$, ∞ elsewhere	R_L at $(\omega_p - \omega_q)$, ∞ elsewhere	no	$R_s = R_L$ ‡	
R_s at ω_q , $(2\omega_p - \omega_q)$, 0 elsewhere	R_L at $(\omega_p - \omega_q)$, 0 elsewhere	no	$R_s \neq R_L$	

† m odd. ‡ For $r_2 = 0$, see note.

Table 3. Second-order ring modulators and mixers

Termination at input port	Termination at idler port	Condition satisfied (c)	Calculated terminations for minimum loss	Comments
R_s at ω_q , R_L at $(2\omega_p - \omega_q)$, ∞ elsewhere	Z at $(\omega_p - \omega_q)$, 0 elsewhere	yes	$R_s = R_L$	also with parallel and series tuning interchanged
R_s at ω_q , R_L at $(2\omega_p - \omega_q)$, 0 elsewhere	Z at $(\omega_p - \omega_q)$, 0 elsewhere	yes	$R_s = R_L$	also with series in place of parallel tuning
R_s at ω_q , R_L at $(2\omega_p - \omega_q)$, ∞ elsewhere	Z at $(\omega_p + \omega_q)$, 0 elsewhere	no	$R_s \neq R_L$	three other forms exist—see above
R_s at ω_q , R_L at $(2\omega_p - \omega_q)$, ∞ elsewhere	Z at $(\omega_p - \omega_q)$, $(\omega_p + \omega_q)$, 0 elsewhere	no	$R_s \neq R_L$	see above
R_s at ω_q , $(4\omega_p - \omega_q)$, R_L at $(2\omega_p - \omega_q)$, ∞ elsewhere	Z at $(\omega_p - \omega_q)$, 0 elsewhere	no	$R_s \neq R_L$	see above
R_s at ω_q , $(4\omega_p - \omega_q)$, R_L at $(2\omega_p - \omega_q)$, ∞ elsewhere	Z at $(\omega_p - \omega_q)$, $(3\omega_p - \omega_q)$, 0 elsewhere	no	$R_s \neq R_L$	see above

true for the combination. There are corresponding forms for the ring modulator equivalent circuits of this type discussed in Table 2 when $r(t)$ contains even harmonics.

References

1. Peterson, E. and Hussey, L. W., 'Equivalent modulator circuits', *Bell Syst. Tech. J.*, **18**, p. 32, 1939.
2. Kruse, S., 'Theory of rectifier modulators', *Ericsson Technics*, **2**, p. 17, 1939.
3. Stieltjes, F. H., 'Application of complex functions to frequency-transposing systems', *Tijdschr. Ned. Radiogenoot.*, **11**, p. 221, 1946.
4. Belevitch, V., 'Théorie des Circuits Non-linéaires en Régime Alternatif' (Louvain University Press, 1959).
5. Van der Graaf, J., Unpublished report. Netherlands Post & Telecommunications Service.

6. Howson, D. P. and Tucker, D. G., 'Rectifier modulators with frequency-selective terminations', *Proc. Instn Elect. Engrs*, **107B**, p. 261, 1960.
7. Torrey, H. C. and Whitmer, C. A., 'Crystal Rectifiers' (McGraw Hill, New York, 1948).
8. Tucker, D. G., 'Circuits with Periodically-varying Parameters' (Macdonald, London, 1964).
9. Tucker, D. G., 'Zero-loss second-order ring modulator', *Electronics Letters*, **1**, p. 245, 1965.
10. Tucker, D. G., 'The second-order ring modulator', *Proc. Instn Elect. Engrs*, **113**, p. 1459, 1966.
11. Howson, D. P., '... Parametric amplifiers with above-pump amplification', Proc. 3rd Microwave Colloquium, Budapest 1966.

Manuscript first received by the Institution on 23rd January 1969 and in final form on 23rd June 1969. Short Contribution No. 122/CC54.

© The Institution of Electronic and Radio Engineers, 1969

STANDARD FREQUENCY TRANSMISSIONS—August 1969

(Communication from the National Physical Laboratory)

August 1969	Deviation from nominal frequency in parts in 10 ¹¹ (24-hour mean centred on 0300 UT)			Relative phase readings in microseconds N.P.L.—Station (Readings at 1500 UT)		August 1969	Deviation from nominal frequency in parts in 10 ¹¹ (24-hour mean centred on 0300 UT)			Relative phase readings in microseconds N.P.L.—Station (Readings at 1500 UT)	
	GBR 16 kHz	MSF 60 kHz	Droitwich 200 kHz	*GBR 16 kHz	†MSF 60 kHz		GBR 16 kHz	MSF 60 kHz	Droitwich 200 kHz	*GBR 16 kHz	†MSF 60 kHz
1	-300.1	0	+0.1	536	456.2	17	-300.1	-0.1	+0.1	545	467.1
2	-300.0	-0.1	+0.1	536	457.5	18	-300.1	-0.1	+0.1	546	467.6
3	-299.9	-	+0.1	535	-	19	-300.0	0	+0.1	546	467.6
4	-300.1	-0.1	+0.1	536	458.0	20	-300.1	-0.1	+0.1	547	468.6
5	-300.1	0	+0.1	537	458.3	21	-300.1	0	0	548	468.7
6	-300.0	0	+0.1	537	458.4	22	-300.0	-0.1	0	548	469.7
7	-300.1	-0.1	+0.1	538	458.9	23	-300.1	-0.1	0	549	471.1
8	-300.0	-0.1	+0.1	538	459.4	24	-300.2	-0.1	0	551	471.6
9	-299.7	-0.1	+0.1	535	460.5	25	-300.1	-0.1	0	552	472.3
10	-300.0	-0.1	+0.1	535	461.0	26	-300.1	-0.1	0	553	472.8
11	-300.1	-0.1	+0.1	536	461.7	27	-300.0	-0.1	0	553	473.9
12	-300.3	-0.1	+0.1	539	462.4	28	-300.0	-0.1	-	553	477.6
13	-300.0	-0.1	+0.1	539	463.2	29	-300.0	0	0	553	477.9
14	-300.3	-0.1	0	542	464.2	30	-300.1	0	+0.1	554	478.1
15	-300.0	-0.1	0	542	465.3	31	-300.0	0	+0.1	554	478.6
16	-300.2	-0.1	+0.1	544	465.9						

All measurements in terms of H.P. Caesium Standard No. 334, which agrees with the N.P.L. Caesium Standard to 1 part in 10¹¹.

* Relative to UTC Scale; (UTC_{NPL} - Station) = + 500 at 1500 UT 31st December 1968.

† Relative to AT Scale; (AT_{NPL} - Station) = + 468.6 at 1500 UT 31st December 1968.

A Multi-level Light Integrator

By

M. J. BEALE,†

A. R. MORMAN, (Graduate)†

AND

R. A. MORRIS, B.Sc.†

Presented at the Second New Zealand Electronics Conference (NELCON II) organized by the New Zealand Section of the I.E.R.E. and the New Zealand Electronics Institute and held in Auckland in August 1968.

Summary: An instrument which integrates the number of minutes during which average light intensity falls between or outside nine pre-set levels is described. The primary use of the equipment is in the study of the response of plants to light. The technique may have other applications.

1. Introduction

In studying the response of growing plants to light, it is necessary to know the amount of photosynthetically active radiation which they are receiving. Several light integrating instruments have been developed for this purpose,^{1, 2} and most of these are designed to give a linear integration of the amount of light received during a given interval.

There is, however, a school of thought which holds that plants have a non-linear response to light. The shape of the response curve can be obtained for various species of plants from a measurement of the carbon dioxide uptake at various light levels for a typical plant of the species at the appropriate stage of growth and growth condition. However, to predict the response of the plant under field conditions it is necessary to know, ideally, the times for which the plant was exposed to all intensity levels of interest. In practice, it is sufficient to measure the total time for which the light was between each of a series of defined levels. The response of the plant can be obtained by multiplying each reading by an appropriate factor derived from the response-curve of that plant.

The principles outlined above were first put forward by McCree,³ and this paper describes an instrument which is designed to obtain the information in a suitable form.

2. Circuit Operation

Referring to the simplified block diagram shown in Fig. 1, it will be seen that the light is detected by an Eppley detector; this is a multi-junction thermocouple which develops a voltage output proportional to the light intensity incident on it. The output voltage of the Eppley detector causes a current to flow through resistor R into the input of a Miller integrator. The voltage at the output of the integrator is therefore a measure of the integrated value of light intensity. The integrator output voltage is allowed to run up to a fixed limit; when it has reached this level, a comparator circuit operates a resetting system which

discharges the polystyrene dielectric integrator capacitor C and allows the charging cycle to recommence. The frequency with which the capacitor is reset is thus proportional to the Eppley detector voltage and hence to light intensity. This section of the circuit is incorporated in the analogue to digital converter of Fig. 2.

Each pulse from the light integrator is accumulated in a scale-of-100 electronic counter (Fig. 1). Once per minute the state of the count is interrogated and analysed into one of ten channels and the register attached to that channel increases its reading by one. To provide control over channel width, the lower limit of each channel may be set by a pair of channel-selector switches to lie anywhere between zero and 100 counts. When interrogation, analysis and registration are complete, the scale-of-100 is reset and accumulation of pulses from the light integrator continues.

3. Circuit Description

The detailed block diagram is shown in Fig. 2.

3.1 Analogue-to-Digital Converter

The analogue-to-digital converter has already been described in Section 2. It is a further development, using a microcircuit amplifier, of work described in outline by Morris and Robotham.²

3.2 Scale-of-100 Pulse Accumulator

The scale-of-100 is made up from two decade dividers each consisting of four J-K flip-flops, as outlined in Ref. 4. Thus, assuming the scale-of-100 to be reset to zero at the beginning of any minute, the average (integrated) value of light intensity over that minute may be deduced from an examination of the states of the flip-flops at the end of the minute, in conjunction with a truth table for the pulse accumulator (Fig. 3).

3.3 Level Recognition Circuitry

To provide ten channel level analysis, nine two-decade switches are provided to pre-select channel thresholds. The switches provide, in conjunction with associated circuitry, facilities for recording the number of minutes during the course of an experiment for

† Physics and Engineering Laboratory Department of Scientific and Industrial Research, Lower Hutt, New Zealand.

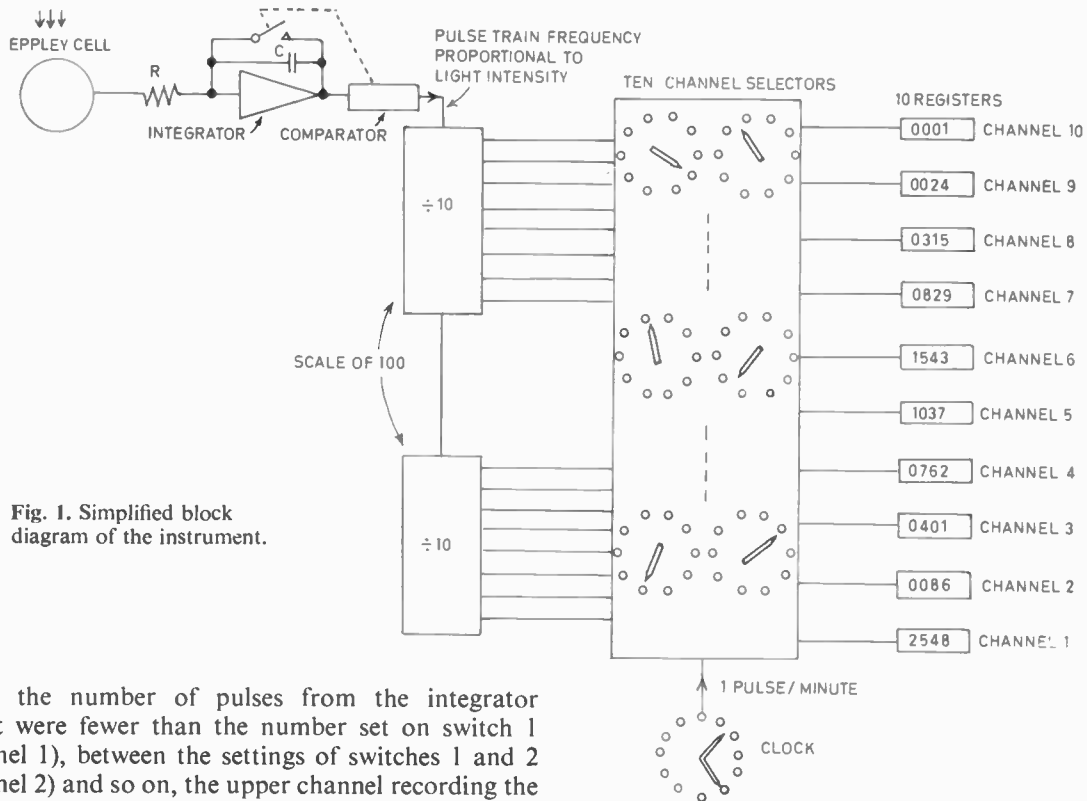


Fig. 1. Simplified block diagram of the instrument.

which the number of pulses from the integrator circuit were fewer than the number set on switch 1 (channel 1), between the settings of switches 1 and 2 (channel 2) and so on, the upper channel recording the number of minutes during which the number of pulses from the integrator circuit was greater than the number to which switch 9 is set (channel 10).

3.3.1 Operation of level recognition circuitry

Assume that the nine pairs of switches have been set as shown in Table 1. Each of the ten position

Table 1

Switch	Setting	Switch	Setting
1	08	6	75
2	17	7	82
3	32	8	88
4	45	9	94
5	63		

switches has four wafers. All the fixed contacts of the switches are wired according to the truth table for the scale-of-100 pulse accumulator (Fig. 3). Each switch wafer then corresponds to a vertical column of the truth table. With the fixed contacts of the switches all connected to the pulse accumulator outputs, and the movable contacts set to the positions specified in Table 1, all the eight wipers of, for example, switch set 1, will be at a logic '1' level when the state of the scale-of-100 is 08 counts, switch 2 when the count equals 17, and so on. Recognition of this condition is achieved in one of nine sets of eight input AND gates.

Therefore, as the pulse accumulator fills from zero to 99 counts, all nine channel selecting AND gates will recognize the state of count corresponding to their respective switch settings, beginning with level 1 and ending with level 9.

If in a given minute, light intensity is only sufficient to generate, for example, 56 pulses in the light integrator circuit, levels 1 to 4 inclusive will have been recognized, and levels 5 to 9 inclusive will not have been recognized. To determine where this discontinuity occurs, each AND gate output registration is stored in an R-S flip-flop initially reset at the beginning of the minute. Thus as the scaled count passes through a value set on a switch pair, the memory for that switch set has its state reversed. For the example cited above, flip-flops 1 to 4 inclusive will therefore be set to the '1' state, flip-flops 5 to 9 inclusive will remain at '0'.

3.4 Channel Analysis, Interrogation and Registration

By wiring the normal output of each flip-flop and the inverted output of the next higher-order flip-flop to two inputs of a three input AND gate and interrogating the third input at the end of every minute, an output pulse will appear only at the output of that AND gate for which the 'lower' flip-flop is '1' and the 'higher' flip-flop is '0'. As noted later, this pulse is used for registration.

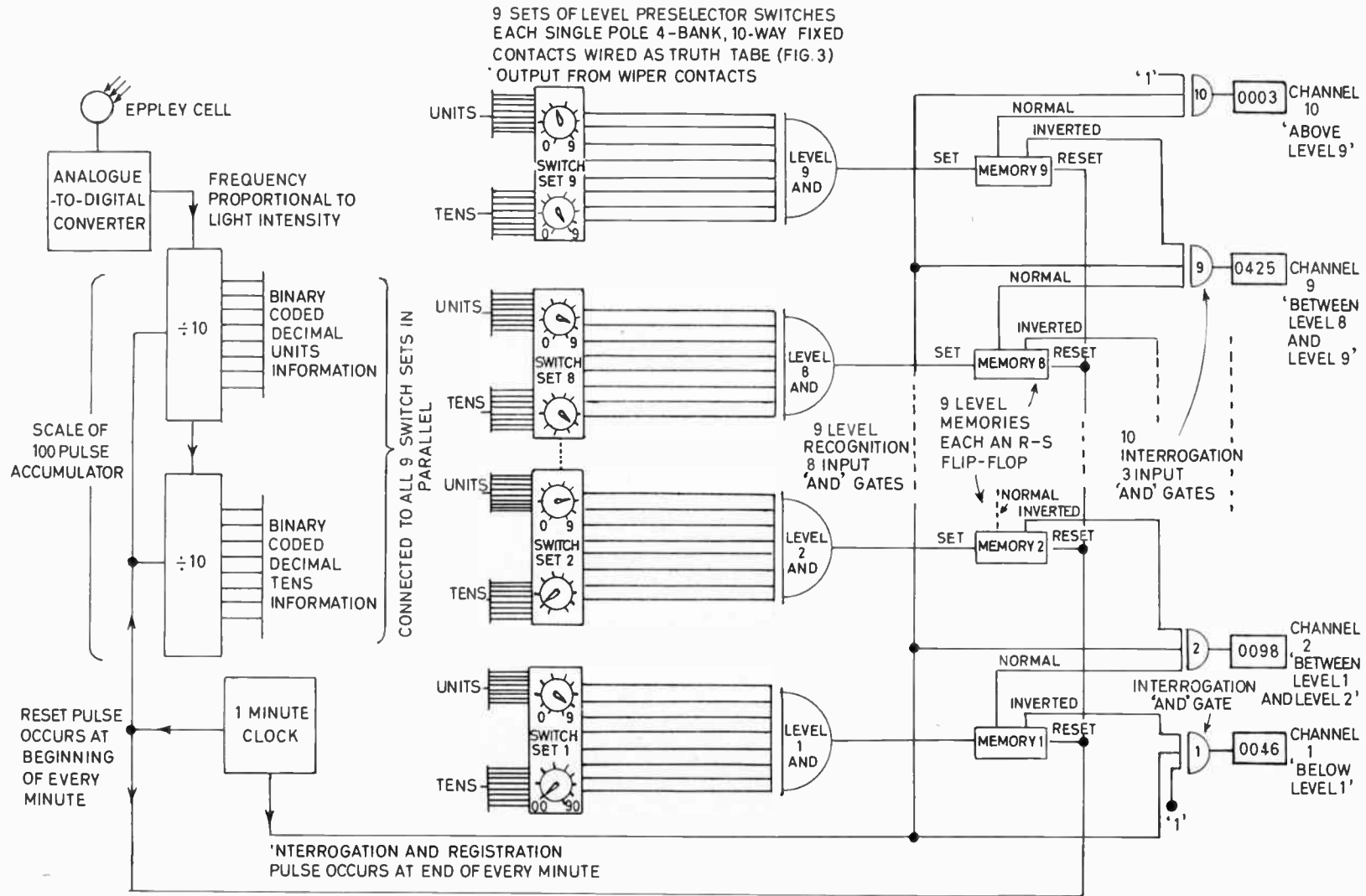


Fig. 2. Detailed block diagram.

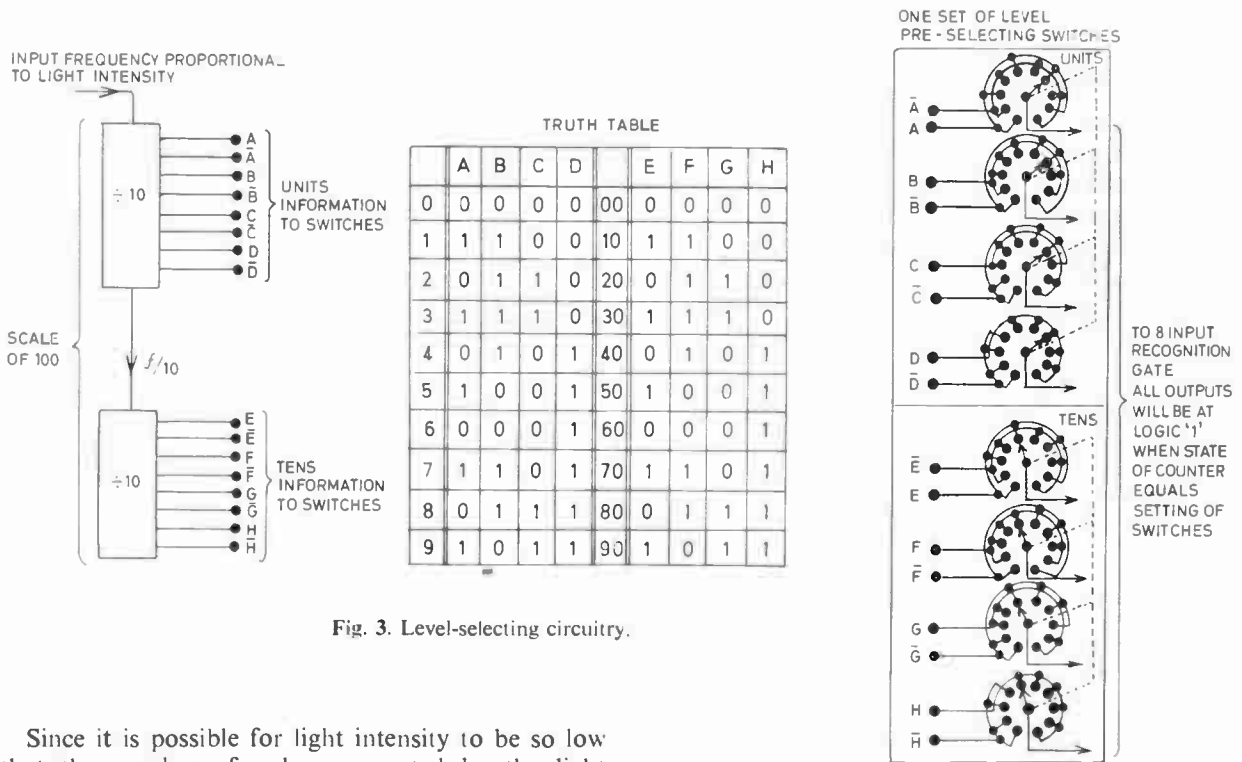


Fig. 3. Level-selecting circuitry.

Since it is possible for light intensity to be so low that the number of pulses generated by the light integrator is below the setting of switch set 1, level-sensing AND gate 1 is wired to sense the condition that pulses accumulated are between zero and (in the case cited for the setting of switch 1) 08. This is achieved by permanently wiring the 'lower' input of the AND gate to a '1' level. Thus, with the interrogation AND gate associated with channel 1 wired to the inverted output of the first flip-flop (logic '1' in reset state), channel 1 will be energized only if the number of pulses accumulated over a minute is less than the numerical setting of switch set 1.

Channel 10, similarly, has in this case its 'upper' interrogation AND gate 'enabling input' permanently wired 'open' so that when the count passes the setting of switch 9, channel 10 is energized, thus signifying that during that minute integrated light intensity was above the value corresponding to switch 9.

Outputs of AND gates for channel analysis and interrogation are amplified to drive the electro-mechanical registers used for read-out.

4. Conclusion

An instrument which integrates light intensity over a minute and analyses the average intensity into one of ten pre-selected channels has been described. The number of counts registered in each channel represents the total number of minutes during which average light intensity fell between the specified limits for each channel. The prototype instrument has been

operated by a plant physiologist for a year and has helped in the determination of plant-light relationships.

While the equipment described was developed for use in plant physiology studies, it is felt that the technique may be useful in the multi-level integration of any slowly-changing direct voltage of greater magnitude than about 1 mV. Detailed circuit diagrams and setting up notes may be found from Reference 5.

5. References

1. Allan, A. H. and McCree, K. J., 'Integrating meters for comparing light intensities in plant growth studies', *J. Sci. Instrum.*, **32**, pp. 422-424, November 1955.
2. Morris, R. A. and Robotham, R. W., 'Electronic light integrator', Paper presented at the 1st New Zealand Electronics Conference, Auckland, 1966.
3. McCree, K. J., 'Light measurements in plant growth investigations', *Nature*, **206**, No. 4983, pp. 527-528, 1st May 1965, and **210**, No. 5037, pp. 752-753, 14th May 1966.
4. Fairchild Application Bulletin No. APP 120.
5. Beale, M. J., Morman, A. R. and Morris, R. A., 'A Light Intensity Spectrometer', Physics and Engineering Laboratory Report D.S.I.R., New Zealand.

Manuscript first received by the Institution on 25th November 1968 and in final form on 7th March 1969. (Short Contribution No. 122/IC11)

© The Institution of Electronic and Radio Engineers, 1969

Digital Techniques in Load Cell Weighing

By

L. LENG,
B.Sc.Tech., C.Eng., M.I.E.E.†

Reprinted from the Proceedings of the Conference on 'Electronic Weighing' held in London on 30th-31st October 1968.

Summary: Typical load cell characteristics are listed and some factors concerning loading are given. An all-electronic system for digitizing the output of load cells directly is described, and details are given of some basic systems used to obtain control and information facilities from the digital weight-signals, with some fundamentals of the binary arithmetic used. Some weighing applications are mentioned and a computer-controlled weighing system is briefly described.

1. Introduction

Precision-grade load cells have brought load cell systems into the field of accurate weighing. The first occasion on which a load cell weigher was stamped by a 'Weights and Measures' inspector for unrestricted trade use was in November 1963, and since then many accurate load cell weighing systems have been installed. The basic instrumentation used is mainly of the analogue type with pointer indication of weight on a dial, and if digital signals are needed a digital transducer can be added.

With the greater involvement of weighing in so many fields of activity, needing considerable flexibility of the control and data processing functions which can be incorporated, there is an increasing requirement for accurate weighing systems involving signals in digital form and in which there is little need for dial indication of weight. For example, load cell weighing installations in which the weight information is presented solely in digital form have recently been given similar official approval for trade purposes.¹

This paper describes a basic instrumentation equipment which is essentially of digital type, and some systems into which it can be incorporated to give a wide range of load cell weighing facilities.

2. Load Cells

Since the design of the instrumentation is related to the load cells' characteristics it is pertinent to list here their main characteristics together with a brief note on relevant aspects of the loading of the cells.

2.1. Characteristics

For a precision grade strain gauge load cell the main characteristics affecting accuracy and instrumentation are typically as follows:

Output voltage (at rated load)	$1.750\text{mV} \pm 0.1\%$ per volt of excitation voltage.
Output resistance	$480 \pm 5 \Omega$.

† Technical Division, W. & T. Avery Ltd., Soho Foundry, Birmingham, 40.

Excitation voltage	20 V r.m.s.
Non-linearity (maximum)	0.15% of rated output.
Hysteresis (maximum)	0.03% of rated output.
Creep (maximum) at rated load	0.03% of rated output.
Repeatability (maximum)	$\pm 0.02\%$ of rated output.
Temperature effects over the range	-10°C to 45°C .
On zero balance	$\pm 0.0023\%$ per degC of rated output.
On calibration values	$\pm 0.0014\%$ per degC of rated output.

Non-linearity is defined² as the maximum deviation of the calibration curve from a straight line drawn between the no-load and rated load outputs, expressed as a percentage of the rated output and measured on increasing load only.

Hysteresis is defined² as the maximum difference between load cell output readings for the same applied load; one reading obtained by increasing the load from zero and the other by decreasing the load from rated load. It is measured at half rated output and expressed in percent of rated output.

2.2. Loading

In a load cell weighing installation the choice of the total rated capacity of the cells is made in relation to the total load comprising that of the weighing structure plus the rated capacity of the weighing installation, due allowance being made for any larger-than-normal overload capacity which may be needed because of the nature of the intended use of the weigher.

In general, the smaller the maximum load applied to a load cell in relation to its normal rated load the more accurate will be its performance; the errors due to creep, hysteresis, non-linearity and repeatability are generally reduced by factors greater than that by which the maximum loading of the cell is reduced below rated load; those due to internal temperature variation are reasonably constant for each cell within its rated load. Reduction of the maximum loading will also result in a smaller output voltage from each

load cell and so in choosing the cells and the extent of their loading in any installation the aim should be that when the cells' outputs are suitably combined satisfactory total voltage conditions are obtained in terms of accuracy, magnitude and immunity to the effects of strays and of noise, and that the effects due to temperature variation are acceptable.

In the detail of the manner in which the load is applied factors such as the minimizing of any side-thrust which may be applied to the cells are of great importance, and it must be emphasized that unless such details are properly engineered unsatisfactory weighing will result and no amount of expertise applied to the associated instrumentation can correct for it.

3. Instrumentation

The instrumentation basically provides the excitation supplies for the load cells, combines the weight-signals of the cells and processes the resulting signal to produce weight information.

One form of instrumentation³ comprises a precision potentiometric electromechanical servo which drives a pointer to indicate weight values on a dial. This form of instrumentation is not within the scope of this paper but is mentioned here because for some applications a digital transducer may be mechanically coupled to the servo to obtain an electrical output in digital form corresponding to weight and this output may be used for providing the basis for various control and information systems on the lines of those given in Section 3.2.

3.1. Digitizer

To produce weight information in digital form directly from the load cells' output without the need for an electromechanical servo an all-electronic equipment, developed specifically for use in weighing systems, may be used to digitize the load cells' output directly. This operates fundamentally in a manner similar to that of a digital voltmeter of the continuous balance type in that it comprises essentially a self-balancing digital servo system. The basic system of this equipment is shown in Fig. 1.

The load cells are excited with 180 Hz alternating current and their combined output, which could be typically some 12 mV at the rated load of the weighing installation, is first amplified to a level of 2 V. The input network to the amplifier includes resistances to produce two adjustable voltages in opposition to the weight-signal: one, for backing off the voltage due to the dead weight of the loading structure, is initially preset; the other in the form of a screwdriver-controlled potentiometer is used by the operator for day-to-day adjustment of the zero of the weighing installation and is known as the fine balance control. Also included in the input network are two sets of resistors each with a panel-mounted switch for disconnecting the weight-signal from the amplifier and injecting preset voltages corresponding to zero and full load respectively for test purposes.

The amplified a.c. weight-signal is applied to the demodulator which is of the synchronous switching type, the switching transistors being controlled by a

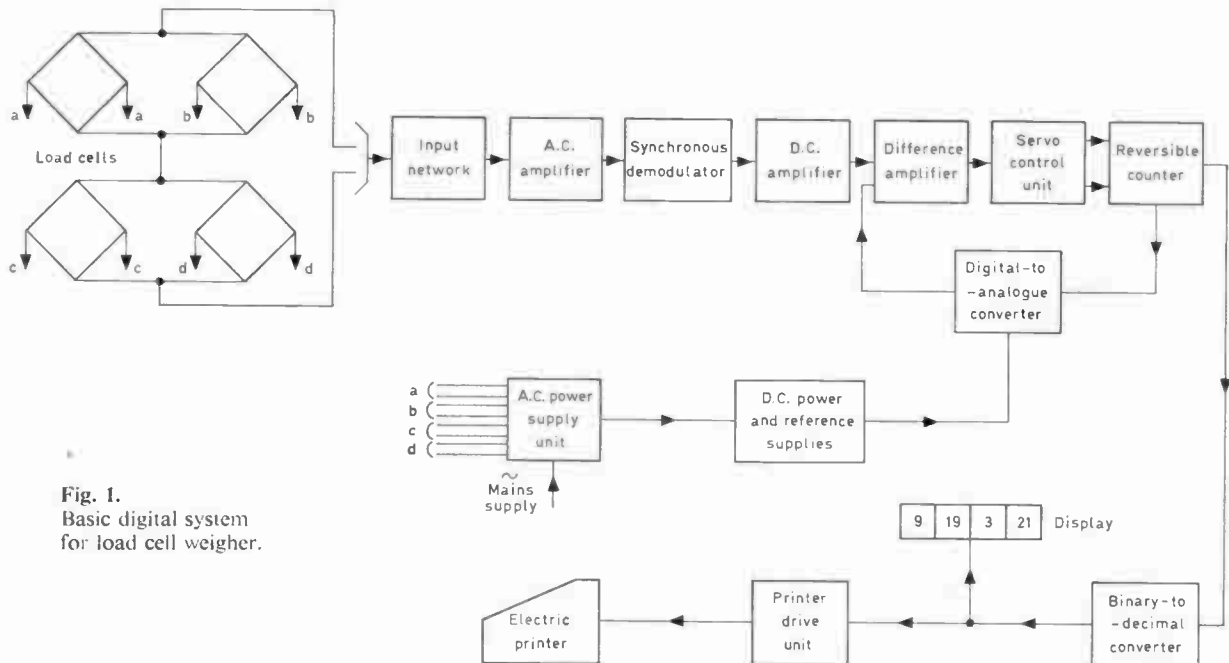


Fig. 1. Basic digital system for load cell weigher.

square-wave switching signal of the same frequency and phase as the a.c. weight-signal. The demodulator is followed by a low-pass L-C-R filter to remove the ripple component from its output. The filter has an adjustable time-constant which may be set to suit various conditions of site vibration in static weighing applications.

The resulting d.c. weight-signal is then amplified to a level of 6 V. An integrated circuit amplifier is used with a zero drift of typically $\pm 5 \mu\text{V}$ per degC referred to its input. The maximum d.c. output from the demodulator is normally 1.8 V so that the drift is negligible over a wide range of ambient temperature.

To effectively reduce by a considerable factor the deviation from linearity of the load cells' output a linearity correction circuit is incorporated in the instrumentation. This circuit processes an output from the d.c. signal amplifier to supply a four-segment correction characteristic to the input of the amplifier. The segments are adjusted by potentiometer setting during initial dead weight testing of the installation.

The d.c. weight-signal is now applied to the self-balancing digital servo in conjunction with a reference direct voltage. The reference voltage originates from the same power source as that of the load cells' excitation supply and is demodulated and amplified in a manner similar to that in which the a.c. weight-signal is processed. In the digital servo the signal voltage is applied to the difference amplifier the output of which is applied to the control unit. When the difference amplifier output exceeds a pre-set threshold level, trigger circuits in the control units are operated, causing pulses to be generated. These pulses drive a reversible counter in a direction determined by the polarity of the input to the control unit.

The reversible counter basically translates the pulse train from the control unit into a parallel binary representation. It comprises bi-stable transistor circuit elements arranged in suitable counting stages. The direction of count is determined by the states of diode resistor gates which are inserted between counting stages and their states are controlled by the control unit. The counter has steady electrical outputs in binary form which represent the state of the count at any instant, and these outputs are applied to the digital input of a digital-to-analogue converter, and are also taken as the output of the digitizer.

The digital-to-analogue converter consists basically of a number of transistors functioning as switches. Each switch is driven from one of the counter's inputs and connects one side of a precision resistor to the reference voltage line. Each of the counter's outputs can be either a definite voltage or zero, thus controlling each transistor switch to either the 'on' or 'off' condition. The other side of each resistor is connected

to a common output line so that a current flows into the output line from each resistor which is connected to the reference supply, and the value of each precision resistor is chosen so that the current flowing through it to the output is proportional to the weight value represented by the output counter switching it. Thus the analogue output of the converter is proportional not only to the numerical value of the digital input at any instant but also to the magnitude of the reference voltage.

The output voltage from the converter is applied to the input of the difference amplifier in such a way as to oppose the weight-signal voltage. When the difference between the two inputs to the difference amplifier is small enough to cause the output to fall below the preset threshold level the control unit will stop sending out pulses, and the reversible counter will stop. The digital servo will then be in balance and the outputs of the reversible counter will correspond to the weight-signal voltage in digital form. Each of the counters' outputs can be either a definite voltage or zero, representing the '1' and '0' conditions in a standard binary notation. They form the output of the digitizer, and by a suitable combination of transistor logic circuit elements, are generally converted to system of coding appropriate to the output business machinery.

Whenever the amplitude of the weight-signal voltage changes by an amount corresponding to more than one digital increment the reversible counter and the digital-to-analogue converter will be automatically caused to run in the appropriate direction to restore the balance. For every increment of weight-signal voltage there will be a corresponding balancing voltage from the digital-to-analogue converter and hence a corresponding digital output from the reversible counter.

Thus the d.c. weight-signal is digitized in terms of the reference voltage and by adjusting the system calibration the digital output from the reversible counter will in fact be in terms of weight in the units of any desired system of avoirdupois or metric, the provision for the weight-system units being made in the configuration of the digital-to-analogue converter and of the reversible counter.

A small centre-zero electrical meter is provided and is so connected into the control unit of the servo that when the weighing system is properly set up its pointer swings equally in either direction before the digital indication changes in response to appropriate changes in weight on the load cells. This facility is useful for testing and commissioning and it also enables the weighing system to be set precisely to zero by means of the fine balance control provided for the operator's use. In weighing terms the operational adjustment to zero of the weight-indicating system when the weigher

is unloaded is known as 'balancing', and is usually restricted in extent to a very small proportion of the total capacity of the weigher.

The reversible counter is driven at a uniform pulse rate of about 50 kHz when the digital servo is running, and so it takes nominally 80 ms to run from zero to 4000 increments. The time taken to respond to a weight change may be varied to suit site-conditions by changing the time-constant of the filter at the demodulator output.

The performance of the equipment is such that when forming part of a weighing system using precision grade load cells the maximum displayed weighing error corresponds to 1 digital increment in a range of 4000 increments. The load cells should be suitably loaded in relation to their rating and sufficient thermal inertia, and if necessary thermal shielding, should be designed into their mountings and loading structures to limit their internal temperature variations within overall accuracy margins and operating cycles.

3.2. Systems

An electrically-operated printer is included in the system shown basically in Fig. 1 to print-out automatically the weight value on command. To prevent a print being made unless the weight value is steady, part of the control unit of the digital servo is electrically interlocked with the printer drive circuit so that the printer cannot operate unless the digital servo is at balance and has been in that state for a certain period. Also the digitizer can be electrically locked during the printer operation by disconnecting the control unit from the counter so that any pulses resulting from a weight change cannot reach the counter.

In automatic feed control systems signals corresponding to pre-set values of required weight for control

purposes may be obtained in various ways, one of which is by representing the pre-set weight information as an analogue voltage at the input of the difference amplifier as shown in Fig. 2. In this the pre-set weight input information is initially disconnected while the digital servo runs to balance; the servo is then locked at balance and the pre-set weight information is entered so that the control unit will not reach balance again until the required weight has been fed into the weigher, at which point the control unit causes the feed to stop. Finally, on disconnecting the pre-set weight input information, unlocking the digital servo and allowing it to run to balance again, the gross weight can be printed out and the pre-set weight information for the next feed can then be presented and controlled as though the weigher had been automatically tared.

Another way of obtaining signals corresponding to pre-set weight values is to monitor the binary output of the digitizer with parallel input binary adders. These comprise a series of half adders, two being needed for each complete stage of binary addition. In the general case of monitoring weight to obtain signals for controlling the feed of material into the weigh-hopper signals in b.c.d. form corresponding to the actual weight of material in the weigh hopper are applied to an arithmetic function block which contains the appropriate numbers of half-adders, together with signals corresponding to the difference between the full capacity of the resulting adders and the required weight value. The latter signals are the complement of the required weight and are obtained from hand-set switches, punched cards, etc., which are set up in terms of the required weight, but which are wired in such a way as to give the particular complement of the required weight, thus if the capacity of the adders in the arithmetic unit is 999 units then the complement needed is the 'nine's complement', and so if three ten-position switches each calibrated

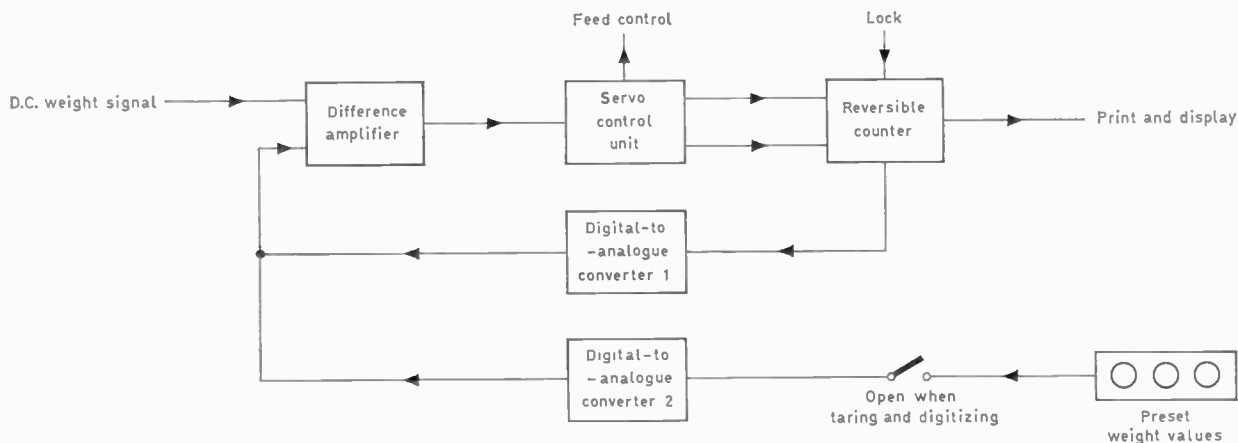


Fig. 2. Pre-set weight signal system (analogue).

0 to 9 are used for setting up the required weight the output contacts for each decade are wired to correspond to 9 minus the switch setting.

As the material is fed into the weigh hopper the corresponding weight value of the signal being fed into the arithmetic unit increases and adds to the complement of the required cut-off value which is already in the adders. The adders reach their maximum capacity, and when the weight value increases by one further increment the unit gives out a 'carry' signal which is used as the cut-off signal. This 'carry' signal is present as long as the actual weight exceeds the required weight. Thus the cut-off signal is obtained by taking the adders to one increment above their maximum value and therefore to prevent an error of one increment in the cut-off value a standing signal of one increment is applied to the arithmetic unit.

Auxiliary adding circuits are usually included in the arithmetic unit so that an intermediate cut-off signal to slow down the feeder drive may be obtained in advance of the final cut-off signal by a variable preset amount, and also so that the final cut-off signal may be advanced by a small variable preset amount to allow for the overrun of the feeder. This minimizes any final difference between the actual weight of material fed and the weight set on the required weight switches.

The basis on which this system is applied to the digital servo is shown in Fig. 3. In this case the digital servo is in continuous operation and an auxiliary reversible counter (RC2) runs together with the main counter but is reset to zero after each feed so that successive feeds are monitored from zero weight. Thus information for print and display of gross weight is obtained from the main counter and of net weight from the auxiliary counter.

In weighing terms the operational adjustment to zero of the weight indicating system when the weigher is loaded, with say an empty container, is known as

'taring'. The principle of taring is the same as that of balancing, referred to in Section 3.1, except that taring can be carried out to the extent of a considerable proportion of the capacity of the weight indicating system. Balancing and taring may be carried out by hand or, on receipt of an initiating signal, automatically. For manual operation, resistances in the input network may be switched to produce a voltage in opposition to the weight-signal, as in the case of the fine balance control. For automatic operation part of the digital servo loop is duplicated as shown in Fig. 4; to back-off any weight information existing in the main servo loop 1, RC1 is first reset to zero and locked, RC2 is then unlocked and its servo loop runs to balance thus taking to zero the net input to the difference amplifier. RC2 is again locked, RC1 is unlocked and the main servo loop 1 indicates zero weight although the weight-signal input to the digital servo is not zero.

Thus by suitable disposition of the main function blocks on lines similar to those of the examples of systems just given a wide variety of control and indication facilities may be obtained. These include:

- (i) manual calibrated tare,
- (ii) automatic tare,
- (iii) obtaining signals at pre-set weight values from information given in either analogue or digital form,
- (iv) monitoring of weight dispensed from a weighed container,
- (v) digital display and printing of gross, tare and net weights and
- (vi) analogue display of weight.

The weight information in analogue form for item (vi) above is obtained from the output of the d.c. amplifier of Fig. 1. This ranges from 0 to 6 V and may be applied in conjunction with the reference voltage to a self-balancing potentiometric instrument for accurate weight display or may be applied to a less

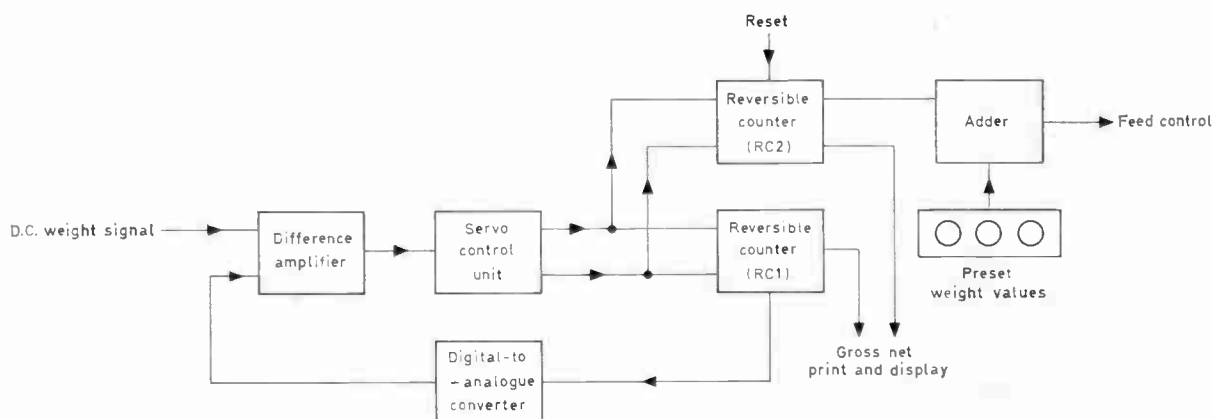
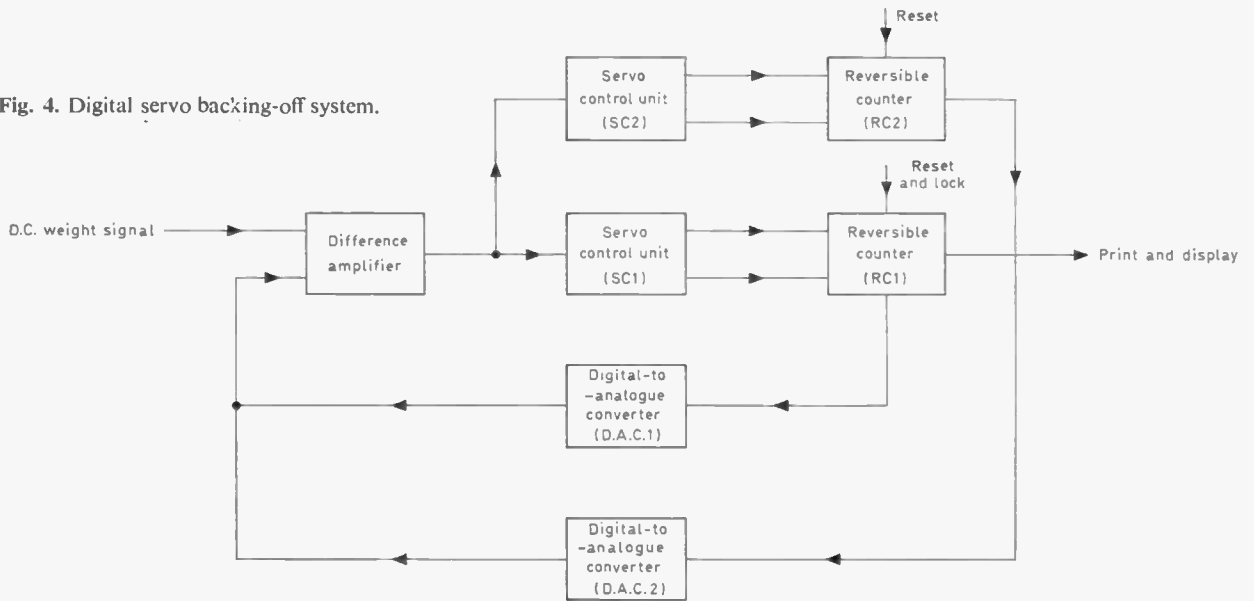


Fig. 3. Pre-set weight signal system (digital).

Fig. 4. Digital servo backing-off system.



accurate instrument such as a commercial grade voltmeter for approximate weight display.

3.3. Applications

Applications of the digitizer include load cell weighbridges which meet Board of Trade stamping requirements.⁴ The weighbridge office interior of one such application is shown in Fig. 5. The installation is a 40 ft x 10 ft (12.2 m x 3.05 m) weighbridge of capacity 39 tons 19 cwt 3 qr involving 3199 increments

of 1 qr.[†] Weight is indicated on the five digital display tubes which can be seen on the vertical front of the display unit to the right of the printer. The fine balance control and the edgewise centre-zero meter which are used as a routine by the operator for accurately adjusting the zero of the system when the weighbridge is unloaded are at the left-hand side of the display unit. Weight is recorded automatically on the electrical add-listing printer on the left of the display unit. The rows of pushbuttons in front of the

† 1 ton = 20 cwt = 1016.05 kg 1 cwt = 112 lb = 50.80 kg 1 qr = 28 lb = 12.70 kg

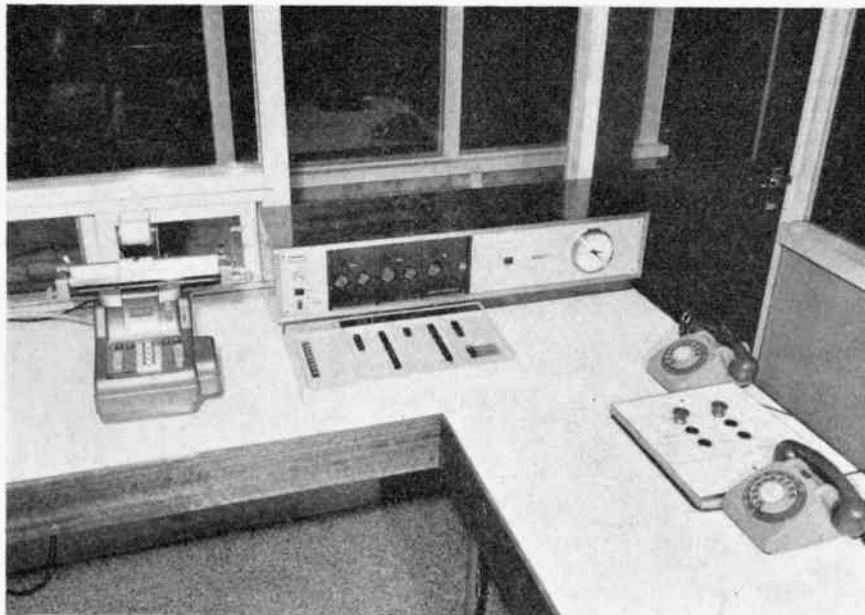


Fig. 5. Interior view of a 40-ton load cell weighbridge office.

display units are for adding various identifying codes to the print out and also for keying gross or tare weights into the printer which can then automatically calculate and print out net weights. The digitizer and the electronic circuits of the printer are housed in a cubicle which is located under the office counter.

Other applications which meet stamping requirements include weighbridges with up to 4000 weight increments, a typical capacity being 100 tons by 56 lb, and industrial applications such as weighers with selectable print out in either avoirdupois or metric units. This latter facility is obtained by incorporating two digital servos, only one of which can be operative at any time, the selection being made quite simply by a switch: one digital servo is calibrated in avoirdupois (tons, cwts, qrs) and the other in metric units. In those dual-unit systems where the tons are to be subdivided into decimal increments the two systems of units can be obtained with one digital servo, the difference in scaling factor between the major units of 1 ton and 1000 kg being obtained by changing the gain of the a.c. signal amplifier, a typical capacity being 80 tons by 0.02 tons and 80000 kg by 20 kg.

4. Computers in Weighing

In blending plants associated with some process industries the basic control requirement is usually for a group of weighers to be automatically controlled to weigh and govern the feeding of the selected materials which form each blend. Typically, there may be a total of 72 material storage bins and 2-rate feeders associated with the group of weighers numbering from say, 2 to 12, the exact number depending on many layout and operational requirements of the plant. A blend may contain 10 or more materials. The materials involved in a blend and the required weights of each are to be in accordance with a preset blend formulation, and there may be a hundred or so different formulations available for general use at any time.

The information concerning the materials and weights involved in each formulation can be given to the control system by means of punched cards, there being one card for each formulation. At the start of each blend the card appropriate to the required formulation is put into the punched card reader. Associated with each weigher is a control system which accepts information from the card reader via a main control unit and gives out signals for selecting and controlling those of the material feeders associated with that weigher which are involved in that blend. All the weighers involved in each blend usually operate concurrently in order to minimize the blend cycle time—usually of a few minutes' duration. On completing the feed of each material the control system automatically checks that the actual weight fed is within a preset tolerance of the required weight,

and if this is satisfactory the weigh hopper is discharged and the feed of the next selected material associated with the weigher is started, or if weighings are to be cumulative there would be no hopper discharge between consecutive materials. When all the weighings called for on the punched card associated with the formulation of a given blend are completed a 'blend complete' signal is given and after the final discharge of the weigh hoppers the next blend may be started with the same or another card as required.

Current industrial trends are such that some blending plants involve so many materials and different blend formulations which may need to be frequently changed that the requirements of the medium for supplying the system with input information are more readily provided by magnetic core storage with punched tape input. Also the complexity of the blending system, the flexibility in its operation and the extent of the output data required can be such that the use of a programmed digital processor is justified for its control. Core storage and a digital processor together comprise the essentials of a digital computer of the type which are available in small capacities mainly for industrial control and data logging purposes.

Figure 6 shows the basic diagram of a load cell multiweigher blending plant which uses a small computer for storing the information covering a large number of formulations, for controlling the weighers and feeders and for giving a printed record of the performance of each weigher, and of the main events in each blending cycle. The information for all the formulations is put into the store by means of punched tape, which can be generated by manual operation of the printer, and a formulation is called from the store by a simple switch operation on the operator's panel at the start of each blend. The digital processor will operate during each blend in accordance with a program which is also held in the store.

Associated with each weigher is a minimum of instrumentation but sufficient of the type described in Section 3 of this paper to provide weight information in suitable electrical form for the digital processor to provide the control function. It does this by sequentially scanning the electrical outputs of the weighers, which are shown as 5 in this case, at a high rate and instantaneously comparing the weight signal from each weigher with the required values in accordance with the formulation. As each feed is completed the actual weight fed is printed and automatically checked to be within a preset tolerance; if this is satisfactory the digital processor will either initiate the next selected material feed, or will first discharge the hopper if the weighings are to be non-cumulative. In addition to the control of the weighers, feeders and main sequence the

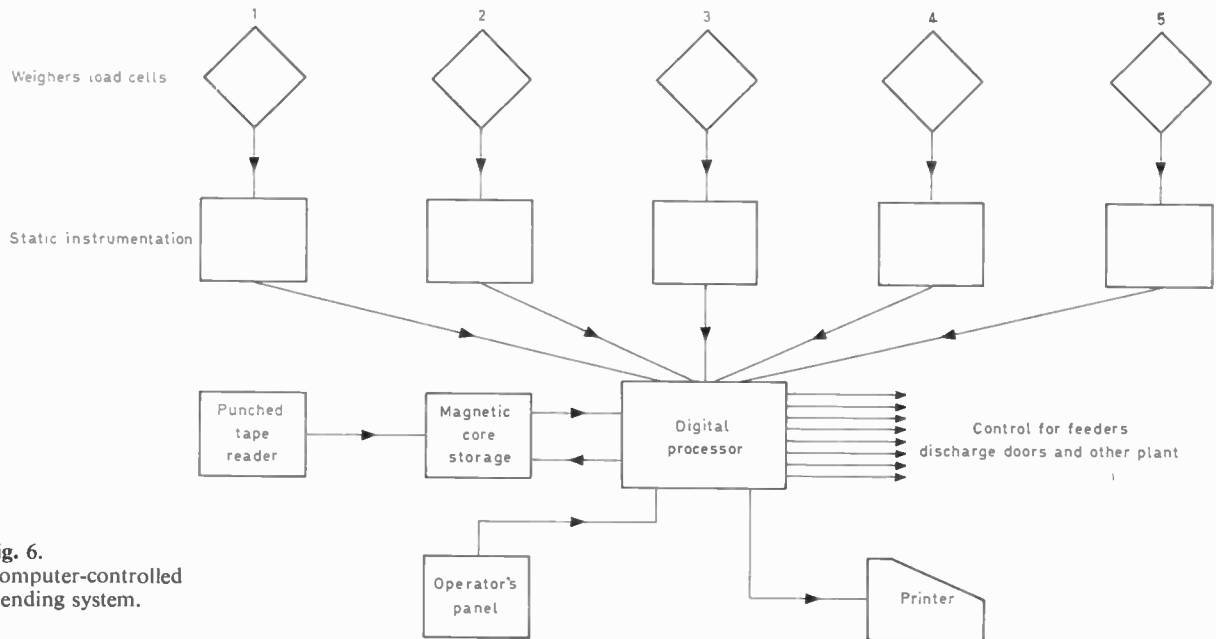


Fig. 6.
Computer-controlled
blending system.

digital processor can be programmed to carry out various optimizing sub-routines such as the selection of the order in which the feeders and weighers are to be used to give minimum blend-cycle times, or of the order in which various blends should be put through the system to optimize the operation of subsequent process plant. Various degrees of control of an interlocking with parts of the main plant not connected with weighing but associated with the blending plant can also be carried out with advantage by the digital processor. Changes in the requirements of any operational sequence controlled by the digital processor can be obtained by change of its program which is effected by reading in to the system program changes on punched tape.

By means of the control and indication facilities included on the operator's control panel the operator can select the formulations which are needed for the next several blends, start or stop the blending cycle, modify formulations, adjust the operational factors which affect accuracy and initiate various automatic printings which will give information on the progress of the blend cycle. The computer, the instrumentation associated with each weighing and the operator's control panel can be housed in a control room adjacent to the plant. A weight display for each weigher is provided in the control room so that the performance of each weigher can be observed in operation if required.

5. Conclusion

Digital techniques are being successfully applied to accurate load cell weighing both in conjunction with

electromechanical servos and by means of all-electronic systems involving the basic instrumentation described.

The complexity now required of so many weighing functions leads to considerable use of digital systems, and this together with advancing techniques in micro-electronics will no doubt give greater emphasis to all-electronic digital equipments.

6. Acknowledgments

Acknowledgment is made to the Directors of W. & T. Avery Limited for permission to publish the paper. The author wishes to acknowledge with thanks the help of his colleagues in W. & T. Avery's Technical Division in providing information and material in connection with the paper.

7. References

1. Board of Trade Notice 1474 of 1968. 'Notes for Guidance of Inspectors', Item (6). (Authorizes the use for trade purposes of the basic digital system described in this paper.)
2. 'Load cell terminology and test procedure recommendations', The Scale Manufacturers Association, Inc. Washington, D.C.
3. Leng, L., 'Electronics in Weighing', Paper published by the Institute of Weights & Measures Administration. (Describes the basic instrumentation mentioned in Section 3 of this paper.)
4. Board of Trade Notice 1710 of 1963. (This states the accuracies required of weighing equipment which is to be used for trade purposes.)

Manuscript first received by the Institution on 18th July 1968, and in revised form on 4th October 1968. (Paper No. 1278/IC12.)

Latitude, Altitude, Azimuth and Polarization Angle Dependence of Scattering of Radio Waves in the Ionosphere Considering Anisotropy

By
S. S. DE, M.Sc.†

Summary: This paper describes the latitude, altitude, azimuth and polarization angle dependence of scattering of radio waves in the ionosphere. The anisotropic behaviour which arises due to the presence of the geomagnetic field has been taken into account. The formula obtained for scattering cross-section may be verified experimentally and the importance of the geomagnetic field in the production of anisotropy may then be analysed.

1. Introduction

Ignoring the Earth's magnetic field Booker and Gordon¹ deduced the formula for scattering cross-section per unit volume of a randomly inhomogeneous but isotropic dielectric. From their work when the scale of turbulence is small compared with $\lambda/2\pi$, the formula for scattering cross-section obtained, is given by

$$\Omega = \frac{(\frac{\Delta\epsilon}{\epsilon})^2 (2\pi l)^3}{\lambda} \sin^2 \chi \quad \dots\dots(1)$$

where Ω is the scattered power per unit incident power density per unit macroscopic element of volume and per unit solid angle in a direction making an angle θ with the direction of incidence; l is the scale of turbulence; χ is the angle between the incident electric field and the direction of scatter and $\sin^2 \chi$ is the polarization factor. $(\Delta\epsilon/\epsilon)^2$ is the mean squared variation in dielectric constant and λ is the wavelength of the radio wave. For small scale turbulence the non-dependence of Ω on θ has been taken, for which θ term in eqn. (1) is omitted.

When the Earth's magnetic field is considered, the scattering volume is no longer isotropic in nature. It is worthwhile to note that the scattered electromagnetic wave is due to the vibrations of the electrons in the medium, in short, due to the elementary Hertzian oscillators. The directions of vibrations of electrons are solely determined by the directions of the forces experienced by them. The directions of the forces which are really the directions of \mathbf{D} are however not identical with the directions of \mathbf{E} , which is true only in the case of isotropic medium. Thus accounting for the geomagnetic field which causes anisotropy in the scattering medium leads to different orientations of the Hertzian oscillators unlike the case of Booker and

Gordon. So in the anisotropic medium, the polarization angle χ will depend on the orientation of the displacement vector \mathbf{D} instead of \mathbf{E} , as in the case of isotropic medium. In this case, $\Delta\epsilon$ will be a matrix. The magnetic field at a particular place is dependent on latitude in particular. For a fixed latitude, the variations of altitude and azimuth angles for the scattered ray should also be taken into account. Taking into account these variations, the expression for χ can be obtained which will give the required cross-section from eqn. (1). We therefore now proceed to compute χ .

2. Computation of χ

For the computation of χ , it is at first necessary to compute the expression $1+4\pi\sigma^{-1}$ where σ is the susceptibility tensor. The anisotropic nature of the magneto-ionic medium is represented by

$$-\epsilon_0 R \begin{pmatrix} E_x \\ E_y \\ E_z \end{pmatrix} = \begin{pmatrix} U & inY & -imY \\ -inY & U & ilY \\ imY & -ilY & U \end{pmatrix} \begin{pmatrix} P_x \\ P_y \\ P_z \end{pmatrix} \quad \dots\dots(2)$$

where l, m, n are the direction cosines of the vector \mathbf{Y} and other symbols have the following meaning:

$$z = \frac{\nu}{\omega} = \frac{\text{frequency of collision of electrons with heavy particles}}{\text{angular wave frequency}}$$

$$U = 1 - iz$$

$$R = \frac{Ne^2}{\epsilon_0 m_e \omega^2}$$

$$\mathbf{Y} = \frac{\mu_0 \mathbf{H} e}{m_e \omega}$$

$$\mathbf{P} = -\epsilon_0 \frac{R}{1 - iz} \mathbf{E}$$

μ_0 magnetic permeability of free space

† Institute of Radio Physics and Electronics, University of Calcutta, India.

- m_e mass of electron
- ϵ_0 electric permittivity of free space
- e charge of an electron
- N number density of electrons
- H magnetic wave field
- E electric wave field

Equation (2) may also be written as $E = \sigma P$

where

$$\sigma = -\frac{1}{\epsilon_0 R} \begin{pmatrix} U & inY & -imY \\ -inY & U & ilY \\ imY & -ilY & U \end{pmatrix}$$

Now,

$$D = E + 4\pi P = E + 4\pi\sigma^{-1}E \quad \dots\dots(3)$$

According to Banerjee² and Budden³ the inverse of σ , i.e., inverse susceptibility tensor, turns out to be

$$\sigma^{-1} = -\frac{\epsilon_0 R}{U(U^2 - Y^2)} \begin{pmatrix} U^2 - l^2 Y^2 & -inYU - lmY^2 & imYU - lnY^2 \\ inYU - lmY^2 & U^2 - m^2 Y^2 & -ilYU - mnY^2 \\ -imYU - lnY^2 & ilYU - mnY^2 & U^2 - n^2 Y^2 \end{pmatrix}$$

Substituting the value of σ^{-1} in eqn. (3) and neglecting H^2 terms, we obtain

$$1 + 4\pi\sigma^{-1} = \begin{pmatrix} 1 & 0 & 0 \\ 0 & 1 & 0 \\ 0 & 0 & 1 \end{pmatrix} - \frac{4\pi\epsilon_0 R}{U^2} \begin{pmatrix} U & -inY & imY \\ inY & U & -ilY \\ -imY & ilY & U \end{pmatrix}$$

$$= \frac{4\pi\epsilon_0 R}{U^2} \begin{pmatrix} U - \frac{U^2}{4\pi\epsilon_0 R} & -inY & imY \\ inY & U - \frac{U^2}{4\pi\epsilon_0 R} & -ilY \\ -imY & ilY & U - \frac{U^2}{4\pi\epsilon_0 R} \end{pmatrix} \quad \dots\dots(4)$$

Let Z be the direction of propagation of electromagnetic waves from the transmitter and let X-axis lie in the vertical plane passing through the direction of propagation which makes an angle α with the direction of E at the scattering volume under consideration in the ionosphere where there are irregularities. Let θ be the angle between the direction of propagation and the direction of reception. Also let $(\lambda_1, \mu_1, \nu_1)$ be the direction cosines of D . Thus the direction cosines of E become $(\cos \alpha, \sin \alpha, 0)$ and that of the receiving wave is $(\sin \theta, 0, \cos \theta)$. Here the direction of the received wave is perpendicular to the Y-axis. We can write

$$\begin{pmatrix} D_x \\ D_y \\ D_z \end{pmatrix} = \begin{pmatrix} a_{11} & a_{12} & a_{13} \\ a_{21} & a_{22} & a_{23} \\ a_{31} & a_{32} & a_{33} \end{pmatrix} \begin{pmatrix} \cos \alpha \\ \sin \alpha \\ 0 \end{pmatrix} E_0$$

where the matrix a_{ij} is used for brevity in place of the elements in $1 + 4\pi\sigma^{-1}$.

Therefore,

$$\lambda_1 \propto \frac{D_x}{E_0} = a_{11} \cos \alpha + a_{12} \sin \alpha$$

$$\mu_1 \propto \frac{D_y}{E_0} = a_{21} \cos \alpha + a_{22} \sin \alpha$$

$$\nu_1 \propto \frac{D_z}{E_0} = a_{31} \cos \alpha + a_{32} \sin \alpha$$

Thus,

$$\lambda_1 = \frac{a_{11} \cos \alpha + a_{12} \sin \alpha}{\Delta}$$

$$\nu_1 = \frac{a_{31} \cos \alpha + a_{32} \sin \alpha}{\Delta}$$

where

$$\Delta^2 = (a_{11} \cos \alpha + a_{12} \sin \alpha)^2 + (a_{21} \cos \alpha + a_{22} \sin \alpha)^2 + (a_{31} \cos \alpha + a_{32} \sin \alpha)^2$$

From equation (1) we can write, for simplicity,

$$\Omega = c \sin^2 \chi$$

where

$$c = \frac{\left(\frac{\Delta \epsilon}{\epsilon}\right)^2 \left(\frac{2\pi l}{\lambda}\right)^3}{\lambda}$$

$$\Omega = c[1 - (\lambda_1 \sin \theta + \nu_1 \cos \theta)^2]$$

$$= c \left[1 - \frac{(a_{11} \cos \alpha \sin \theta + a_{12} \sin \alpha \sin \theta + a_{31} \cos \alpha \cos \theta + a_{32} \sin \alpha \cos \theta)^2}{(a_{11} \cos \alpha + a_{12} \sin \alpha)^2 + (a_{21} \cos \alpha + a_{22} \sin \alpha)^2 + (a_{31} \cos \alpha + a_{32} \sin \alpha)^2} \right] \dots\dots(5)$$

Let (l_3, m_3, n_3) be the direction cosines of the transmitting direction, i.e. Z-direction, and (l_1, m_1, n_1) and (l_2, m_2, n_2) be the direction cosines of X-axis and Y-axis respectively. In this system of co-ordinates (see Fig. 1) the geomagnetic potential

$$V = - \frac{\cos \phi}{r^2}$$

where ϕ is the co-latitude of the place and r is radius of the Earth.

If β be the latitude of the place then the direction cosines of the geomagnetic field become $(\cos \beta, 0, 2 \sin \beta)$.

Thus,

$$\left. \begin{aligned} H_x &\propto l_1 \cos \beta + 2n_1 \sin \beta = l \\ H_y &\propto l_2 \cos \beta + 2n_2 \sin \beta = m \\ H_z &\propto l_3 \cos \beta + 2n_3 \sin \beta = n \end{aligned} \right\} \dots\dots(6)$$

Let this system be transformed to a system of co-ordinates with the Z-axis as the direction of zenith, the X-axis as the direction of North and the Y-axis as the direction of East. The X-Y plane is the plane of the Earth which is the horizontal. Also let A be the altitude and a be the azimuth of the place.

Then,

$$\left. \begin{aligned} l_3 &= \cos A \cos a, & l_2 &= -\sin a, & l_1 &= -\sin A \cos a \\ m_3 &= \cos A \sin a, & m_2 &= \cos a, & m_1 &= -\sin A \sin a \\ n_3 &= \sin A, & n_2 &= 0, & n_1 &= \cos A \end{aligned} \right\} \dots\dots(7)$$

Substituting the values of (l, m, n) from eqns. (6) and substituting the value of Y in eqn. (4) we get

$$1 + 4\pi\sigma^{-1} = \frac{4\pi\epsilon_0 R}{U^2} \begin{pmatrix} U - \frac{U^2}{4\pi\epsilon_0 R} & -\frac{i\mu_0 He}{m_e \omega} (l_3 \cos \beta + 2n_3 \sin \beta) & \frac{i\mu_0 He}{m_e \omega} (l_2 \cos \beta + 2n_2 \sin \beta) \\ \frac{i\mu_0 He}{m_e \omega} (l_3 \cos \beta + 2n_3 \sin \beta) & U - \frac{U^2}{4\pi\epsilon_0 R} & -\frac{i\mu_0 He}{m_e \omega} (l_1 \cos \beta + 2n_1 \sin \beta) \\ -\frac{i\mu_0 He}{m_e \omega} (l_2 \cos \beta + 2n_2 \sin \beta) & \frac{i\mu_0 He}{m_e \omega} (l_1 \cos \beta + 2n_1 \sin \beta) & U - \frac{U^2}{4\pi\epsilon_0 R} \end{pmatrix} \dots\dots(8)$$

3. Computation of Ω

Equation (8) gives an expression for $1 + 4\pi\sigma^{-1}$. By making use of this an expression for the scattering cross-section may now be obtained.

$$\Omega = c \left[1 - \left(\frac{4\pi\epsilon_0 R}{U^2} \right)^2 \left\{ U \cos \alpha \sin \theta - \frac{U^2}{4\pi\epsilon_0 R} \cos \alpha \sin \theta - \frac{i\mu_0 He}{m_e \omega} \cos A \cos a \sin \alpha \sin \theta \cos \beta - \frac{i\mu_0 He}{m_e \omega} 2 \sin A \sin \beta \sin \alpha \sin \theta + \frac{i\mu_0 He}{m_e \omega} \sin a \cos \beta \cos \alpha \cos \theta - \frac{i\mu_0 He}{m_e \omega} \sin A \cos a \cos \beta \sin \alpha \cos \theta + \frac{i\mu_0 He}{m_e \omega} 2 \cos A \sin \beta \sin \alpha \cos \theta \right\}^2 \times \right.$$

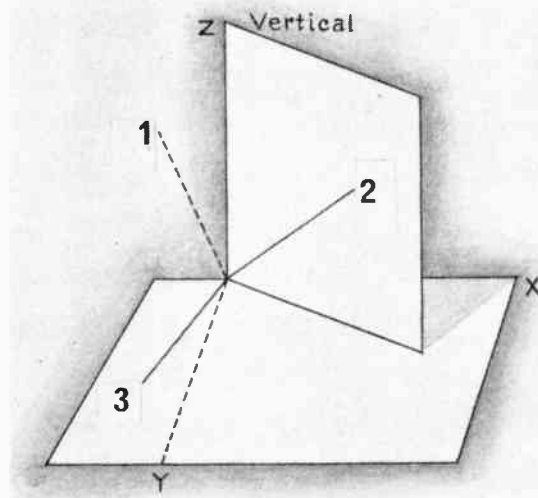


Fig. 1.

$$\begin{aligned} & \times \left(\frac{4\pi\epsilon_0 R}{U^2} \right)^{-2} \left\{ \left(U \cos \alpha - \frac{U^2}{4\pi\epsilon_0 R} \cos \alpha - \frac{i\mu_0 H e}{m_e \omega} \cos A \cos a \cos \beta \sin \alpha - \right. \right. \\ & \left. \left. - \frac{i\mu_0 H e}{m_e \omega} 2 \sin A \sin \beta \sin \alpha \right)^2 + \left(\frac{i\mu_0 H e}{m_e \omega} \cos A \cos a \cos \beta \cos \alpha + \frac{i\mu_0 H e}{m_e \omega} 2 \sin A \sin \beta \cos \alpha + \right. \right. \\ & \left. \left. + U \sin \alpha - \frac{U^2}{4\pi\epsilon_0 R} \sin \alpha \right)^2 + \left(\frac{i\mu_0 H e}{m_e \omega} \sin a \cos \beta \cos \alpha - \frac{i\mu_0 H e}{m_e \omega} \sin A \cos a \cos \beta \sin \alpha + \right. \right. \\ & \left. \left. + \frac{i\mu_0 H e}{m_e \omega} 2 \cos A \sin \beta \sin \alpha \right)^2 \right\}^{-1} \end{aligned}$$

Neglecting H^2 terms we get on simplification the expression for Ω as

$$\Omega = c(1 - \cos^2 \alpha \sin^2 \theta) + c \frac{2 \frac{i\mu_0 H e}{m_e \omega} \cos \alpha \sin \theta (R_1 + R_2 + R_3)}{R_4} \dots\dots(9)$$

where

$$\begin{aligned} R_1 &= \cos a \sin \alpha \cos \beta \sin (A + \theta) \\ R_2 &= -2 \sin \beta \sin \alpha \cos (A + \theta) \\ R_3 &= -\sin a \cos \beta \cos \alpha \cos \theta \\ R_4 &= U \left(1 - \frac{U}{4\pi\epsilon_0 R} \right) \end{aligned}$$

4. Analytical Consequences

From the modified formula for scattering cross-section deduced above in eqn. (9), it is clearly seen that the first term of the right-hand side expression is identical with the expression deduced by Booker and Gordon.¹ That the first term of eqn. (9) is similar to the expression given by eqn. (1) may be easily proved with the help of, for example, spherical trigonometry.

The second term or the last term of eqn. (9) arises due to the anisotropic behaviour of the ionosphere as a result of the effect of the geomagnetic field. This is obvious since if we make $H = 0$ the second term in eqn. (9) drops out. Thus the first term of right-hand side of eqn. (9) is the isotropic part and the last term of the right-hand side of eqn. (9) is the anisotropic content. For a fixed latitude the effect of the geomagnetic field on the scattering or radio waves in the ionosphere can be analysed experimentally using eqn. (9) and the subsequent variations of scattering cross-section with variations of altitude and azimuth angle may be tested simultaneously or separately.

The effect of the geomagnetic field takes a prominent role when the propagation is perpendicular to the lines of force of the geomagnetic field. The effect of the

geomagnetic field is minimum when the propagation is parallel with the lines of force of the geomagnetic field.

It is expected that by taking into account the deduced parametric variations, the formula obtained by eqn. (9) should approach more closely towards experimental observations.

5. Acknowledgments

The author is indebted to Professor J. N. Bhar, Head of the Department of Radio Physics and Electronics, University of Calcutta, for his keen interest in the subject. The author is also grateful to Professor A. K. Choudhury and Dr. S. Basu, for helpful discussions and constant encouragement.

6. References and Bibliography

1. Booker, H. G. and Gordon, W. E., 'A theory of radio scattering in the troposphere', *Proc. Inst. Radio Engrs*, **38**, pp. 401-12, April 1950.
2. Banerjee, B. K., 'On the propagation of electromagnetic waves through the atmosphere', *Proc. Roy. Soc., A*, **190**, pp. 67-81, 17th June 1947.
3. Budden, K. G., 'Radio Waves in the Ionosphere' (Cambridge University Press, 1961).
4. Booker, H. G., 'Radio scattering in the lower ionosphere', *J. Geophys Res.*, **64**, pp. 2164-77, December 1959.
5. Fejer, J. A., 'Scattering of radio waves by an ionised gas in thermal equilibrium', *Canadian J. Phys.*, **38**, pp. 1114-33, August 1960.

Manuscript first received by the Institution on 22nd July 1968 and in final form on 17th February 1969. (Short Contribution No. 124/Com. 21.)

© The Institution of Electronic and Radio Engineers, 1969

A Survey of the Developments in Antenna Servo Techniques

By

D. R. WILSON, M.Sc.(Tech.),
Ph.D., C.Eng., M.I.E.E.†

Summary: The paper considers the factors that influence the servo design for satellite tracking antennae. The methods of servo compensation are discussed and simple adaptive techniques are illustrated. The importance of the mechanics in relation to the servo performance is emphasized and the application of digital computers in servo tracking loops is discussed. A 'design' example is given.

1. Introduction

The 1947 Servomechanism and Regulators Conference¹ provided a record of the progress made during the 1939–45 War in the art of servo control of large masses, i.e. gun controls, radar mountings, searchlights, etc. The basic concept of closed-loop stability in an engineering sense, as stated by Nyquist,² was interpreted into physical design criteria³ by the engineers of that decade and, in general, the concepts that were expounded are as valid today as when they were first applied. Further, in 1958 Tustin⁴ and his collaborators presented in great detail a treatise on the position control of massive objects. One may well ask what can yet be said about position servo control that has not been said or inferred by previous authors. The answer to such a question is, in terms of academic fundamentals, very little, but in terms of engineering design and more importantly—engineering implementation of the designs—very much indeed.

In the last decade servo specifications have laid down increasingly stringent figures for the dynamic and static performance and therefore in order to improve servo performance the servocomponents that have been used, both for high and low powers, have undergone considerable development in the past 10 years. This development, coupled with the related advances in the application of the improved component, has meant that real progress has been made. The 1967 Servocomponents Conference⁵ covered many facets of servo component development, which for the purpose of this paper may be conveniently broken down into the following sections:

- (i) Transducers,
- (ii) Error processing,
- (iii) Power amplification.

Of the first, synchro systems have been universally applied to measure positional error in aerial and gun control systems and the like, but the use of conductive plastic⁶ materials has put new life into the much maligned potentiometer as a reliable servocomponent.

† G.E.C.-A.E.I. (Electronics) Ltd., New Parks, Leicester.

However, when extreme positional accuracy is required there is no alternative to a digital encoder. As an example, the pointing accuracy demanded of a large (say 90 ft) diameter antenna for a satellite communication Earth station would, typically, necessitate the use of a 17-bit digital encoder as the data position transducer. The customer, however, pays heavily for increased resolution and accuracy in comparison with a synchro position-control system. Further servocomponents such as brushless tachometers,⁷ brushless synchros,⁸ the hi-syn⁹ etc. are indications of the trend to seek improved components to measure the state variables of a servo control system, e.g. position, velocity, acceleration, drive armature current etc. The second and third topics listed above are fully discussed in the paper.

However, in spite of considerable electrical progress, the limiting component in a servo control system is still the drive mechanics and supporting structure. In the case of a large antenna the drive mechanics includes the motor, gearbox and associated backing structure of the aerial that is within the servo loop during an active tracking period. This applies both to high dynamic performance aerials, such as radar trackers, and to the larger aerials for satellite communication links which, although they have a negligible dynamic performance, have an extremely stringent accuracy specification of the order of 0.01° r.m.s. maximum positional error, i.e. 0.03° peak, assuming a Gaussian distribution. The fundamental problem of backlash and gearbox resilience coupled with aerial structural resonances are the limiting factors in current servo design practice and performance in the field. This is particularly so with light-weight air transportable equipment, where to reduce the dead weight of an equipment means reducing the overall stiffness of the drive and hence introducing low mechanical resonant frequencies into the servo control system, thus producing extremely difficult stability problems for the system designer. There is a considerable need for more effort to be applied to dynamic structural analysis of servo mechanism loads.¹⁰ System designers have, in the

past, almost invariably assumed a lumped inertia load for the most complex mechanical drives, which usually means that the servo has to be tuned on site with anti-resonant elements. This problem is further aggravated by the fact that nearly all such equipments need to be independently tuned if the mechanical resonance is critical; however large antennae still tend to be 'one-off' jobs rather than production equipments and consequently this is not as embarrassing as it could be.

The paper considers various aspects of the problems discussed in this section. In Section 2 analytic methods are reviewed and system design objectives illustrated. Section 3 discusses low-level (i.e. low-power) error signal processing and servo compensation. Section 4 discusses power amplification, while Section 5 discusses the application of digital techniques in antenna control systems.

2. Analytical Design

Servomechanism fundamentals are well documented in numerous texts and it is sufficient to note that the frequency-response method of design, albeit in several different forms, such as Bode, Nyquist, inverse Nyquist, root-locus, Nichols' charts etc. or the use of standard forms,¹¹ remains the basis of deterministic position control system design, i.e. where it is required to position a load, such as a gun or missile launcher, under local or remote control by synchros, digital encoders or other position transducers. The pointing of a large antenna at a desired point in the sky either by manual effort at the control desk or by prepared paper tape predictions, falls into this category.

The second major class of control system is defined by those operating on stochastic signals of the type generated in an automatic tracking radar. Such systems are used to track and illuminate a target as part of a missile weapon system. Similarly, a large antenna is used to track a satellite as part of a communication link, but with the advent of stationary satellites the need for relatively high-performance satellite tracking is being removed. However, it should be noted that a stationary satellite drifts in relation to the aerial and still needs to be tracked, albeit very slowly. In this mode of operation, namely, tracking slowly drifting synchronous satellites, it is convenient to track the satellite by a beam-swinging technique, such as sub-reflector tracking, and in this mode the main drive motors may be switched off and the dish locked in position. However, sub-reflector tracking imposes a particularly difficult problem for the adequate maintenance of a brushgear on a d.c. motor drive and for this reason a power servo using a two phase a.c. induction motor¹² is considered to be the optimum choice of electric drive.

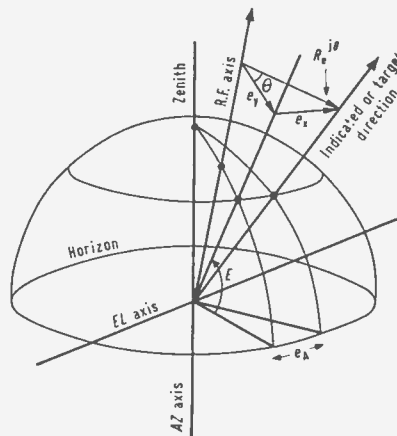


Fig. 1. Angular error components.
 $e_y = R \cos \theta$, $e_x = R \sin \theta$, $e_a = e_x \sec E$.

In a monopulse tracking system an autotrack receiver generates an error signal which is proportional to the angular offset from the centre of the beam with respect to the target, i.e. the satellite. Figure 1 illustrates the geometry of satellite tracking. In view of the geometry of an azimuth-elevation mount, i.e. az-el or elevation over azimuth, it follows that (in this type of mount) the actual servo errors are related to the space errors e_x and e_y , that are detected with respect to the r.f. beam axis, are:

$$\text{azimuth servo error } e_a = e_x \sec E \quad \dots\dots(1)$$

$$\text{elevation servo error } e_y = e_y \quad \dots\dots(2)$$

The two-axis block diagram of a satellite tracking antenna can therefore be as shown in Fig. 2, where the space-error is represented by $Re^{j\theta}$. However, in general for an az-el mount a single axis non-interacting servo is postulated for design purposes, such as in Fig. 3, where θ_n and T_w represent disturbance inputs due to receiver noise and wind gust torques respectively. It follows that

$$\epsilon = \frac{\theta_i}{1 + G_1 G_2} + \frac{G_2 G_1}{1 + G_1 G_2} \cdot \theta_n + \frac{G_1}{1 + G_1 G_2} \cdot T_w \quad \dots\dots(3)$$

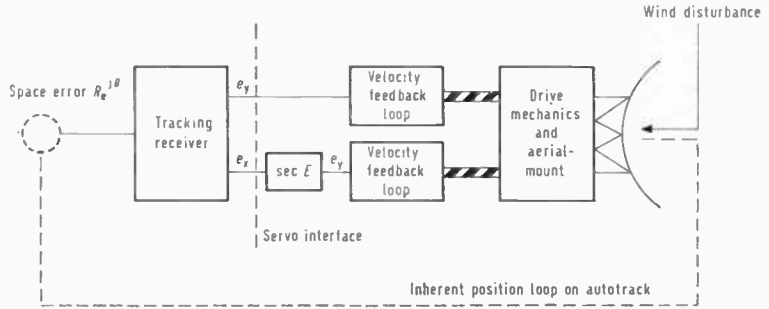
In general the object of the system designer is to minimize tracking error by appropriate design and selection of the elements which are defined by the transfer functions G_1 and G_2 .

2.1. Autotrack Error

The autotrack error has four components:

- (i) that due to receiver noise;
- (ii) that due to wind gust on the antenna;
- (iii) that due to input derivatives of a higher order than the servo can track (normally this is acceleration lag in a type-2 servo);
- (iv) null axes shift.

Fig. 2. Two-axis model of an autotrack aerial control system.



Considering these factors in reverse order the last of these error sources is not within the control of the servo designer in that it represents an angular misalignment between the communication beam and the tracking beam as received by the communications equipment, i.e. the autotrack error is the difference between where the communication beam to the satellite is pointing and the angle defining the communication beam peak, which is the line of maximum transmit and receive gain. Typically, this effective d.c. offset is 0.003°.

The acceleration lag in the steady state is a function of the acceleration constant of the servo and hence can be computed, i.e. if the forward path transfer function of the servo is $G(s)$, then:

$$\text{acceleration lag} = \frac{\bar{\theta}}{K_a}$$

where $K_a = \lim_{s \rightarrow 0} s^2 G(s)$

and typically $\bar{\theta} = 0.02^\circ/(\text{second})^2$. In practice acceleration lag has a second-order effect, when tracking synchronous satellites.

The error due to gusting can be evaluated from the spectral density as shown in the Appendix. However, it should be noted that it is only the gusting effect that introduces servo errors in that a constant wind torque error would be integrated out by the tracking servo.

The input quantities θ_n and T_w are usually estimated in terms of their spectral densities, Φ_n , Φ_w respectively and hence the mean square errors associated with receiver noise and wind gust disturbances, may be

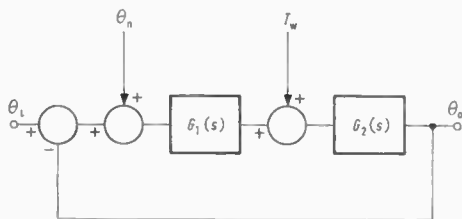


Fig. 3. Single-axis model of an aerial servomechanism with disturbances.

calculated as follows:

$$\sigma_n^2 = \int_{-\infty}^{+\infty} \left| \frac{G_2 G_1}{1 + G_1 G_2} \right|^2 \Phi_n(\omega) d\omega \text{ (rad)}^2 \dots\dots(4)$$

$$\sigma_w^2 = \int_{-\infty}^{+\infty} \left| \frac{G_1}{1 + G_1 G_2} \right|^2 \Phi_w(\omega) d\omega \text{ (rad)}^2 \dots\dots(5)$$

and hence the composite random error is given by

$$\text{error} = \sqrt{\sigma_n^2 + \sigma_w^2} \dots\dots(6)$$

which is to be minimized in conjunction with the bias errors from sources (iii) and (iv) above, if they are significant.

$\Phi_n(\omega)$ and $\Phi_w(\omega)$ will, at their simplest, be of the form:

$$\Phi_n = \frac{k_n}{\omega^2 + a^2} \text{ (volts)}^2/\text{rad/s} \dots\dots(7)$$

$$\Phi_w = \frac{k_w}{\omega^2 + b^2} \text{ (lb-ft)}^2/\text{rad/s} \dots\dots(8)$$

The design trend therefore is away from the conventional one of transient response, but one of optimal filter design, i.e. the servomechanism is considered to be a filter, which is to be synthesized. This implies a specification for a filter bandwidth, such that the disturbance inputs are rejected and thereby the aerial is allowed to remain pointing accurately at the target in space. In general however, the bandwidth requirements are contradictory, i.e. narrow bandwidth to reduce noise errors, wide bandwidths to reduce wind torque disturbances.

Wiener¹³ made a significant contribution to the solution of the optimal filter concept by attempting to specify the general form of the transfer function $G_1(s)$ assuming the elements of $G_2(s)$, namely, motors, gearing etc. to be fixed. It is well known that the absolute optimum filter in the Wiener minimum mean square sense is, if not absolutely unrealizable, impractical because of the high derivative content of such optimum filters, and hence an optimum servo in that sense is also unrealizable. However, the results of optimal control design are relevant to servo control provided the results are interpreted as engineering ideals and not as specific objectives.¹⁴

Quasi-optimum solutions of the servo tracking problem have interested servo analysts for two decades and in the case of the large satellite tracking antennas (≥ 90 ft diameter) the optimum servo bandwidth can be shown¹⁵ to occur at a point where the errors due to wind torque disturbances equal those due to receiver noise. The smaller transportable communications antennae (≤ 30 ft diameter) do not have such optimum bandwidths because the wind errors are usually negligible for normal specifications, i.e. 80 km/h (50 miles/h) mean wind speed, gusting to 104 km/h (65 miles/h),¹⁶ and therefore the servo design criteria reduces to one of minimizing the servo response to receiver noise. (See Appendix.) It follows therefore that the realization of the quasi-optimum filter, i.e. the servomechanism, reduces to designing a servo with a specified bandwidth and providing facilities for the bandwidth to be switched in discrete intervals appropriate to the conditions in which the antenna control system is operating.

include square root functions to generate optimum run in performance to large slews of position, implementation of the sec *E* function in the azimuth servo drive, generation of appropriate scanning routines such that the aerial searches selected space angles in a chosen manner, e.g. a spiral scan, and coarse/fine changeover elements. Further diode limiting circuits can conveniently be included around the feedback path of an integrated circuit to limit effectively any particular variable, such as the acceleration of the load to a specified maximum to prevent mechanical damage to the mount bearings or the drive motor.

Conventional compensation routines such as phase advance or integral plus phase advance are easily implemented as shown in Fig. 4. Included in the phase advance circuit are typical amplifier stabilizing components, which include two fast-acting diodes across pins 2 and 3 to protect the amplifier from high input voltages. The components R_1, R_2, R_3, C are varied to achieve the type of compensation required, which is of the form

$$\frac{e_o}{e_i} = \beta \frac{(1+sT)}{(1+\alpha sT)} \quad \dots\dots(9)$$

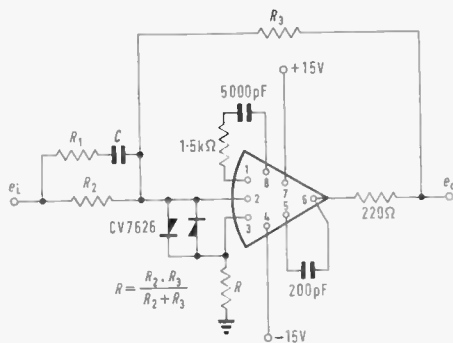
where

$$\beta = \frac{R_3}{R_2}, \quad T = (R_1 + R_2)C, \quad \alpha = \frac{R_1}{R_1 + R_2}, \quad \text{i.e. } \alpha < 1$$

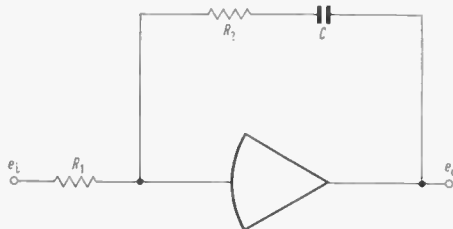
Therefore, the compensation characterization is of a 'phase advance' type. The integral plus phase advance transfer function is:

$$\frac{e_o}{e_i} = \frac{R_2}{R_1} \frac{s + \frac{1}{CR_2}}{s} \quad \dots\dots(10)$$

A simple method¹⁶ of introducing a signal-adaptive compensation network is shown in Fig. 5, whereby the effective transfer function of the compensation network is modified as a function of the input signal to the network, i.e. for a large misalignment and therefore a large error signal the diode chain will conduct connecting in circuit the capacitances C_1, C_2, C_3 , while for a small error signal, that is when the load is running into its new position, the capacitance in circuit will be C_3 . The overall effect of this technique is to vary the damping of the servo during the run-in from a large misalignment in that, initially, a lightly-damped servo is required to produce high rates of acceleration and finally, when the servo is approaching correspondence, an overdamped servo characteristic is required to prevent final overshoot of the required position. This circuit has been proved in practice to be extremely effective and it is a good illustration of the relatively simple optimization circuits that can be built into the error-processing channel of a servomechanism.



(a) Phase advance amplifier with circuit details.

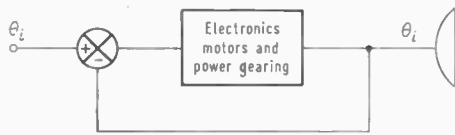


(b) Integral plus phase advance.

Fig. 4.

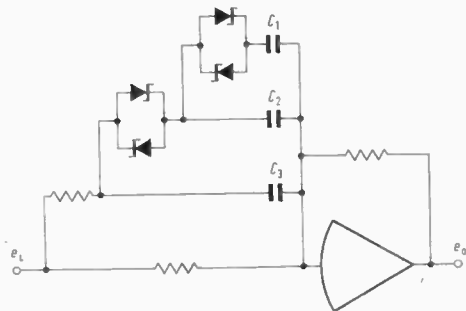
3. Error Processing and Compensation

The use of integrated circuits such as the Fairchild 709 has enabled relatively sophisticated circuitry to be implemented in the error process channel of a servomechanism. Often an effective analogue computer is built round several integrated circuits, which are high gain d.c. amplifiers, to generate the required compensation signals. Elements which are synthesized

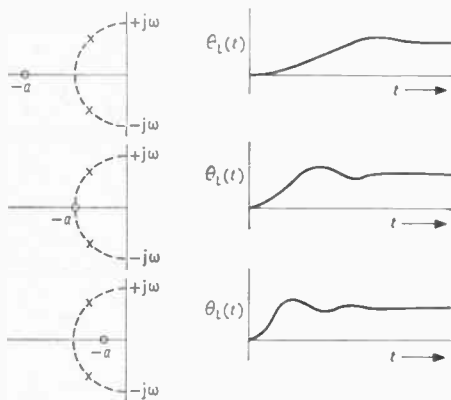


(a) Closed loop servo with

$$\frac{\theta_o}{\theta_i} \approx \frac{\omega^2 (s+a)}{s^2 + 2\zeta\omega s + \omega^2}$$



(b) Signal adaptive optimizing network forming part of the forward loop transfer function in (a).



(c) Theory of zero switching. The final servo response is a composite function of the three characteristics.

Fig. 5.

4. Power Amplification

Two principal modes of power amplification are used in high-power servomechanisms:

- (a) rotary power amplifiers,
- (b) static thyristor amplifiers.

The rotary power amplifiers include Ward-Leonard and metadyne generator systems. Their main advantage, apart from their capacity to generate large powers, is their ability to withstand shock loads on the servo, and as such act as a buffer for such an impact

load from the supply, which in the case of a local power source on a transportable equipment could have serious effects on other equipments if such an impact load was not adequately protected. An important disadvantage of rotary power amplifiers is their inherent large time-constants within the servo loop, which increases servo stability problems and reduces the speed of response of the servo. The static thyristor amplifier is very much in favour at the present time as a servo power amplifier in that it has a negligible time-constant and can often have a time-constant introduced to make it compatible with the performance of the motor; further, the absence of moving parts increases reliability and maintainability and the power capacity of thyristors is now no longer a limitation in that amplifiers of 150 kVA capacity are currently being manufactured.

The method of power amplifier design is one that can be improved by considering what is the fundamental power amplification required. The power output of a servo drive is torque at the output shaft, i.e. torque at the load. The input is a low-level signal at the output of the error channel processing circuits. The overall power amplifier therefore includes:

- (i) electrical power amplifier,
- (ii) torque converter (servo motor),
- (iii) gearbox to transmit torque to the load.

These three components of the servo amplifier are invariably designed as separate units and are finally brought together at the manufacturing stage. Under such conditions it is unlikely that the resulting overall torque amplifier will be an optimum one. The application of a.c. induction motors has been slow because of the complex control schemes that are associated with such machines in spite of their increased reliability and maintainability. However, application^{1,2} of a new mode of a.c. motor control is expected to lead to better results in the future.

5. Digital Methods

The criterion for digital control is either one where a multi-loop process has to be controlled, for instance, a nuclear reactor or process control system such as can be found in the chemical industry or where the specification on the controllability of the load specifies precise positioning accuracy, as in the case of machine tools or large aerials for satellite communication systems. Only the latter type is considered in this Section.

The digital computers that are used in the control of larger aerials are basically of two distinct types:

- (i) general-purpose computers,
- (ii) special-purpose wired (i.e. fixed program) computers.

Type (i) is available in principle from the computer manufacturers and thus by writing the appropriate programs and designing the appropriate interfaces for the computer, with the servo hardware, a digital system can be implemented. This is, usually, at the present time, an expensive proposition, for the majority of general-purpose computers have been designed and built with the process control industry in mind and therefore tend to be much larger machines than can be efficiently utilized in an aerial control mode unless considerable off-line data processing work is available to keep the computer fully loaded.

In view of this and because the modes of operation of an aerial control scheme can be specified unambiguously, as

- (i) manual control by the aerial control station operator,
- (ii) auto-track from the satellite beacon,
- (iii) programmed tracks,
- (iv) slew control,
- (v) scan about a manual setting,
- (vi) stand-by,

it follows that the various routines can be built into a fixed program and the various modes of operation selected from a front-panel switch on the control console. A typical sampling time associated with such a digital computer would be of the order of $1/32$ s. Since the widest closed-loop bandwidth of the servo for a large satellite communication aerial is of the order of 1 Hz, it follows that intersample ripple associated with a digital control system will not be a problem and the error signal will, as far as the servo mechanics are concerned, appear as an analogue signal. Servo design is therefore not a particularly difficult problem with a special-purpose wired computer.

6. Conclusions

The paper has surveyed servo techniques with particular reference to large antenna systems, although the methods in principle are applicable to any servo control design problem. Attention has been drawn to areas where increased design effort is still warranted to improve overall system performance and a discussion of digital control has intimated that large general purpose computers are not suitable for servo control schemes.

7. Acknowledgments

The author wishes to thank the Directors of GEC-AEI for permission to publish this paper and the author's colleagues for many helpful discussions, particularly Mr. D. Wilson for the technical details given in Section 3.

8. References

1. Convention on Automatic Regulators and Servo Mechanisms. *Proc. Instn Elect. Engrs*, **94**, Part IIA, No. 2, 1947.
2. Nyquist, H., 'Regeneration theory', *Bell Syst. Tech. J.*, **11**, p. 126, 1932.
3. Whiteley, A. L., 'Fundamental principles of automatic regulators and servomechanisms', *J. Instn Elect. Engrs*, **94**, Part IIA, p. 5, 1947.
4. Tustin, A. *et al.*, 'The design of systems for automatic control of the position of massive objects', *Proc. I.E.E.*, **105**, Part C Supplement, p. 1, 1958.
5. Proc. I.E.E. Conference on 'Servocomponents', London, November 1967 (I.E.E. Conference Publication No. 37).
6. Mitchell, W. S. E., 'Precision potentiometers for servo applications', *ibid*, p. 78.
7. Byrne, J. V., Evans, D. A. and Lloyd, N., 'Low-ripple brushless tachogenerators', *ibid*, p. 13.
8. Driver, K. L., 'The design problem of the brushless synchro', *ibid*, p. 19.
9. Howbrook, E., 'A new synchro', *ibid*, p. 7.
10. Mercurio, S. F. and Niechodowicz, F. E., 'Dynamic response analysis of complex mechanical systems', 34th Symposium of Shock, Vibration and Associated Environments, October 1964.
11. Whiteley, A. L., 'Theory of servo systems with particular reference to stabilization', *Proc. I.E.E.*, **93**, Part II, p. 353, August 1946.
12. Wilson, D. R., 'Two phase power servo drives', *Electronics Letters*, **4**, p. 512, November 1968.
13. Wiener, N., 'The Extrapolation, Interpolation and Smoothing of Stationary Time Series' (Wiley, New York, 1949).
14. Wilson, D. R. and James, D. R., 'An engineering interpretation of optimal control', *Control and Instrumentation*. To be published.
15. Heckert, J. P. and Sordal, C. D., 'Autotracking accuracy of large antenna systems for satellite communication applications', Proc. I.E.E. Conference on Design and Construction of Large Steerable Aerials, London, June 1966 (I.E.E. Conference Publication No. 21).
16. Bowler, P., 'A compensation technique for optimising large and small signal servo responses', Proc. I.E.E. Conference on Servocomponents, p. 188, London, November 1967 (I.E.E. Conference Publication No. 37).

9. Appendix

Figure 6 illustrates the component parts of a servomechanism suitable for a satellite tracking antenna. This configuration is independent of antenna diameter, but for the purposes of this discussion a small antenna of 20 ft diameter will be considered.

The basic configuration has the following three feedback loops:

- (i) torque loop round the thyristor amplifier,
- (ii) velocity loop,
- (iii) position loop incorporating the satellite beacon and tracking receiver.

A thyristor amplifier can be considered as a simple gain (K_A , A/V) for the purposes of the servo design

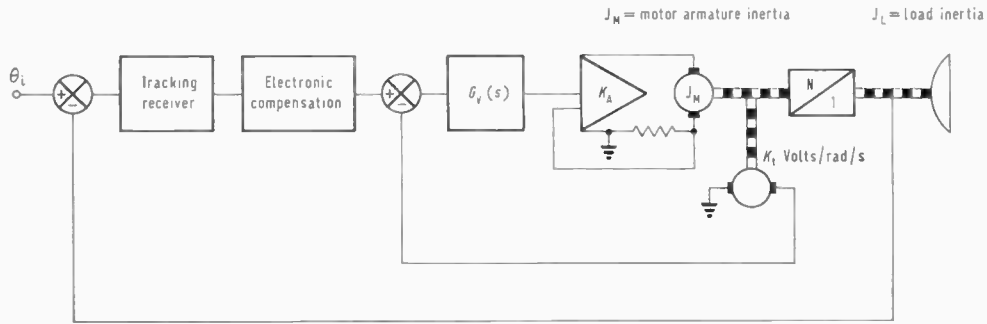


Fig. 6. Servo control system for a satellite tracking antenna.

$$\frac{i}{V_2} = \frac{K_A}{1 + K_A R} \quad \dots\dots(11)$$

Normally, $K_A R \gg 1$

Therefore

$$\frac{i}{V_2} \approx \frac{1}{R} \quad \dots\dots(12)$$

where R is the feedback resistor which is connected in series with the armature. This resistor will dissipate several watts, i.e. power consumed by the armature feedback resistor = $I^2 R$.

The velocity loop requires lag compensation in order to cut down the bandwidth, and therefore the term $K_2/(1 + ST_1)$ is incorporated. The transfer function is:

$$\frac{\dot{\theta}_m}{V_1} = \frac{\frac{K_2}{T_1 R} \frac{K_T}{J}}{\left(s^2 + \frac{1}{T_1} s + \frac{K_2}{T_1 R} \frac{K_T}{J} K_1 K_t \right)} \quad \dots\dots(13)$$

The position loop incorporates integral compensation to implement a type-2 servo. The transfer function is:

$$\frac{\theta_1}{\theta_i} = \frac{\frac{G_R}{T_R} \frac{K_2}{T_1 R} \frac{K_T}{J} \frac{1}{N} (S + 1/T)}{s^2 (s + 1/T_R) \left(s^2 + \frac{1}{T_1} s + \frac{K_2}{T_1 R} \frac{K_T}{J} K_1 K_t \right)} \quad \dots\dots (14)$$

The parameters of a typical 20 ft antenna are:

antenna load inertia, $J_L = 2000$ slug-ft²

receiver sensitivity, $G_R = 5$ volts/degree

receiver cut-off frequency = 20 Hz, i.e. $T_R = \frac{1}{40\pi}$

tachometer constant, $K_t = 0.172$ volts/rad/s

The motor can be selected from the desired slew speed, tracking performance in wind, and the drive to stow conditions. Normally, the torque necessary to accelerate the antenna is a second-order effect when

tracking a satellite, and is virtually negligible when tracking a synchronous satellite. During a slew an acceleration of 1°/(second)² is normally adequate. Therefore, the steady wind torque opposing the direction of an intended slew is normally the worst case or point of peak motor torque rating.

For the case considered here assume a motor with a maximum speed of 2500 rev/min, a torque constant $K_T = 0.36$ lb-ft/A and a maximum armature current of 10 A. A gear ratio of 12 000 : 1 will therefore produce a maximum slew speed of 1.5°/second and 43×10^3 lb-ft at the antenna. The motor would have a peak horse power rating of

$$\text{hp} = \frac{2\pi NT}{33000} = 1.7$$

The inertia of the armature of a motor of this capacity is 5.23×10^{-3} slug-ft². It follows that all the electromechanical constants of the above system are defined and the servo system can be developed.

9.1. Torque Loop

The torque loop equation is:

$$\frac{i}{V_2} = \frac{1}{R}$$

Assume that the maximum voltage swing of V_2 is ± 10 V and the range of armature current is ± 10 A. Therefore, in order for the full linear range of the variable to be used it follows:

$$R = 1 \text{ ohm}$$

and that the peak power dissipated in that resistor is 100 W.

9.2. Velocity Loop

The steady-state velocity is defined by

$$\frac{\dot{\theta}_m}{V_1} = \frac{1}{K_1 K_t} \quad \dots\dots(15)$$

Noting that $\dot{\theta}_m = 2500$ rev/min and that the maximum range of V_1 is ± 10 V, it follows:

$$K_1 K_t = \frac{1}{26.2} \text{ volts/rad/s}$$

Since the denominator of equation (13) can be written in the form

$$s^2 + 2\zeta\omega s + \omega^2$$

it follows that the form of the rate-loop response can be specified:

Let $\omega = \sqrt{10^3}$ rad/s ($f = 5$ Hz) and $\zeta = 1.0$

Therefore

$$T_1 = \frac{1}{20\pi}$$

and

$$\frac{K_2}{T_1} \frac{1}{R} \frac{K_T}{J} K_1 K_t \approx 10^3$$

Hence $K_2/T_1 = 381$, from which $K_2 = 6.05$.

Thus

$$\frac{\theta_m}{V_1} = \frac{26.2 \times 10^3}{s^2 + 20\pi s + 10^3} \quad \dots\dots(16)$$

9.3. Position Loop

The position loop characteristic can be varied by appropriate selection of the parameters α and $1/T$. The type of characteristic and bandwidth required is a function of the system, and in this case the object is to minimize receiver tracking noise as it will be shown that wind gust torques introduce negligible tracking jitter. The object therefore is to design a servo-mechanism with a low-pass filter characteristic.

The root locus technique allows the parameters α and $1/T$ to be specified for a desired predominant closed-loop pole pair, which is chosen to ensure a satisfactory response. In this example for a 0.1 Hz bandwidth the parameters are

$$\alpha = 10$$

$$1/T = 2.2$$

The open-loop transfer function is:

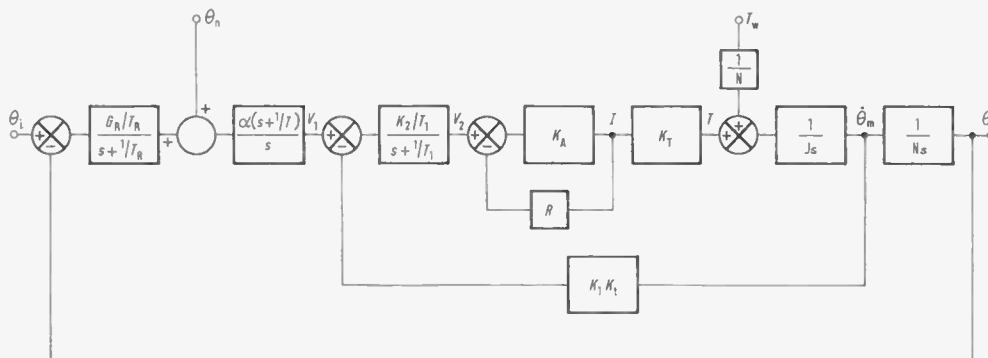


Fig. 7. Servo block diagram and disturbance input points.

$$\frac{7.8 \times 10^5 (s + 2.2)}{s^2 (s^2 + 62.84s + 10^3) (s + 125.68)}$$

and thus the closed-loop transfer function can be derived:

$$\theta_L = \frac{7.8 \times 10^5 s + 17.15 \times 10^5}{s^5 + 188.5s^4 + 8905s^3 + 1.26 \times 10^5 s^2 + 7.8 \times 10^5 s + 17.15 \times 10^5}$$

from which the frequency response, Fig. 8, is plotted. Figure 7 illustrates the point in the servo loop that the wind torque disturbance appears. Figure 9 gives the rearranged diagram which facilitates analysis.

$$G_w(s) = \frac{1}{N} \frac{1}{K_T} R \frac{(s + 1/T_1)}{K_2/T_1} \frac{s}{\alpha(s + 1/T)} \frac{(s + 1/T_R)}{G_R/T_R}$$

and

$$\theta_L(s) = G_w(s) \cdot \frac{G(s)}{1 + G(s)} \cdot T_w(s)$$

Noting that the frequencies of the wind gusts are much less than the frequencies $1/T_1, 1/T_R$, it follows that:

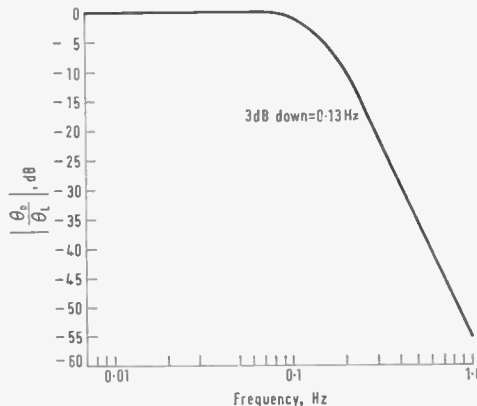


Fig. 8. Closed-loop transfer function $G(s)/1 + G(s)$ where:

$$G(s) = \frac{7.8 \times 10^5 (s + 2.2)}{s^2 (s + 125.68) (s^2 + 67.89s + 1005)}$$

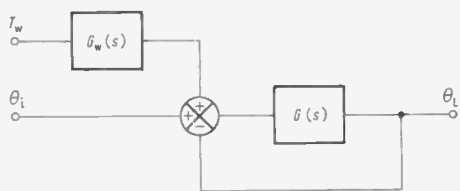


Fig. 9. Rearranged block diagram showing the wind disturbance reflected to the input.

$$\frac{\theta_L}{T_w} = \frac{1}{JN^2 T_1 T_R} \times \frac{s}{s^5 + s^4 \left(\frac{1}{T_R} + \frac{1}{T_1} \right) + s^3 \left(\frac{1}{T_1 T_R} + \frac{K_2 K_T K_1 K_i}{R J T_1} \right) + s^2 \left(\frac{K_2 K_T K_1 K_i}{R J T_1 T_R} \right) + \frac{G_R \alpha K_2 K_T}{T_R N R J T_1} s + \frac{G_R \alpha K_2 K_T}{T_R N R J T_1}}$$

$$\frac{\theta_L}{T_w} = \frac{105.2 \times 10^{-4} s}{s^5 + 188.52s^4 + 8905s^3 + 1.26 \times 10^5 s^2 + 7.8 \times 10^5 s + 17.15 \times 10^5}$$

The wind spectrum for a 48 km/h (30 miles/h) wind gusting to 63 km/h (45 miles/h) (3σ) is (assuming a 20ft diameter antenna):

$$\Phi_T(s) = \frac{60.4 \times 10^3}{-s^2 + (0.11)^2} \text{ lb-ft/rad/s}$$

Therefore,

$$\sigma_T^2 = 2\pi \left\{ \frac{1}{2\pi j} \int_{-j\infty}^{+j\infty} \left| \frac{\theta_L(s)}{T_w(s)} \right|^2 \Phi_T(s) ds \right\}$$

$$= 2\pi I_6$$

where I_6 is the value of the integral within the brackets. This can be evaluated from standard forms, and in this

particular case

$$I_6 = 2.918 \times 10^{-12}$$

$$\sigma_T^2 = 2\pi \times 2.918 \times 10^{-12}$$

$$\sigma_T = 2.46 \times 10^{-4} \text{ degrees}$$

Thus the wind gust jitter for the stated conditions is negligible for this size of antenna with the proposed control system.

The definition of the noise term in Fig. 3 in an auto-tracking servo loop is a function of the transmitted power of the satellite beacon, the sky attenuation, the aerial gain and the 1st stage of microwave amplification. This may use a tunnel diode amplifier, travelling-wave tube or parametric amplifier with cryogenic cooling if an extremely low-noise tracking receiver is essential. However, a typical figure for the noise spectral density, which is assumed white, is 52 dB down with respect to (1 degree)²/Hz, i.e. $2 \times 6.309 \times 10^{-6}$ (deg)²/rad/s.

Noting

$$\theta_L(s) = \frac{G(s)}{1+G(s)} \theta_n(s)$$

$$\sigma_n^2 = 2\pi \left\{ \frac{1}{2\pi j} \int_{-j\infty}^{+j\infty} \left| \frac{G(s)}{1+G(s)} \right|^2 \Phi_n(s) ds \right\}$$

which can be evaluated by standard forms using the definition of $G(s)$ above, i.e.

$$\sigma_n = 0.0376 \text{ degrees}$$

It follows that the peak value of σ would be 0.113° and that the antenna would satisfy all current design specifications for performance in poor tracking conditions.

Manuscript first received by the Institution on 19th August 1968 and in final form on 18th April 1969. (Paper No. 1279/IC 13.)

Complementary Monostable Multivibrator

By
J. J. SAINSBURY
 (Graduate)†

Summary: The circuit described has good stability and long delay periods with good load-driving capabilities. A modified circuit is also presented which has stable delay periods even when large transient voltages are present on the supply, such as can be experienced in an industrial environment.

1. Introduction

The circuit shown in Fig. 1 is very similar to that described in a recent paper by Ho.‡

This circuit has been used for many years and generally works very well. However, it is prone to shortening of the delay period due to transient voltages on the supply when used in industrial environments. It is possible to compensate for this effect. Unlike Ho's circuit, the transistors in this circuit are 'off' during the delay, or timing period.

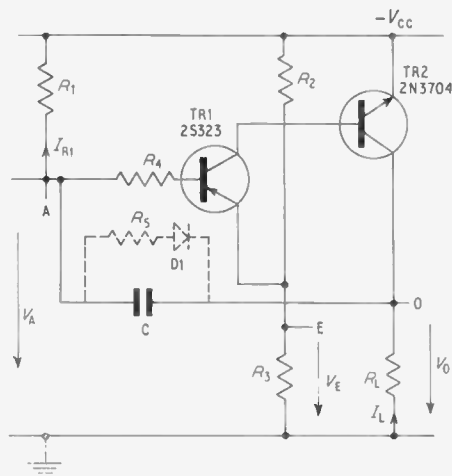


Fig. 1. Complementary monostable multivibrator.

2. Circuit Description

Referring to Fig. 1, let us start with the assumption that $V_A = 0$, and transistors TR1 and TR2 are off. V_A will fall exponentially as the capacitor charges through the two resistors R_1 and R_L . R_L is much smaller than R_1 , and can be neglected when calculating the value of R_1 to give the correct time-constant.

When V_A is about 0.6 V (V_{EB} more negative than

V_E) TR1 and hence TR2 conducts, V_0 falls, which causes V_A , via the capacitor, to fall further. Thus there is a regenerative action resulting in TR1 and TR2 being fully conductive.

If R_1 is of such a value that there is just sufficient base current through it to maintain the current in TR1 and TR2, and hence the load, the circuit will stay in the conducting state.

Let this value of R_1 be R_C .

If $R_1 < R_C$ the transistors will stay on.

If $R_1 > R_C$ the circuit will become an astable multivibrator similar to Ho's circuit (Fig. 6). Alternatively, one-shot operation can be preserved by connecting a 'hold-in' diode D1, and resistor R_5 , across the timing capacitor C, as shown dotted in Fig. 1. The diode is reverse-biased and has no effect in the delay period. When TR1 and TR2 are conducting the diode becomes forward-biased and, in conjunction with R_4 , R_5 and TR2, supplies base current to TR1 to keep it conducting.

R_4 is included to limit the base current to a safe value when the capacitor discharges. R_4 will not be required if the effective parallel resistance of R_2 and R_3 is sufficiently high.

Let $R_1 = R_C$ (i.e. the value required to just hold the circuit 'on').

$$\text{Current through } R_C = I_{RC} = I_L / h_{FE1} h_{FE2}.$$

Voltage across $R_C = V_{RC} = V_{CC} - V_E - V_{EB}$ (assuming R_4 to be small).

$$\text{Therefore, } R_C = V_{RC} / I_{RC}$$

$$= \frac{(V_{CC} - V_E - V_{EB}) h_{FE1} h_{FE2}}{I_L} \dots\dots(1)$$

For the normal cross-coupled monostable circuit, shown in Fig. 2, the maximum value for the resistor, R_{MAX} , that determines the delay period is given by:

$$R_{MAX} = \frac{(V_{CC} - V_{EB}) h_{FE}}{I_L} \dots\dots(2)$$

From eqns. (1) and (2) and assuming $V_{EB} < V_{RC}$

$$R_C \simeq \frac{R_2}{R_2 + R_3} \times h_{FE2} R_{MAX}$$

† Fords (Finsbury) Ltd., Chantry Avenue, Kempston, Bedfordshire.

‡ Ho, C. F., 'Zero quiescent current monostable multivibrator', *The Radio and Electronic Engineer*, 37, pp. 22-4, January 1969.

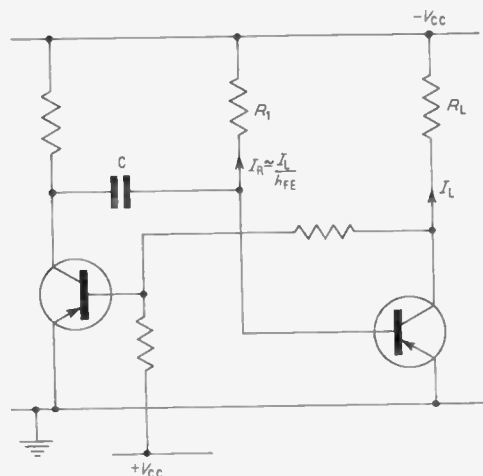


Fig. 2. Normal monostable circuit.

Hence R_C can be much larger in value and the capacitor can be smaller for a given delay period and load.

However, R_1 can be much larger than R_C if a hold-in diode circuit is used, and very long delay periods can be achieved. In practice, the limits for R_1 are set by the leakage currents of TR1 and the diode, and the input circuitry.

The delay period or 'off' period is given by

$$t = CR_1 \ln \left[\frac{V_{CC}}{V_{CC} - V_E - V_{EB}} \right]$$

and is independent of the current gain of the transistors.

3. Supply Transient Compensation

Although this type of circuit will give very good time stability for changes in the supply voltage, it will not tolerate very large transients on the supply during the delay period, such as can be experienced in industrial environments.

Transient voltages are decoupled from the base of TR1, whereas the emitter follows the transient instantaneously, though reduced in amplitude by the potential divider formed by R_2 and R_3 . The transient usually causes a reduction in the supply voltage and hence a reduction in the voltage across R_3 . The base-emitter junction of TR1 can become forward biased, and prematurely end the delay period. Fast and medium-speed transients can easily be decoupled in the normal manner by using resistance capacitance decoupling. In practice however, large, very slow transients, lasting for say half a second, do occur in industrial environments. Decoupling these requires

very large and expensive capacitors if the current taken from the supply is greater than say, 100 mA. The circuit shown in Fig. 3 will overcome this problem. C_1 and C_2 are effectively in parallel when calculating the time-constant, but in series to the transients on the supply. The values of R_6 and the relative values of C_1 and C_2 are chosen so that the transient voltage at the base (point A), is equal to that on the emitter (point E). The transistor will then not switch 'on' and shorten the delay period. R_6 compensates for the effect of R_L when fast transients are present and the capacitors are effective short-circuits. If R_L is small and fast transients are decoupled, R_6 is not required.

The formulae for calculating the value of R_6 and the relative values of C_1 and C_2 , are derived in the Appendix.

4. Practical Considerations

In Figs. 1 and 3, TR1 is a silicon alloy transistor. This type was selected because it has a high emitter-to-base breakdown voltage. Alternatively a planar transistor with a silicon diode in series with the base circuit could be used. This arrangement may slightly increase the change of delay period with change in ambient temperature, due to change in the diode forward voltage. The delay period may be varied by varying V_E in Fig. 1. If this method is used for the circuit shown in Fig. 3, the transient compensation will not be effective unless the values of R_6 and C_1 are also re-adjusted.

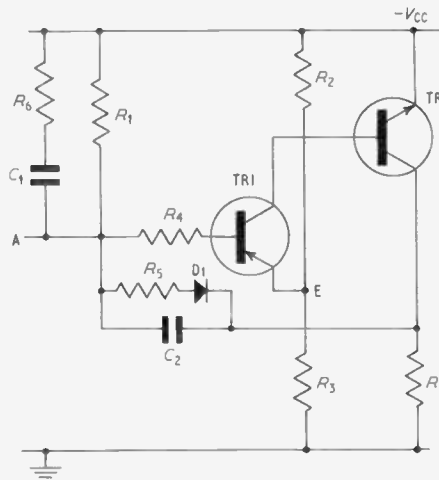


Fig. 3. Circuit for supply transient compensation. $C_1 = (R_3/R_2)C_2$, $R_6 = (R_2/R_3)R_L$

and

$$t = R_1(C_1 + C_2) \ln \left(\frac{V_{CC}}{V_{CC} - V_E - V_{EB}} \right)$$

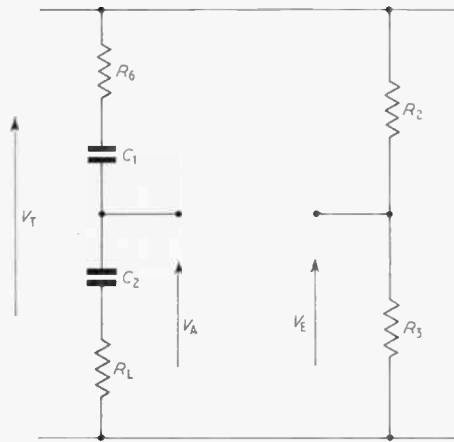


Fig. 4. Compensation circuit.

Resetting the circuit can be achieved by applying a positive pulse to point A, or a negative pulse to E.

5. Acknowledgments

The author wishes to thank Messrs. K. Linger, R. A. Fravel and K. A. Newman for their help with the preparation of this paper, and also the Directors of Fords (Finsbury) Limited for permission to publish it.

6. Appendix: Compensation Formulae

Consider only transient voltages occurring in the delay period. Assume that R_1 is very large and can be neglected. The relevant parts of Fig. 3 can be redrawn

as shown in Fig. 4. For complete compensation, V_A should equal V_E .

Take the transforms of Fig. 4.

$$V_A(P) = \frac{\left(\frac{1}{PC_2} + R_L\right) V_T(P)}{\frac{1}{PC_2} + R_L + \frac{1}{PC_1} + R_6}$$

$$= \frac{(C_1 + PC_1 C_2 R_L) V_T(P)}{C_1 + C_2 + PC_1 C_2 (R_L + R_6)}$$

$$V_E(P) = V_A(P) = \frac{R_3 V_T(P)}{R_2 + R_3}$$

$$\frac{R_3}{R_2 + R_3} = \frac{C_1 + PC_1 C_2 R_L}{C_1 + C_2 + PC_1 C_2 (R_L + R_6)}$$

$$C_2 R_3 + PC_1 C_2 R_3 (R_L + R_6) = C_1 R_2 + PC_1 C_2 R_L (R_2 + R_3)$$

For the above equation to be valid for all transient voltage waveforms the following conditions have to be satisfied:

$$C_2 R_3 = C_1 R_2 \quad \dots\dots(i)$$

and

$$R_3 (R_L + R_6) = R_L (R_2 + R_3) \quad \dots\dots(ii)$$

Condition (ii) gives

$$R_6 = R_L (R_2 / R_3)$$

Manuscript first received by the Institution on 26th March 1969 and in final form on 16th June 1969. (Short Contribution No. 125/CC55.)

© The Institution of Electronic and Radio Engineers, 1969

Multi-mode Excitation of Large Aperture Horns to Produce Electronic Deflection of Directional Pattern

By

ALLEN DAS, M.Sc.†

Summary: A method for producing electronic deflection of directional pattern of apertures, large compared to the wavelength, by exciting a number of modes, particularly in a horn, is discussed. Such electronic deflection of directional pattern of apertures could be usefully employed, amongst others, as hardened antennas for application in ground systems of navigation satellites, satellite-controlled satellites, etc., where the scan angle is between 10 to 15 beamwidths. It might also be used, depending on the number of modes that could be independently excited, for radars associated with the ballistic missile defence and for flush-mounted aircraft applications.

1. Introduction

The horn antenna has been used for the satellite communication ground station because of its broad-band and low-noise properties. The suitability and performance of large aperture horn antennas are amply reflected in the success of the *Echo* and *Telstar* projects.^{1, 2}

Techniques requiring generation and radiation of several waveguide modes have been utilized for beam shaping,³ for suppressing side-lobes and equalizing beamwidths⁴⁻⁷ and for monopulse feeds.⁸ Applications of multi-mode radiation have been generally confined to small apertures,^{3-6, 8} except that reported by Profera⁷ who used multi-modes for obtaining low side-lobe radiation from a 23.7λ aperture at 16 GHz. This contribution proposes the use of multi-modes for producing electronic deflection of directional pattern of large aperture horns.

2. Theory

Although a horn reflector type² antenna is of primary interest, radiation from an oversized rectangular waveguide is discussed here for simplicity. A horn with the same excitations as discussed in the following paragraphs will have radiation patterns similar to that of the oversized rectangular waveguide. Assuming $n = 0$, $\phi = 0$ and no reflections, the radiation patterns of TE_{m0} modes from a rectangular waveguide are given by⁹

$$E_{\phi} = (\text{constant}) \times (\beta_{m0}/\kappa + \cos \theta) \frac{\sin \left(\frac{\pi a}{\lambda} \sin \theta + \frac{m\pi}{2} \right)}{\left(\frac{\pi a}{\lambda} \sin \theta \right)^2 - \left(\frac{m\pi}{2} \right)^2} \quad \dots(1)$$

where m, n represent the number of sinusoids in the

intensity of two orthogonal field components and the other symbols have the following meaning:

- θ angle of elevation
- ϕ azimuth angle
- λ wavelength of radiation
- β_{m0} phase constant for the TE_{m0} -mode of propagation
- κ propagation constant, $2\pi/\lambda$

As the factor $(\beta_{m0}/\kappa + \cos \theta)$ varies slowly with θ , its effect is neglected in the following discussions. Equation (1) simplifies to

$$|E_{\phi}| = \text{constant} \times \frac{|\cos \psi|}{\left| \psi^2 - \left(\frac{m\pi}{2} \right)^2 \right|}, \quad \text{for } m = 1, 3, 5 \quad \dots(2)$$

$$\text{and } |E_{\phi}| = \text{constant} \times \frac{|\sin \psi|}{\left| \psi^2 - \left(\frac{m\pi}{2} \right)^2 \right|}, \quad \text{for } m = 2, 4, 6 \quad \dots(3)$$

where $\psi = (\pi a/\lambda) \sin \theta$ and a is the aperture of the waveguide.

The H-plane normalized radiation patterns of the rectangular waveguide are plotted in Figs. 1 and 2 for odd-mode and even-mode excitations, respectively. These figures represent the general nature, but not the detailed character, of the radiation patterns. From Figs. 1 and 2, it can be seen that the directional pattern can be pointed electronically to different directions by exciting one or a combination of the higher-order modes. The high side-lobes of the higher-order modes (Figs. 1 and 2) may be reduced by the combination of the TE and the TM modes.

Let us assume that $a/\lambda = 30$. Then the sixth-order mode is pointed approximately at an angle $\theta = \arcsin \{(23\pi)/8\pi \times 60\} \simeq 5.8^\circ$. To obtain a larger

† Consultant; formerly with TRW Systems, California, U.S.A.

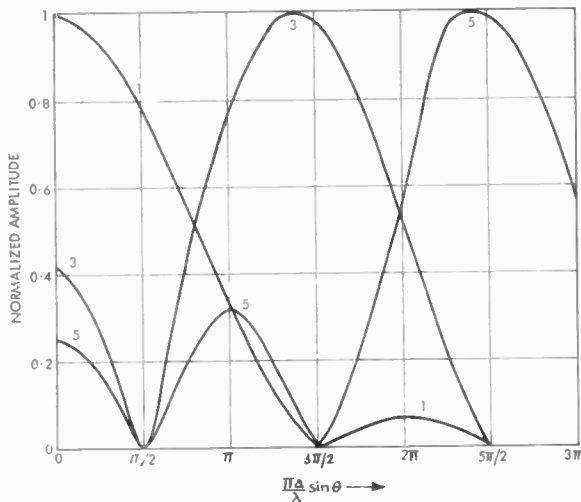


Fig. 1. Normalized amplitude of the radiation pattern of oversized rectangular guide for odd-mode excitations.

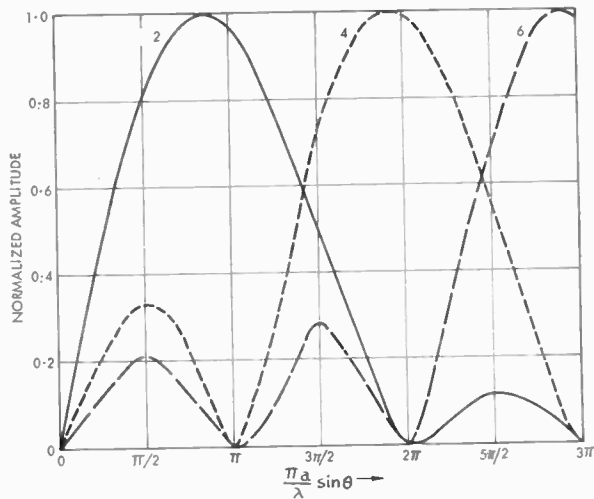


Fig. 2. Normalized amplitude of the radiation pattern of oversized rectangular guide for even-mode excitations.

angle for the beam deflection, a greater number of higher-order modes would have to be excited. For obtaining a beam deflection of 45° , modes up to the 42nd would be required.

If the higher-order modes are excited in the part of the horn where these modes can exist, then they will propagate down the flared horn and finally radiate. As a result, the radiation from a larger aperture can be controlled by the feed network located at a comparatively smaller aperture. For the above-mentioned example, the condition for radiation¹⁰ $\beta a \leq \kappa a$ will be satisfied for the 60th mode. The following factors, however, are to be considered: (i) the phase error across a large aperture horn will cause a distorted radiation pattern; (ii) the losses in the large aperture horn with a reasonable flare angle could be large; (iii) the higher-order modes have different phase velocities which will result in these modes undergoing different phase changes during their travel to the mouth of the horn; (iv) the radiation efficiency for the higher-order modes would have to be calculated; and (v) it would be necessary to prevent unwanted mode conversion.

3. Applications

The successful theoretical and experimental work of the horn-reflector antenna² shows that the factors (i) and (ii) can be adequately taken care of—at least for the dominant-mode propagation. From the knowledge of the dimensions of the horn and of the phase velocities, the relative phase of the higher-order modes at the aperture can be calculated. In addition to the use as a multi-beam aperture with electronic deflection

of its directional pattern for various purposes, multi-mode-excited horns would appear to have special attractiveness as hardened antennas. Figure 3 shows such a horn placed inside a mountain, perhaps inside a cave. The feed network is located inside the horn, and the electronic system is protected from nuclear radiation by the metallic portions of the horn. The beams can be deflected as shown in Fig. 4, by separately selecting different or a combination of higher-order modes. To obtain scanning in both planes, multi-modes have to be excited in both planes.

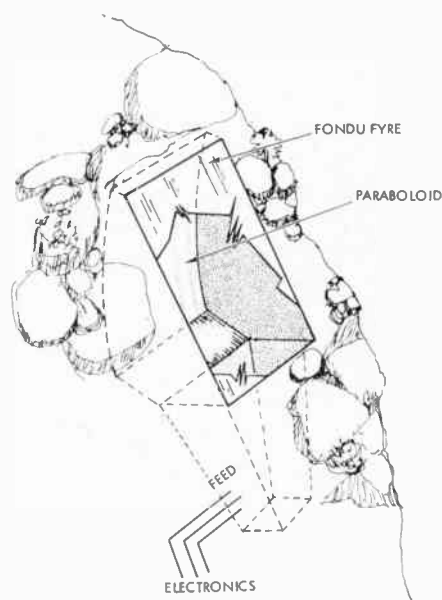


Fig. 3. Hardened multi-mode excited horn.

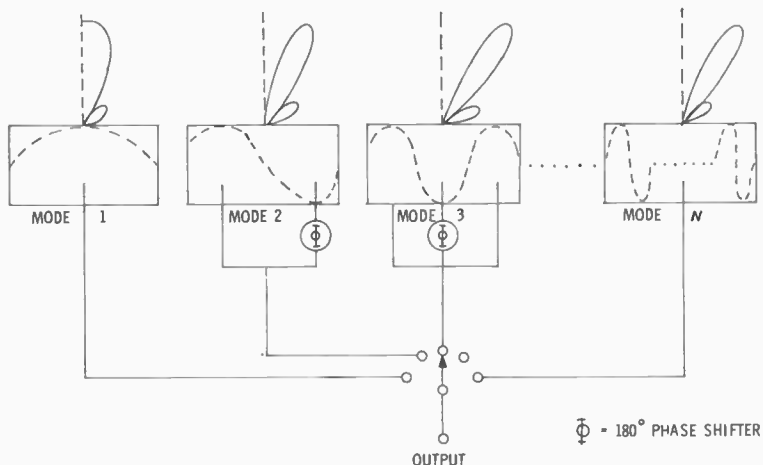


Fig. 4. Beam deflection by multi-mode excitation.

The horn will be completely filled with a low-loss, shock-resistant material such as 'Fondu Fyre',¹¹ which is believed to withstand large overpressures and attendant thermal effects. The ablation, as a result of one or multiple nuclear bursts, would probably reduce the diameter of the aperture, gradually lowering its gain and increasing its beamwidth.

It would be necessary to design feeds for exciting the different higher order modes independent of one another. Coaxial³ and waveguide feeds¹² have been developed to excite a small number of higher order modes. These feed networks, which have yet to be designed, should have very little interaction with one another. This is similar to very little mutual coupling required between the elements of a phased array. Hardened multi-mode-excited horns for L to X-band operation would appear to be of immediate application where (a) the physical dimensions of the aperture are not very large, and (b) the mechanical tolerances required may not be too expensive or difficult to achieve.

4. Conclusions

A new method of producing electronic deflection of directional patterns of large apertures is proposed. In view of the applications mentioned, further work in such multi-mode-excited apertures is recommended.

5. References

1. Crawford, A. B., Hogg, D. C. and Hunt, L. E., 'A horn-reflector antenna for space communications', *Bell Syst. Tech. J.*, **40**, pp. 1095-1116, July 1961.
2. Hines, J. N., Tingye Li and Turrin, R. H., 'The electrical characteristics of the conical horn-reflector antenna', *Bell Syst. Tech. J.*, **42**, pp. 1187-1211, July 1963.

3. 'Techniques for Integrating Solid-State Circuitry into Antennas,' Interim Technical Reports Nos: 2142-7, 1 September 1966; 2142-8, 3 March 1967; 2142-10, 19 May 1967; 2142-11, 30 June 1967; 2142-12, 30 September 1967; 2142-13, 22 December 1967; Ohio State University Research Foundation, Contract No. AF33(615)-3384-WPAFB.
4. Potter, P. D., 'A New Horn Antenna with Suppressed Side lobes and Equal Beamwidths', Technical Report No. 32-354, JPL California Institute of Technology, Pasadena, California; 25 February 1963.
5. Jensen, P. A., 'A Low-Noise Multi-Mode Cassegrain Monopulse Feed with Polarization Diversity', NEREM Record, pp. 94-95, 1963.
6. Drabowitch, S. W., 'Multimode antennas', *Microwave Journal*, **9**, pp. 41-51, January 1966.
7. Profera, C. E., Jr., 'Phased Arrays for Meteorological Satellite', Contract No. NAS12-149, RCA, June 1967.
8. Profera, C. E., Jr. and Yorinks, L. H., 'A high efficiency dual frequency multi-mode monopulse antenna feed system', *Suppl. to I.E.E.E. Trans. on Aerospace and Electronic Systems*, **AES-2**, pp. 314-22, November 1966.
9. Silver, S., 'Microwave Antenna Theory and Design', pp. 341-347 (Boston Technical Publishers, 1964).
10. Jones, K. E. and Mitra, R., 'Some Interpretations and Applications of κ - β Diagram', University of Illinois, Technical Report No. AFAL-TR-65-78, April 1965.
11. 'A Study of Structural Vulnerability of Fixed Portions of Hardened Command and Control Systems', CCNI to AF04 (694)-982, BSDTR-67-208, TRW No. 07379-6015-R100, September 1967.
12. Sharp, E. D. and Jones, E. M. T., 'A sampling measurement of multi-mode waveguide power', *I.R.E. Trans. on Microwave Theory and Techniques*, **MTT-10**, pp. 73-82, January 1962.

Manuscript first received by the Institution on 24th March 1969 and in final form on 23rd June 1969. (Short Contribution No. 126/Comm. 22.)

© The Institution of Electronic and Radio Engineers, 1969

Radio Engineering Overseas . . .

The following abstracts are taken from Commonwealth, European and Asian journals received by the Institution's Library. Abstracts of papers published in American journals are not included because they are available in many other publications. Members who wish to consult any of the papers quoted should apply to the Librarian giving full bibliographical details, i.e. title, author, journal and date, of the paper required. All papers are in the language of the country of origin of the journal unless otherwise stated. Translations cannot be supplied.

INTEGRATED CIRCUIT PRODUCTION

The photographic process used in the production of integrated circuits requires a set of photomasks that register very accurately with each other. These are made by photographic reduction of mask patterns; in this process 100 to 10 000 single images of the pattern for a circuit, each typically 1×1 mm, are formed on one mask for the purposes of quantity production. One method now widely used for making the masks employs a step-and-repeat camera, in a multi-barrel arrangement, for producing several masks simultaneously. A six-barrel step-and-repeat camera with carriages moving on hydrostatic bearings and a new grating measuring system for controlling their movements have been developed at the Philips Research Laboratories, Eindhoven and is described in a recent paper. As a result of numerous refinements in the bearings, in the measurement of displacement and in the adjustment of the object plates with the mask patterns and the focusing of the objectives, together with close control of the temperature, the total "repetition error", i.e. the relative error between two masks when one is placed on top of the other (whether produced simultaneously or successively), has been kept down to $\pm 0.2 \mu\text{m}$.

'A step-and-repeat camera for making photomasks for integrated circuits', F. T. Klostermann. *Philips Technical Review*, 30, pp. 57-70, No. 3, August 1969 (In English).

DIRECTIONAL ANTENNA SYSTEMS AND THEIR RESOLUTION

A large antenna array for ionospheric research and a numerical method for increasing its resolution are the subjects of two recently published Australian papers. The work was carried out by the Ionospheric Group at the University of Queensland for the Radio Research Board of Australia.

The first paper outlines the design and construction of a 1 km square cross array. The array is capable of operating in the frequency range 2-6 MHz. One arm is used for transmitting and one for receiving and both beams can be electronically steered to provide a steerable pencil beam radar system for ionospheric sounding.

The second paper first discusses the limitations imposed upon directional antenna systems by their beamwidth and side-lobes and then describes a method which allows for the extraction of signal information from otherwise unresolved signals. However, the method is applicable only for the case where the unresolved signal is due to two discrete signals and where the directional system gives amplitude and phase information as a function of beam direction. The method relies on a knowledge of the direction pattern of the system and using one of its weighted forms it is possible to analyse the output data from one complete sweep to determine the angular separation and then the actual angles of arrival of the

signals. Once these are found, the amplitude and phase of each signal may be evaluated.

'A large antenna array for ionospheric research', D. F. Mines. (pp. 28-32); 'A numerical method for increasing the resolution of directional antenna systems', L. G. Dryburgh (pp. 33-37). *Australian Telecommunication Research*, 3, No. 1, May 1969.

COMMUNICATIONS SYSTEM FOR SUPERSONIC AIR TRANSPORT

As a result of some experimental work carried out at the Radio Research Laboratories of the Japanese Ministry of Post and Telecommunications, a recently published paper describes a polarization diversity reception system for communication between aircraft and ground stations via a satellite in stationary orbit.

The signals in v.h.f. space communications fluctuate rapidly on the propagation path through the ionosphere, and fading is of the nature of Rayleigh distribution if circularly-polarized waves are received. The diversity effect on v.h.f. communications between the ground station and the satellite in a stationary orbit is about 10-20 dB, where linearly-polarized waves are transmitted and reception is by the use of circular or linear polarization diversity, when fading exists.

The system outlined is effective in diminishing the time when signals fade out and provides a method of more reliable v.h.f. space communication through the turbulent ionosphere.

'Diversity reception in v.h.f. space communications', K. Takashi, M. Kajikawa et al., *Journal of the Radio Research Laboratories*, Tokyo, 15, No. 80-81, pp. 187-98, July-September 1968 (In English).

TESTING TELEVISION RECORDING TAPES

The technical quality of television programmes obtained from tape-recordings remains rather unpredictable, because of faults in the tapes. The situation is more serious if, instead of restricting the argument to new tapes, consideration has also to be given to the use of tapes that have been used before.

An installation for testing television recording tapes has therefore been developed by the Research Department of the Office de Radiodiffusion-Télévision Française, for the purpose of assessing tapes taken into service, either for the first time or subsequently. The first step in verifying the quality of television tapes is to record measuring signals on the tape to be tested and then, on reproduction, signals characteristic of the fault observed are recorded on the sound track. A specially-designed rewinding machine for the used tapes makes it possible to discard faulty lengths of tape and to join up the lengths of perfect tape.

'Equipment for systematic testing of television recording tapes', C. Akrich and G. Eymery, *E.B.U. Review*, 114-A, pp. 54-9, April 1969 (In English).